UNIVERSIDADE BEIRA INTERIOR

Improvement on Cellulose Dissolution of Prehydrolyzed-kraft Pulps, their Characterization and Potential for the Lyocell Process

Versão final após defesa

Thalita Pedroso Damaceno

Dissertação para obtenção do Grau de Mestre em

Química Industrial

(2º ciclo de estudos)

Orientador: Prof. Dr. Álvaro Frederico Campos Vaz

Co-orientador: Prof. Dr. Rogério Manuel dos Santos Simões

Julho 2023

Declaração de Integridade

Eu, Thalita Pedroso Damaceno, que abaixo assino, estudante com o número de inscrição M11830 de Química Industrial da Faculdade de Ciências, declaro ter desenvolvido o presente trabalho e elaborado o presente texto em total consonância com o **Código de Integridades da Universidade da Beira Interior**.

Mais concretamente afirmo não ter incorrido em qualquer das variedades de Fraude Académica, e que aqui declaro conhecer, que em particular atendi à exigida referenciação de frases, extratos, imagens e outras formas de trabalho intelectual, e assumindo assim na íntegra as responsabilidades da autoria.

Universidade da Beira Interior, Covilhã 17 /07 / 2023

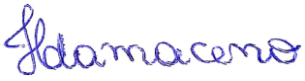

Acknowledgments

I would like to express my sincere gratitude to my supervisors, Professor Doctor Álvaro Vaz and Professor Doctor Rogério Simões, for their continued support and guidance through this work. Their comments and suggestions along the way have helped to prepare me for my future career pathway.

Also, I would like to thank all my laboratory fellows and partners for this journey of knowledge, challenges, and choices. A special thanks to my friend and supporter, MSc. André Cunha, who performed an essential role in this project with all his insights, training on equipment and experiments, availability, and overall assistance.

Finally, I am very grateful for the support given by the Fiber Materials and Environmental Technologies (FibEnTech-UBI) research unit under the project reference UIDB/00195/2020, funded by the Fundação para a Ciência e a Tecnologia (FCT), IP/MCTES through national funds (PIDDAC).

Resumo

A indústria têxtil introduziu o processo lyocell seguindo a crescente demanda por fibras de celulose regeneradas e como uma alternativa ambientalmente correta ao consolidado processo viscose. Algumas propriedades da pasta são necessárias para garantir a dissolução da polpa e a preservação da resistência mecânica da fibra regenerada, , como alto teor de α-celulose, moderado grau de polimerização (DP) e alta pureza (baixo teor de íons metálicos e cinzas).

Este trabalho envolveu o entendimento da influência das condições de pré-hidrólise nas propriedades da *dissolving pulp* de madeira (DWP) de *Eucalyptus globulus*, e a melhoria da dissolução de celulose da pasta de papel reciclada (RPP) por meio de otimizações no processo de cozimento kraft. A madeira de *E. globulus* submetida à hidrólise ácida em fluxo contínuo (FTR) apresentou, entre outras propriedades, menor teor de hemicelulose (3,8%) e viscosidade intrínseca (549 cm^3/g) quando comparada a correspondente polpa em que a auto-hidrólise ocorreu em um reator batch, com 4,9% de hemiceluloses e 874 cm^3/g de viscosidade intrínseca. Esses resultados evidenciaram a eficiência da hidrólise ácida na remoção de hemiceluloses e seu efeito na degradação da cadeia de celulose, visto como um resultado positivo, com maior reatividade no teste Fock (71% para DWP-FTR vs. 57% para DWP-Batch). Para a RPP, o desempenho ótimo foi obtido com cozimento kraft a 170°C, fator H em torno de 2.000, onde a polpa tratada apresentou teores de celulose e hemicelulose de 89% e 5%, respetivamente. Esse processamento resultou em um prominente aumento de 84% na reatividade da polpa e uma redução de 82% na matéria insolúvel quando comparada à polpa não tratada (RPP Original). A extensão e o tempo de dissolução para todas as pastas estudadas nos sistemas de solventes LiCl/DMAc e NMMO/H_2O foram discutidos em termos de suas propriedades físico-químicas. As *dissolving pulps* produzidas no âmbito deste trabalho mostraram grande potencial como matérias-primas para aplicações têxteis, com destaque para a pasta de papel reciclada e o inovador processo desenvolvido para melhorar a sua solubilidade. Entretanto, ainda são necessários alguns ajustes para aumentar a sua pureza.

Palavras-chave Caracterização de pastas; dissolução de celulose; *dissolving pulp*; papel reciclado; pré hidrólise-kraft

Abstract

The textile industry introduced the lyocell process following the increasing demand for regenerated cellulose fibers and as an environmentally friendly alternative to the consolidated viscose process. Some pulp properties are required to ensure pulp dissolution and regenerated fiber mechanical strength preservation, such as high *α*-cellulose content, a moderate degree of polymerization (DP), and high purity (low metal ion and ash content).

This work involved the understanding of the influence of prehydrolysis conditions on the properties of dissolving wood pulp (DWP) from *Eucalyptus globulus*, and the improvement of cellulose dissolution from the recycled paper pulp (RPP) by optimizations in the kraft cooking process. The *E. globulus* wood chips submitted to a flow-through (FTR) acid-hydrolysis showed, between other properties, lower hemicellulose content (3.8%) and intrinsic viscosity (549 cm^3/g) when compared to a DWP which the auto-hydrolysis occurred in a batch reactor, with 4.9% of hemicelluloses and 874 cm^3/g of intrinsic viscosity. These results evidenced the efficiency of acid-hydrolysis on hemicellulose removal and its effect on cellulose-chain degradation, seen as a positive outcome, with a greater Fock's test reactivity (71% for DWP-FTR vs. 57% for DWP-Batch). For the RPP, the optimum performance was obtained with a kraft cooking at 170°C, H-factor around 2,000, where the treated pulp showed a cellulose and hemicellulose content of 89% and 5%, respectively. This processing resulted in a remarkable increase of 84% in pulp reactivity, and a reduction of 82% in the insoluble matter compared to the untreated pulp (RPP Original).

The dissolution extension and time to all studied pulps in solvent systems LiCl/DMAc, and NMMO/H_2O were discussed regarding their physicochemical properties. The dissolving pulps produced under this work showed great potential as raw materials for textile applications, with a particular highlight on recycled paper pulp and the innovative process developed to improve its solubility. However, some adjustments are still necessary to increase its purity.

Keywords

Cellulose dissolution; dissolving pulp; recycled paper; prehydrolysis-kraft; pulp characterization

List of Papers and Conferences

The following publications comprise the foundation of this thesis:

I. Damaceno, T., Cunha, A., Simões, R., and Vaz, A. Sustainable Feedstocks for Lyocell Fibers: Emerging Commercial Processes. Submitted to Environmental Process & Sustainable Energy, May 2023.

II. Damaceno, T., Cunha, A., Simões, R., and Vaz, A. Conversion of Recycled Paper into Dissolving-grade Pulp: A new path for circular bioeconomy. Under development.

Results from this thesis have been presented at the following conferences:

I. XII Iberoamerican Congress on Pulp and Paper Research (CIADICYP), from June 28th to July 1st of 2022, University of Girona, Girona, Spain. Conference posters P.FPP.13 and P.FPP.14. Book of Abstracts, ISBN: 978 84 8458 621 0.

a. Damaceno, T., Cunha, A., Simões, R., and Vaz, A. Solvent exchange: effect on cellulose fibers dissolution in LiCl/DMAc.

b. Damaceno, T., Cunha, A., Simões, R., and Vaz, A. Characterization of cellulose fibers and their potential for lyocell process.

II. International Congress on Engineering – Innovation and Sustainability Praxis (ICEUBI), from November 28-30, 2022, University of Beira Interior, Covilha, Portugal. Oral presentation, conference paper 1359.

Damaceno, T., Cunha, A., Simões, R., and Vaz, A. A new path for the circular economy: Improving cellulose dissolution from recycled paper.

III. XXVI International Conference - Forest Biobased Materials - TECNICELPA 2023, from 11 to 13, October 2023. Pre-approved conference poster.

Cunha, A., Damaceno, T., Vaz, A., and Simões, R. The influence of prehydrolysis kraft conditions on pulp Fock reactivity.

Table of contents

List of Figures

List of Tables

List of de Acronyms

AA	Active Alkali
AE	Effective Alkali
AGU	D-anhydroglucopyranose unit
AN	Acceptor Number
AOX	Absorbable Organic Halide
AS	Acid Sulfite
CAGR	Compound Annual Growth Rate
CIADICYP	Iberoamerican Congress on Pulp and Paper Research
CMC	Carboxymethyl Cellulose
DDJ	Dynamic Drainage Jar
DMAc	N, N - dimethylacetamide
DMSO	Dimethyl sulfoxide
DN	Donor Number
DP	Degree of Polymerization
DTPA	Diethyleneaminepentacetic acid
DWP	Dissolving Wood Pulp
EDA	Ethylene diamine
EDTA	Ethylenediaminetetracetic acid
FCT	Fundação para a Ciência e a Tecnologia
FTR	Flow-through
GPC	Gel Permeation Chromatography
HBA	Hydrogen Bond Acceptor
HBD	Hydrogen Bond Donator
HEC	Hydroxyethyl Cellulose
HMF	Hydroxymethylfurfural
HPLC	High-Pressure Liquid Chromatography
HPMC	Hydroxypropyl Methyl Cellulose
HSP	Hansen's Solubility Parameters
ICEUBI	International Congress on Engineering
IL	Ionic Liquid
KN	Kappa Number
MMCF	Man-made Cellulose Fibers
MWD	Molecular Weight Distribution
NC	Nitrocellulose

NMMO	N-methylmorpholine-N-oxide
PDA	Photodiode Array
PG	Propyl Gallate
PH	Prehydrolysis
PHK	Prehydrolysis Kraft
RCF	Regenerated Cellulose Fibers
RI	Refractive Index
RPP	Recycled Paper Pulp
SEC	Size Exclusion Chromatography
UBI	University of Beira Interior
VTT	Valmistustekniikka Turvallisuustekniikka
XRD	X-Ray Diffraction

Chapter 1: Introductory Considerations

1.1. Introduction

Global textile production increased from 58 million tons in 2000 to 113 million tons in 2021, nearly doubling (Textile Exchange, 2022a). In the years to come, textile production and consumption tend to increase due to the projected 35% population growth by 2050 (Hasanbeigi & Price, 2015). Given the amount of water, energy, solid waste, wastewater, and air pollutants produced by the textile industry, it is considered one of the most environmentally hazardous production systems. Notwithstanding, the fashion industry also encourages irresponsible consumerism by developing trends and seasonal collections that increase waste generation (de Oliveira et al., 2021).

Natural fibers like cotton, silk, and wool have been the resources used to make fabrics for thousands of years. However, as customer demand and environmental concerns increased, the industry began to focus on alternative and renewable sources instead of virgin raw materials (Sayyed et al., 2019; Shen et al., 2010). In the early 20th century, man-made fibers appeared on the market with two main categories (Figure 1.1):

1) Natural polymers, i.e., regenerated cellulose fibers (RCF), made of natural cellulose (from cotton linter, wood, bamboo, etc.) processed by derivatizing or direct dissolving methods (Jiang et al., 2020; Sayyed et al., 2019);
2) Synthetic fibers produced from high-molecular-weight polymers derived from petroleum (Sayyed et al., 2019; Shen et al., 2010).

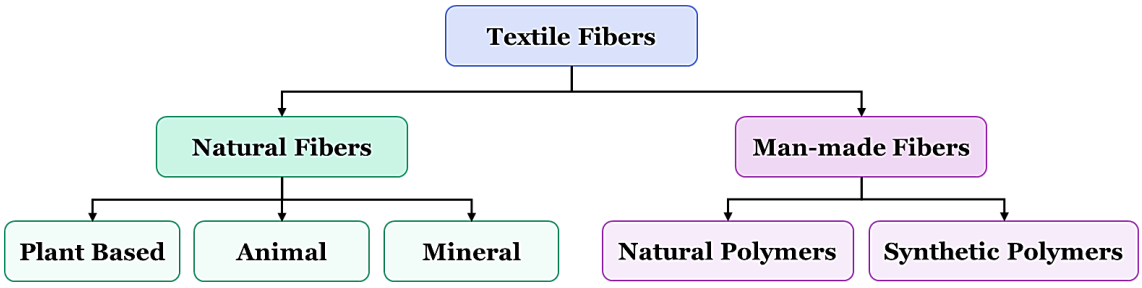

Figure 1.1. Classification of textile fibers (Adapted from Sayyed et al., 2019; Shen et al., 2010).

Cotton is the most widely used natural fiber in the textile industry, with almost a quarter (24%) of the world's total fiber production in the 2020-2021 period (Textile Exchange, 2021, 2022b).

Land occupation, water use (2.6% of the global amount), greenhouse gas emissions, ecotoxicity, and eutrophication are the most significant environmental effects related to its production (de Oliveira et al., 2021; Shen et al., 2010).

Synthetic fibers have dominated fiber production worldwide since the '1960s. Nevertheless, the '2000s sustainable mindset brought an increase in demand for regenerated cellulose as a raw material and an alternative to encourage the use of renewable resources in the textile industry (Shen et al., 2010). As a reflection of this movement, global RCF production more than doubled from over 3 million tons in 1990 to approximately 7.2 million tons in 2021 (Textile Exchange, 2021, 2022a).

The viscose process, which has long been the standard in RCF production, uses the derivative dissolution system NaOH/carbon disulfide (CS_2), which generates hazardous effluent and sulfur compounds such as SO_2, COS, and H_2S (Sayyed et al., 2019). An environmentally friendly substitute, the lyocell process, introduced in the early '80s a technology that uses sustainable feedstocks (such as certified plantation forests or recycled cellulose), and N-methylmorpholine-N-oxide (NMMO) as a non-derivative, non-toxic, environmentally safe, recyclable (>99%), and biodegradable solvent (Jiang et al., 2020; S. Zhang et al., 2018). Lyocell fibers, which had a market share of around 4.2% and a production volume of 0.3 million tons in 2021 (Figure 1.2), were the third most used regenerated cellulose fiber (Textile Exchange, 2022a).

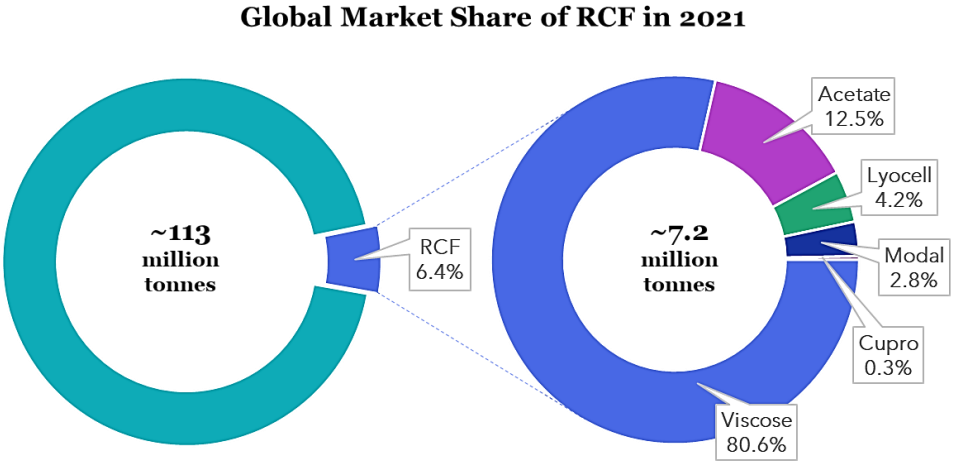

Figure 1.2. Global Market Share of RCF in 2021 (Adapted from Textile Exchange, 2022a).

The primary cellulose source for regenerated cellulose fibers is wood-based dissolving pulp (Björquist et al., 2018; Jiang et al., 2020; Sixta, 2006). For the manufacturing of RCF, particularly

lyocell fibers, specific dissolving pulp properties are required, such as high alpha-cellulose content, a moderate degree of polymerization (DP) and dope viscosity, narrow molecular weight distribution, high reactivity, and high purity (low metal ion and ash content). A balance between these properties is necessary to ensure cellulose dissolution, prevent solvent degradation, and preserve the mechanical strength of regenerated fiber (Chen et al., 2016; Jiang et al., 2020).

1.2. Study Motivation

Sustainability has emerged as a movement in all industries over the past few decades (Venkatesan & Periyasamy, 2019), intending to develop a bioeconomic business model that can balance environmental, customer, and business needs (de Oliveira et al., 2021; Oliveira Duarte et al., 2019). An analysis performed through the Scopus database is shown in Figure 1.3, demonstrating the exponential increase in publications related to the topic "textile" AND "sustainability". It can be noted that more than 84% of the research papers were published in the last ten years, of which almost 73% are from the past five years (2018-2022). This demonstrates that the textile industry's sustainability is a relevant and up-to-date topic.

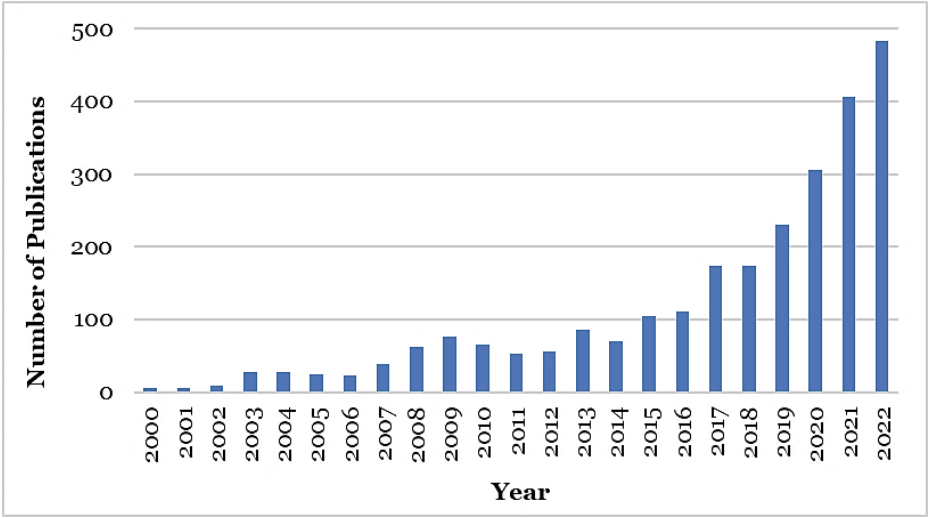

Figure 1.3. Number of published papers throughout the years considering textile sustainability (Source: Scopus).

Innovations in products, processes, and supply chains have been the strategy of the textile industry to achieve a closed-loop production system (Jia et al., 2020). Recently, companies and researchers have tracked the unsustainable steps in the textile value chain by performing life cycle assessments (LCA) of man-made cellulose fibers (MMCF), its results indicating that RCF, especially lyocell, has the lowest overall impact when compared with other MMCF and natural

fibers like cotton, viscose, and PET (Foroughi et al., 2021; Schultz & Suresh, 2017; Shen et al., 2010).

The recent interest in sustainability developments in lyocell processes can be highlighted in Figure 1.4, which shows a network of keywords on publications related to "lyocell" from 2012 to 2022. The analysis performed through the software of data analysis, VOSviewer, shows the allocation of research interest since 2018 on topics such as "sustainable development", "recycling", and "environmental impact".

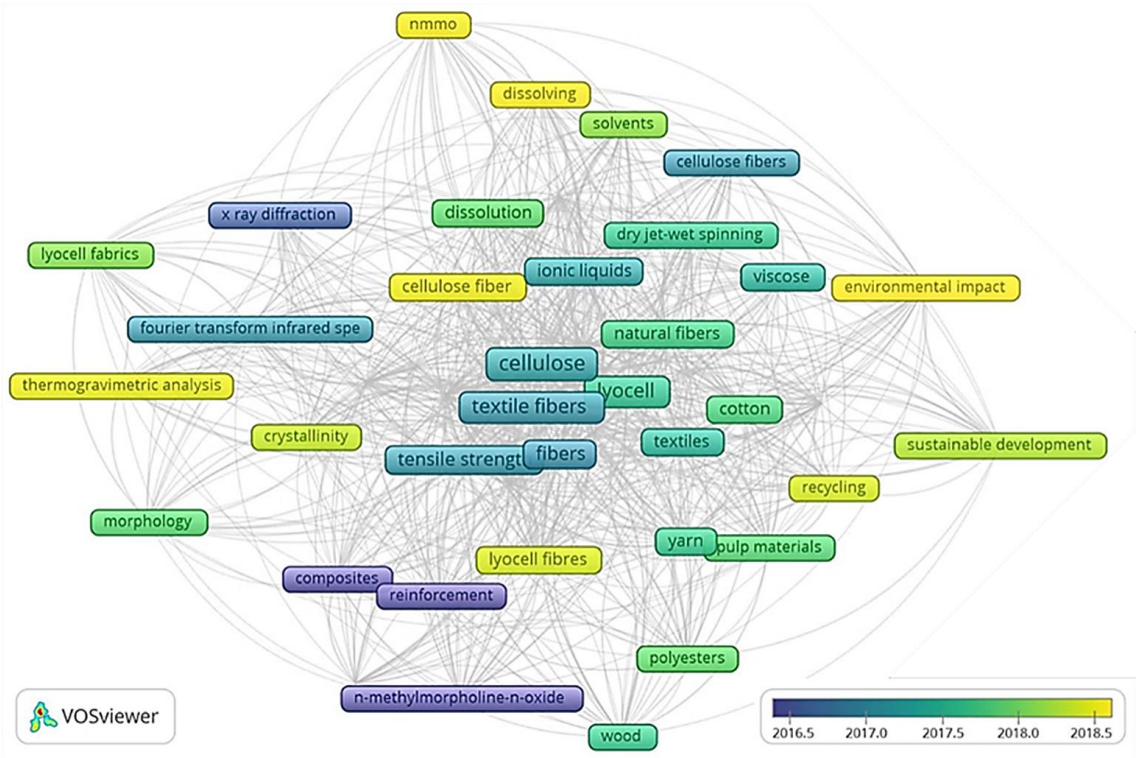

Figure 1.4. Network analysis of publications' keywords from 2012 to 2022 considering lyocell topic performed with data analysis software VOSviewer. The scale highlights the transition of scientific interest between 2016 and 2018 (Source: Scopus).

Most lyocell fibers currently on the market are made of wood pulp, and companies have been focusing on process enhancements, fiber functionalities, and alternative feedstocks to better match their products to market and customer demands. Furthermore, standards like the Organic Content Standard (OCS), Recycled Claim Standard (RCS), Global Recycled Standard (GRS), etc., promote the establishment of sustainability goals like the use of post-consumer recycled materials and certified renewable sources (Textile Exchange, 2021).

This work encompasses different sustainable aspects of renewable and recycled feedstocks used to produce lyocell fibers, from the applied treatments and the recyclability of the involved raw materials to their effective dissolution and application for regenerated cellulose fibers production.

1.3. Objectives

The main objective of this work is to characterize pulps from *Eucalyptus globulus* and recycled paper and investigate the correlation between fibers' structure, composition, and properties with their performance as lyocell fibrous raw materials. For this specific application, dissolving pulps need to fulfill some requirements related to their physical-chemical properties to ensure the quality of the regenerated fiber. To do that, three intermediate objectives are necessary, and they are shown in chronological order:

1. To investigate the influence of pulping processes (prehydrolysis kraft cooking) on wood pulps and recycled paper fibers properties and apply additional treatments such as bleaching and washing to produce high-quality dissolving pulps;
2. To evaluate whether the pulps meet the lyocell process specifications by their characterization in terms of chemical composition and structural and morphologic parameters;
3. To examine pulps dissolution behavior in the solvent systems NMMO/H_2O and LiCl/DMAc, and their reactivity performance by the viscose derivatizing test method (Fock Test), associating with the characteristics of the used lignocellulosic raw materials.

1.4. Project Structure

The structure of this research project was designed considering its complexity and need for time and performance management. Aiming for a better definition and control of the main activities and deliverables, the Work Breakdown Structure (WBS) in Figure 1.5 was developed.

The WBS is used as a hierarchical scope decomposition tool to monitor main activities better and control deadlines, costs, resources, performance, and deliverables. The construction of the WBS requires dividing a project into its stages and subtasks, and each level in the hierarchy has greater detail of the task to be performed (Erik Ernø-Kjølhede, 1999; Project Management Institute, 2021).

The first level of the WBS contains the project itself, followed by the three key work-packages, considering the monitoring tasks and theoretical development under the “Project Definitions”

block; the “Experimental Plan”, describing all stages of the laboratory activities and analyses in chronological order; and the “Deliverables”, consisting of the outcomes of the research project.

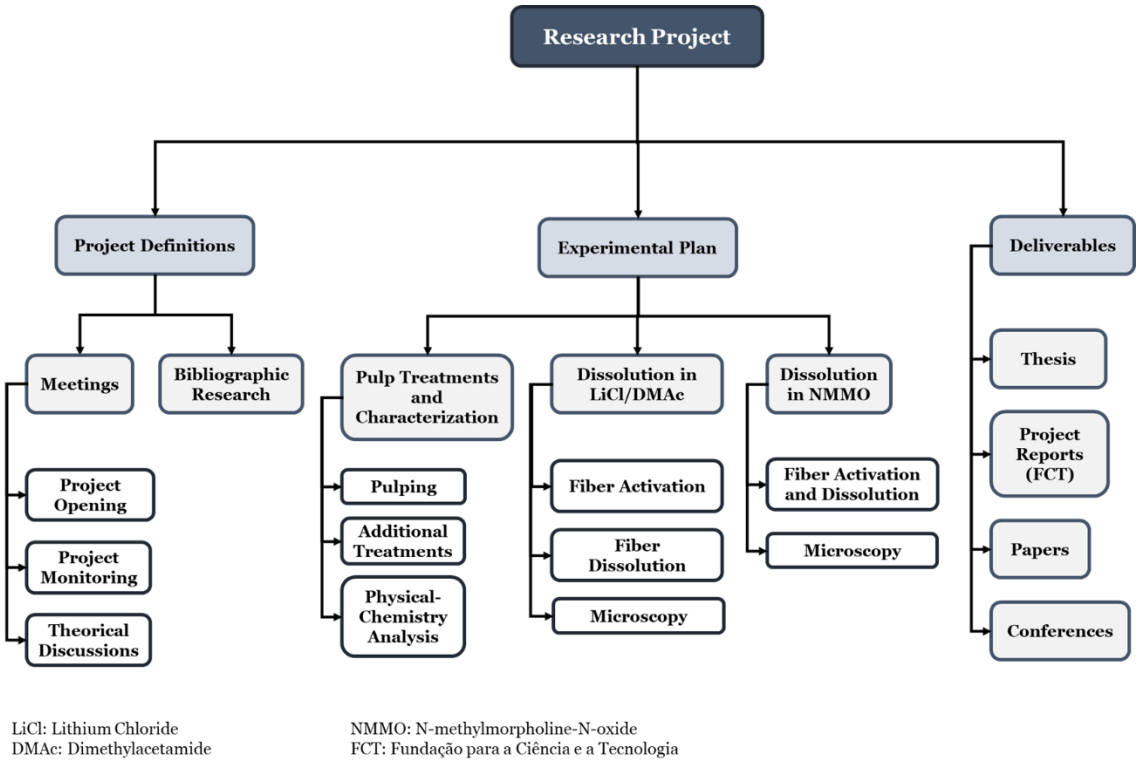

Figure 1.5. Work Breakdown Structure of the research project.

Chapter 2: Literature Review

2.1. Wood Structure and Composition

Wood is the largest source of bio-based materials on earth and the primary source of the cellulose used by paper, board, fibers, films, and other derivative industries (Kennedy et al., 1998; Krässig, 1993). Wood cell wall contains 65-75% of carbohydrates (mainly cellulose and hemicellulose) and around 18-35% of lignin (Rowell et al., 2012). In less extension, extractives such as resins, wax and oils, and inorganic substances can also be found (Heinze, 2016; Sixta, 2006).

Wood can be classified into two main groups: softwoods and hardwoods. Softwood comes from gymnosperms and coniferous trees, also known as evergreens. Some examples include pine, spruce, and cedar, trees with a relatively low density and light color (Asif, 2009; Bajpai, 2018c; Sixta, 2006). Softwood cell wall structure is simpler, composed mostly (90-95%) of longitudinal tracheids cells, responsible for their mechanical strength (Sjöström, 1981).

Hardwoods derive from angiosperm trees, called broadleaves or deciduous trees, that lose their leaves annually (Bajpai, 2018c). Hardwoods are typically darker in color, and have a more complex and condensed structure, including several cell types (such as libriform and parenchyma cells) and vessel elements with large cavities. These trees have a higher density than softwoods, also being more durable and less flexible (Asif, 2009; Sjöström, 1981). Some examples of hardwood are oak, beech, birch, and *Eucalyptus* species (one of the fastest-growing hardwood trees) (Asif, 2009; Salazar et al., 2016).

In summary, softwoods and hardwoods typically differ from each other in terms of their structure (Figure 2.1) (Asif, 2009). The dominant structural feature is the occurrence of vessels and diffuse-porous in hardwoods, while the proportions of cell wall elements, such as cellulose, hemicellulose, and lignin confer exclusive properties for both softwood and hardwood trees (Asif, 2009; Sixta, 2006; Sjöström, 1981).

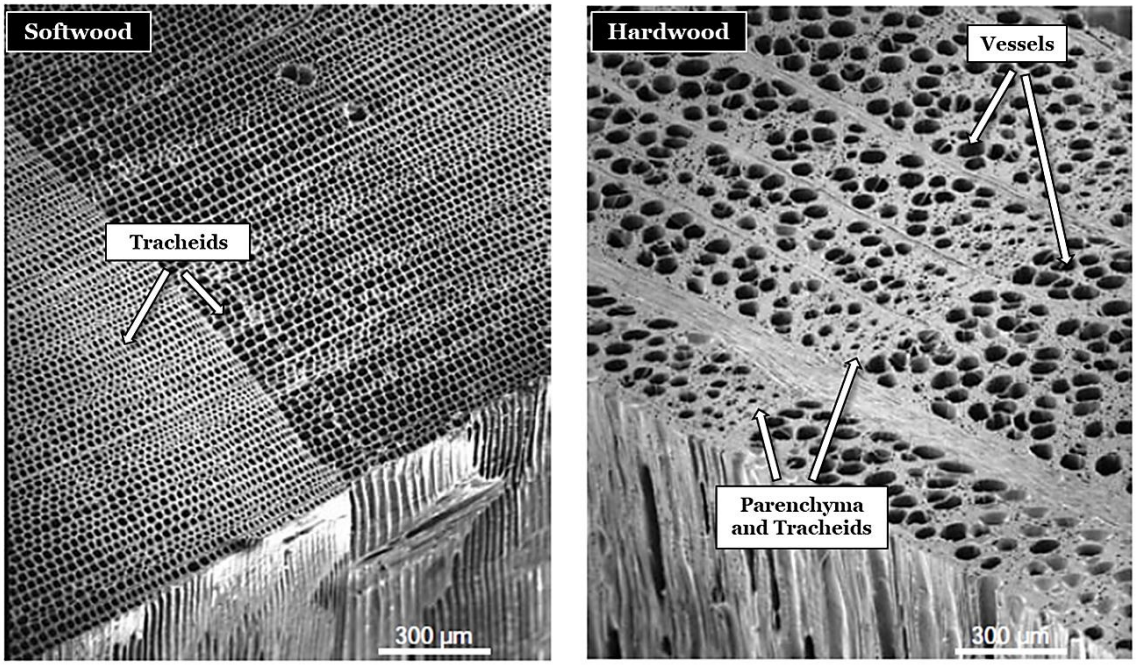

Figure 2.1. Transverse sections of softwood (left) and hardwood (right) with the indication of typical cell types (Adapted from Sixta, 2006).

The plant cell wall comprises cellulosic fibers (macrofibrils), comprising a microfibrils bundle, as described in Figure 2.2. The microfibrils are formed by an aggregate of elementary fibrils, where hemicellulose acts as a protective and binding component, while lignin executes a structural function. Cellulose molecules, in their semi-crystalline structure, form elementary fibrils with crystalline and amorphous regions (Sixta, 2006; X. Zhang et al., 2022). Biological and environmental impacts such as tree species, wood type, geographical location, climate, etc., can affect wood composition in quality and quantity (Çetinkol et al., 2012; Salazar et al., 2016). The typical average values of cellulose, hemicellulose, and lignin content for softwood and hardwood are described in Table 2.1.

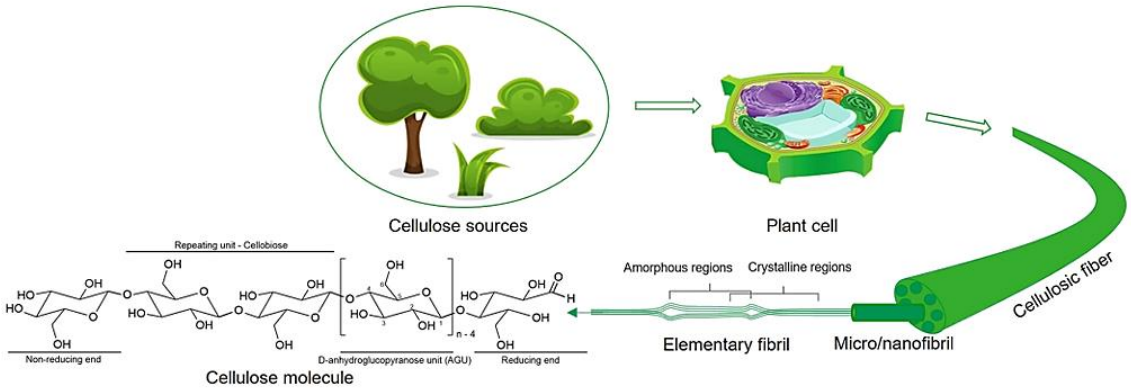

Figure 2.2. Schematic illustration of the fibrillar structure formation hierarchy, from a generic plant cell wall until the cellulose chain (Almeida et al., 2023).

Table 2.1. Chemical composition of wood cell wall (Sixta, 2006).

	Softwoods	**Hardwoods**
Cellulose (%)	40-44	40-44
Hemicellulose (%)	30-32	15-35
Lignin (%)	25-32	18-25

2.1.1. Cellulose

Cellulose, the most abundant biopolymer in nature (Biermann et al., 2001; Kondo, 1998), has a wide range of commercial applications. The primary sources of cellulose for commercial production are woods and plants, such as cotton, jute, sisal, and others (Sixta, 2006). Beyond the plants, cellulose can be produced by some acetic acid-producing bacteria and is found in algae, fungi, and animals, like urochordates, the only animal that produces cellulose (Heinze, 2016; Nakashima et al., 2004; Sixta, 2006).

In 1838, Anselme Payen isolated and determined cellulose composition by the empirical formula $C_6H_{10}O_5$ (Krässig, 1993; Young & Rowell, 1986). Cellulose is a homopolysaccharide consisting of linear D-anhydroglucopyranose units (AGU), linked together by β-(1,4)-glycosidic bonds between C(1) and C(4). The β-link locks the rings in a chair conformation, with the lowest energy and most stable form, which generates a complex supramolecular structure (Bruel et al., 2019; Krässig, 1993; Medronho & Lindman, 2014a; Rosenau, T. et al., 2019).

The macromolecular structure represented in Figure 2.3 was proposed in the late '20s by Haworth (Krässig, 1993). The hydroxyl terminal groups presented at both ends of the cellulose chain are different in nature. The C(1) is a potential aldehyde and a reducing end group, while the C(4) alcoholic hydroxyl is a non-reducing group (Klemm, D. et al., 1998; Krässig, 1993). The average degree of polymerization (DP) can be used to determine the size of the cellulose molecule. The estimated DP and the molecular mass of a single AGU are multiplied to estimate the average molecular weight (Medronho & Lindman, 2014b).

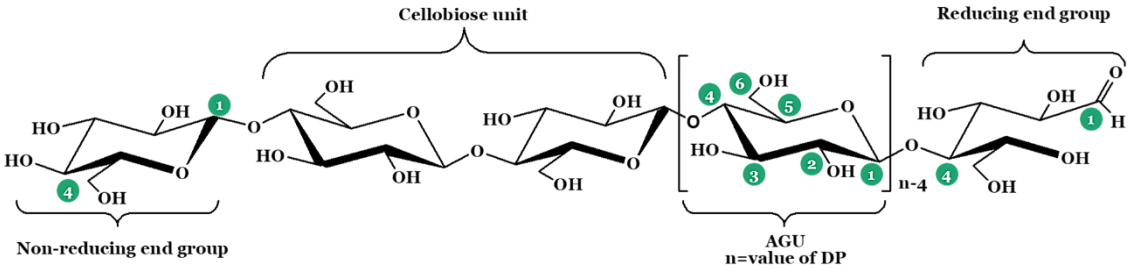

Figure 2.3. The conformational formula of the cellulose molecule (Adapted from Klemm et al., 1998). Developed at ChemDraw Ultra 8.0 by Cambridge Soft Corp.

2.1.2. Hemicellulose

Hemicelluloses, the second most abundant element of wood structure, are heteropolysaccharides, i.e., a mixture of polysaccharides with an average DP of 100-200 (Rowell et al., 2012; Sixta, 2006). The main components are sugars such as hexoses (mannose, galactose, and glucose units), pentoses (xylose and arabinose units), and hexuronic acids (d-glucopyranosyluronic acid and d-galactopyranosyluronic acid) (Rowell et al., 2012; Sixta, 2006). Galactoglucomannans are the major hemicellulose in softwood (10-15%), while glucuronoxylan represents 15-30% of hardwood hemicellulose content (Bajpai, 2018c). Figure 2.4 shows the molecular structure of a typical hardwood xylan and softwood glucomannan. The main chain (backbone) of hemicellulose can be characterized as a homopolymer, such as xylans, where only one monosaccharide unit is observed, or as a heteropolymer, such as glucomannans, with two or more units linked by β-(1,4) bonds. The units are usually linked to the backbone as side groups, such as galactose and 4-O-methylglucuronic acid (Bajpai, 2018c; Sixta, 2006).

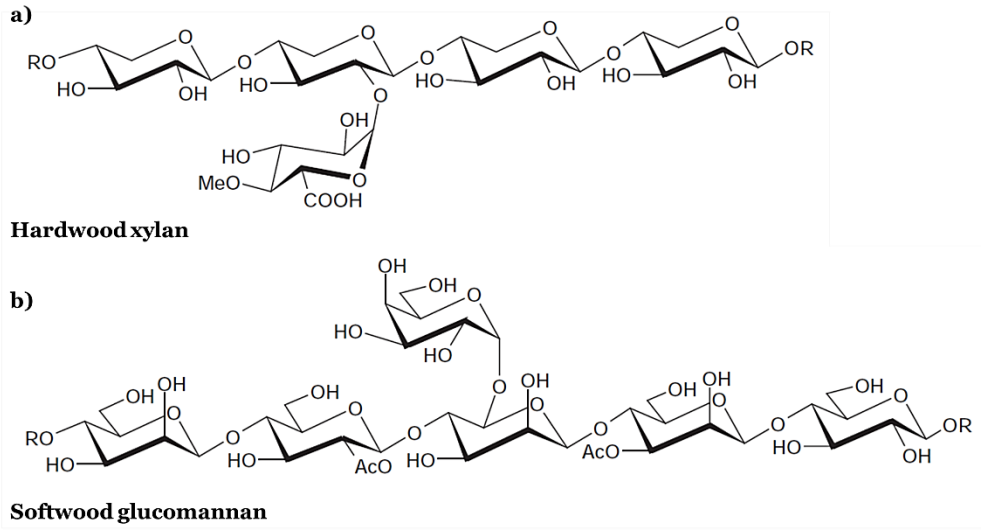

Figure 2.4. Molecular structure of a) hardwood xylan, and b) softwood glucomannan (Adapted from Sixta, 2006).

These compounds give fiber structural elasticity and serve as a binder for cellulose. In the papermaking industry, hemicelluloses are desired components by increasing paper strength during processing. However, a high yield of cellulose is required for dissolving pulps, and hemicelluloses must be removed by chemical pulping (Bajpai, 2018c).

2.1.3. Lignin

Lignin is a complex phenolic polymer, three-dimensional, amorphous, and mainly composed of aromatic molecular structures of its phenylpropane units (Figure 2.5.b) (Bajpai, 2018c; Rowell et al., 2012; Sixta, 2006). The complex polymer structure is formed through enzymatic dehydrogenation of its three precursors: *p*-coumaryl, coniferyl, and sinapyl alcohol, and the recombination of their phenoxy radicals, producing three phenylpropane units, respectively: *p*-hydroxyphenyl (H), guaiacyl (G), syringyl (S), represented in Figure 2.5.a (Kai et al., 2016; Sixta, 2006).

Lignin acts as a structural component that holds the fibers together (Bajpai, 2018c). Softwoods show a higher content of lignin, although their composition is generally uniform, containing mostly coniferyl alcohol (G-lignin), while hardwoods contain both coniferyl alcohol (50-75%) and sinapyl alcohol (25-50%) (Bajpai, 2018c; Sixta, 2006).

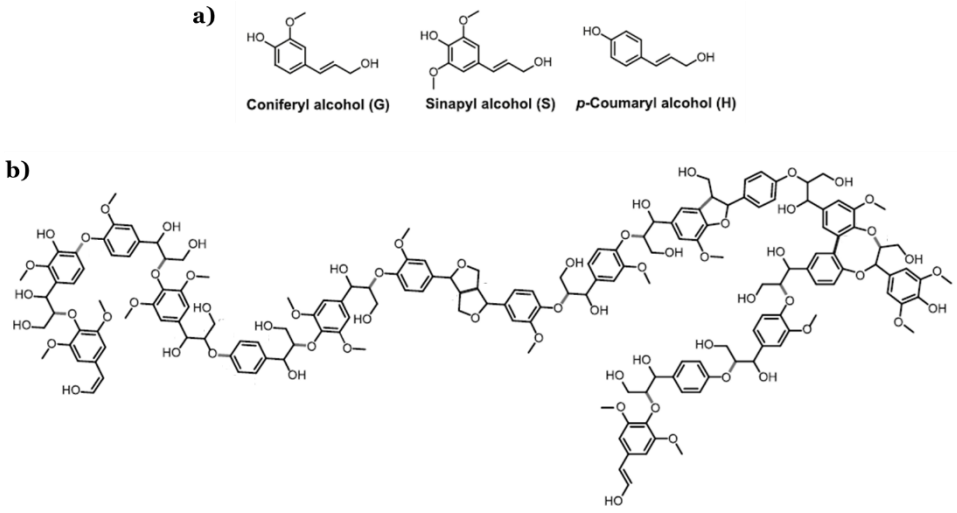

Figure 2.5. The precursors of lignin as phenylpropane units (a) and lignin chemical structure (b) (Adapted from Bertella & Luterbacher, 2020).

2.2. Dissolving Pulp

Dissolving pulp is a high-grade cellulose pulp, also known as dissolving cellulose (Bajpai, 2014a; Kumar & Christopher, 2017). This material contains a high alpha-cellulose content (>90%), with a low amount of hemicellulose (<4%), lignin, and other inorganic components (Hearle et al., 2001; Kumar & Christopher, 2017; Sixta et al., 2013). A high-quality dissolving pulp has properties such as uniform molecular weight distribution, high brightness, and cellulose reactivity (Bajpai, 2014a; Sixta, 2006).

These pulps can be used to manufacture various cellulosic products, like regenerated cellulose films and fibers, for clothing or technical purposes, such as viscose, rayon and lyocell, and cellulose derivative products, like nitrocellulose (NC), used in the production of explosives, and cellulose ethers (carboxymethyl cellulose CMC, hydroxyethyl cellulose HEC, hydroxypropyl methyl cellulose HPMC, etc.), used as rheology modifiers and stabilizers in food, pharmaceuticals, paints, cement and mortars formulations (Bajpai, 2018a; Christoffersson, 2005; Mendes et al., 2021; Sixta, 2006).

Wood-based dissolving pulp is the primary source of cellulose for the production of regenerated cellulose fibers, representing a substantial market share of around 85-88% in the segment (Björquist et al., 2018; Jiang et al., 2020; Sixta, 2006). The dissolving wood pulp (DWP) market shows a compound annual growth rate (CAGR) forecast of 3% between 2021 and 2028 (Data Bridge Market Research, 2021). This rising demand, assigned to RCF production growth, is accompanied by emerging technologies for developing new wood-based products for construction, textile, polymer, and biofuel applications (Hurmekoski et al., 2018; Sixta et al., 2013).

Wood raw materials' chemical pulping processes domain the dissolving pulp production (Chen et al., 2016; Hearle et al., 2001; Sixta, 2006). The most common pulping processes are acid sulfite (AS) and prehydrolysis kraft (PHK) for hemicellulose and lignin removal from the lignocellulosic biomass (Chen et al., 2016; Duan et al., 2015; Hearle et al., 2001).

Dissolving pulp production still shows some process limitations concerning yield and biomass utilization once its components, such as hemicellulose and lignin, must be removed (Silbermann & Weilach, 2018). The implementation of treatments such as acid hydrolysis and autohydrolysis (water prehydrolysis) allow the valorization of the prehydrolyzate liquor byproducts in a biorefinery strategy, adding value to the process and enhancing its sustainability by recovering

the containing short-chain carbohydrates, polysaccharides and other chemical compounds of interest (Bajpai, 2018a; Duan et al., 2015; Kumar & Christopher, 2017; Sixta et al., 2013).

2.2.1. Recycled paper as dissolving pulp

The conversion of paper-grade pulp into dissolving pulp is a well-established topic, with several studies in the literature in the last decades (Chen et al., 2016). Most of the studies report processes such as enzymatic treatments to improve fiber accessibility and caustic extraction for beta and gamma-cellulose fractions removal (Duan et al., 2016; Gong et al., 2022; Köpcke et al., 2008, 2010; H. Wang et al., 2014). The cold or hot alkali extraction is commonly used alongside the AS pulping as a purification step to increase the alpha-cellulose content in the pulp (Sixta, 2006).

Nevertheless, the conversion of recycled paper pulp into dissolving pulp is not usually found in the literature. The composition of recycled paper can vary significantly by its hardwood or softwood, chemical pulp, or mechanical pulp contents, and due to the presence of contaminants (adhesives, plastics, inks, dyes, and other foreign materials) (Scott, 2011). Its reuse in the paper industry is also limited to several cycles due to structural changes and degradation caused by processing operations. Therefore, to overcome this, in what concerns maintaining sustainable goals and reducing landfill occupation, non-paper products from recovered paper have been developed (Han et al., 2021; Scott, 2011).

The only reported processes for obtaining dissolving pulp from wastepaper and cardboard involve multiple steps of well-known methodologies. The patented method, developed by Valmistustekniikka Turvallisuustekniikka (VTT) Technical Research Center, presents as first stage a Super DDJ (Dynamic Drainage Jar) filtration with a 200-mesh wire to remove inorganic impurities, followed by an alkaline soda cooking (20% NaOH, at 165°C, and a H-factor of 1000), oxygen delignification (4% NaOH charge, 100°C, and 13.5 bar of O_2 pressure for 95 min), cold caustic extraction (NaOH 70g/L at room temperature for 1h), bleaching (DEpD), enzymatic treatment with endoglucanase (enzyme charge of 6 mL/kg, at 50°C for 120min), and acid washing (pH 2.5 at room temperature). The final pulp product has less than 0.7% (m/m) of lignin content, 90% of cellulose content, Fock reactivity of over 55%, and a viscosity of more than 250mL/g (Asikainen et al., 2014, 2015). Researchers from Aalto University and VTT presented a method where A4 copy paper sheets and cutting residues of cardboard were filtered and submitted to a classical kraft cooking, 5 mol kg^{-1} of effective alkali charge at a sulfidity of 35% (6:1 liquor to pulp ratio, 160 °C, 190 min). The cold caustic extraction and additional purification steps (bleaching, enzymatic and acid treatments) were followed in line with the earlier techniques developed by Asikainen *et al.* (Ma et al., 2016).

This thesis shows a route proposal for converting recycled paper into dissolving pulp by pre-hydrolysis kraft and other purification processes.

2.2.2. Chemical pulping

Pulping is defined as the process in which the lignocellulosic material is defibrillated, separating the fibers to produce a discrete material able to be dispersed in water: the pulp. Pulping is divided into four main categories: chemical, semi-chemical, mechanical, and a combination of both, the chemimechanical pulping (Bajpai, 2018b; Sixta, 2006).

Chemical pulp is the predominant method applied, accounting for nearly 80% of all pulp produced. In this method, lignin is degraded and dissolved by several chemical reactions at high temperatures (130-170°C). However, this method is not selective, and some hemicellulose and cellulose can be lost in the process, which takes in a fiber yield of 45-55%. The delignification extension and carbohydrate degradation depend on the chemical treatment applied, its conditions, and the characteristics of the lignocellulosic material (Sixta, 2006).

Kraft cooking is the principal chemical pulping method applied worldwide, able to process a wide range of softwood and hardwood species (Hearle et al., 2001; Saka & Matsumura, 2004). Globally, 90% of paper chemical pulp is produced by kraft cooking (Bajpai, 2018a). A different scenario used to be observed for dissolving pulp production, where the acidic sulfite (AS) method was responsible for over 60% of total production, followed by less than 25% for kraft process (Ceccherini et al., 2021; Sixta, 2006). Nowadays, primarily due to sustainable demand, the market interest has shifted to a PHK pulping domain (56%), over 42% of AS process (Ceccherini et al., 2021; Jiang et al., 2020).

The PHK process shows a high recovery of pulping chemicals and a high potential for the implementation of an integrating biorefinery concept. Even so, lower pulp yields (43-45% after bleaching) are observed compared to AS pulping (Bajpai, 2018b; Chen et al., 2016; Sixta, 2006). Besides the process itself, AS pulps and PHK pulps have differences in their properties. PHK pulps show higher alpha-cellulose content (94-96%), narrower molecular weight distribution, and higher fiber strength (Bajpai, 2018b; Duan et al., 2015; Sixta, 2006). However, the PHK pulps showed lower reactivity in several studies (Duan et al., 2015; Li et al., 2018; Sixta, 2000).

2.2.2.1. Prehydrolysis Kraft

The prehydrolysis (PH) was implemented in the mid-80s as a selective hemicellulose removal prior step as part of the developments in the wood pulping industry (Hearle et al., 2001; Sixta, 2006). This process involves the heating (150-180°C) of the cellulosic material in the presence of water (autohydrolysis) or diluted acid (acid hydrolysis). The de-esterification of the hemicellulose acetyl groups causes the formation of acetic acid, which guides acid-catalyzed hydrolysis, resulting in hemicelluloses solubilization and the formation of short-chain polysaccharides (Bajpai, 2018a; Bi et al., 2021; Reyes et al., 2016).

This pretreatment enhances the delignification rate during the kraft cooking by breaking the lignocellulosic structure and improving fiber accessibility. As a consequence, reductions in residence times in the producing plant and energy and chemicals consumption are observed (Araújo, 2008; Hearle et al., 2001; Reyes et al., 2016).

The kraft cooking stage has as main active agents hydroxide and hydrosulfide anions (Reyes et al., 2016; Sixta, 2006). The biomass is cooked at elevated temperatures in a high alkaline (pH 13-14) aqueous solution of sodium hydroxide (NaOH) and sodium sulfide (Na_2S), denoted as white liquor (Bajpai, 2018b; Bi et al., 2021; Sixta, 2006). The hydrosulfide anions promote a delignification selectivity to this process, causing the cleavage of bonds in the phenolic and nonphenolic units in a multistage process (Reyes et al., 2016; Sixta, 2006). The PHK overall process employs a recovery process that involves waste liquor (black liquor), evaporation and incineration, and the regeneration of inorganic compounds, closing part of the chemical cycle of the process (Araújo, 2008; Hearle et al., 2001).

The delignification kinetic model, called H-factor, combines the cooking temperature and time as a single variable, as described in Equation 2.1. The objective of the H-factor is to indicate the delignification rate by predicting the cooking temperature or time to achieve a specific kappa number (Bajpai, 2018b; Sixta, 2006).

$$H = \int_{t_0}^{t} \exp\left(43.19 - \frac{16113}{T}\right) dt \qquad Equation\ 2.1$$

Where t is the time (h), and T is the temperature (°C).

In the work delineated in this thesis, PHK was selected as pulping chemical treatment for DWP production and for improving recycled paper pulp reactivity. The pulping operational conditions

influence the properties of the dissolving pulp. This study evaluated variations in PH reaction systems and kraft cooking conditions (namely time and temperature), and their impact in the final dissolving grade pulp characteristics and dissolution behavior.

2.2.2.2. Bleaching

Bleaching is a chemical process applied as an additional treatment to the cooking process to remove colored compounds from pulp, i.e., residual lignin, chromophores, and other noncarbohydrate impurities (Sixta, 2006). The chemical pulp bleaching, also known as delignifying bleaching, involves multiple stages of oxidative compounds intercalated with alkali extractions (Sjöström, 1981). The typical bleaching chemicals, their conventional symbol (designated letter by TAPPI standard), and their function are described in Table 2.2.

In general, oxidants degrade lignin, and the carboxylic acid groups formed increase the solubility of the lignin fragments. The alkali (NaOH) degrades the oxidized lignin by hydrolysis and ionizes acidic phenolic groups, leading to its dissolution from the pulp (Dence & Reeve, 1996). The procedure, sequence, and chemicals depend on pulp type, target brightness, and need for preservation of strength properties of pulp (Sjöström, 1981). Bleaching selectivity is a crucial factor governed by the reaction rate of the chemical applied with lignin and extractives compared to carbohydrate components (Dence & Reeve, 1996).

Table 2.2. Bleaching chemicals and their respective symbol and function (Dence & Reeve, 1996).

Compound	**Symbol**	**Function**
Chlorine	C	Oxidize and chlorinate lignin
Hypochlorite	H	Oxidize, decolorize, and solubilize lignin
Chlorine dioxide	D	Oxidize, decolorize, and solubilize lignin
Oxygen	O	Oxidize, and solubilize lignin
Hydrogen peroxide	P	Oxidize, and decolorize lignin
Ozone	Z	Oxidize, decolorize, and solubilize lignin
Sodium hydroxide (alkali)	E	Hydrolyze chlorolignin and solubilize lignin
Xylanase (enzyme)	X	Catalyze xylan hydrolysis and aid in lignin removal
EDTA or DTPA (chelants)	Q	Remove metal ions

DTPA: Diethyleneaminepentacetic acid; EDTA: Ethylenediaminetetracetic acid

The elemental chlorine-free (ECF) and totally chlorine-free (TCF) are the most common bleaching processes applied nowadays, developed to reduce the harmful effects of chlorine (Cl_2) bleaching, such as the generation of total and adsorbable organic halides (AOX) (Bajpai, 2005).

A classical ECF sequence for market kraft pulp is given by D(EO)DED (Dence & Reeve, 1996). Generally, the first two stages (prebleaching) are considered the "delignification step", where lignin is decomposed and extracted from pulp, followed by the final steps that aim to improve pulp brightness (Dence & Reeve, 1996; Gellerstedt, 2009; Sjöström, 1981).

Currently, ECF bleaching is the most common method applied globally (Goto et al., 2023), presenting a good selectivity for lignin and chromophores compounds (Gellerstedt, 2009). In the D-stage, the chlorine dioxide (ClO_2) reacts selectively with phenolic and non-phenolic lignin, transferring one electron to produce chlorite ions (ClO_2^-) and generating radical species (phenoxy radical and cation radical, respectively), which follow the chain lignin oxidation reactions to the formation of alkali-soluble compounds to the extraction (E) stage (Dence & Reeve, 1996; Gellerstedt, 2009). Despite presenting itself as an environmental-friendly solution for bleaching, ECF bleaching is a source of environmental concerns. The process reduces but does not eliminate the organo-chlorinated compounds in the effluent, once hypochlorous acid (HOCl) and chlorine (Cl_2) are formed as intermediates in the ClO_2 bleaching reactions (Bajpai, 2005; Dence & Reeve, 1996).

TCF uses non-chlorinated chemicals such as oxygen (O), hydrogen peroxide (P), or ozone (Z) (López et al., 2003; Sixta, 2006). Usually, a chelating stage (Q) is added prior to the hydrogen peroxide to remove transition metals from the pulp to avoid oxidizing agent degradation and maximize bleaching efficiency (Bajpai, 2005; Pinto et al., 2015).

TCF sequences tend to be less selective than ECF, causing cellulose degradation during bleaching. Notwithstanding, TCF also requires low initial lignin content. As a consequence, the fiber loses some strength properties, losing viscosity as well, and does not achieve full brightness values. Despite the absence of chlorine-based compounds, the superiority of TCF over ECF is questionable as it shows lower yields and higher energy consumption in the process (Bajpai, 2005, 2018b).

2.2.2.3. Metal ion removal

The removal of metal ions occurs in the paper industry usually before bleaching, mainly TCF bleaching, as mentioned earlier, and can be done by an acid wash or a chelation stage (Granholm et al., 2010). For the production of dissolving pulp, the management of metal content in pulp is

regularly considered a purification step, applied as a final treatment to ensure a high-quality product (Asikainen et al., 2014; Yaopeng et al., 2020).

Acid washing is an effective, low-cost, and simple method for metal ion removal from pulp. Its effluent recycling capability of up to eight cycles is also a highlighted advantage of this process (Ghasemi et al., 2010). Notwithstanding, the selectivity of this method is low, causing magnesium ions loss, responsible for preventing the degradation of cellulose, which requires the further restoration of this stabilizing ion to the pulp (Ghasemi et al., 2010; Granholm et al., 2010).

The acid washing is typically performed by using sulfuric acid (pH ~2.5), 2-10% pulp consistency, and retention times between 30 minutes and 1 hour (Asikainen et al., 2015; Ghasemi et al., 2010; Gong et al., 2022; Granholm et al., 2010). Temperature, however, is the most critical parameter. An acid treatment at elevated temperatures shows considerably higher yields of metal ions removal. Nevertheless, a decrease in pulp viscosity and strength is observed (Gong et al., 2022; Granholm et al., 2010).

Chelation was presented as more effective than acid washing for transition metal ions removal from hardwood pulp (Ghasemi et al., 2010). Still, environmental concerns related to EDTA and DTPA as soil and aquatic pollutants have been guiding studies for the development of biodegradable chelating agents and alternative eco-friendly methods to reduce harmful transition metal ions content in pulps (Goto et al., 2023; Pinto et al., 2015).

The chelation process occurs through the metal ion complexation by the multidentate chelating agent, forming a ring structural chelate. The effectiveness of this method is strongly affected by the pH and other ligands and cations in the solution once the ions in the system may interfere with the metal chelation reaction. A high concentration of hydrogen ions (i.e., lower pH) tends to increase the complexation rate, which results in improved metal removal from pulp. Notwithstanding, the pH effect can vary considering the pulp origin (hardwood or softwood), the transition metals present, and the affinity of the metal ions to the pulp (Granholm et al., 2010).

Metal ions are bound to pulp mainly by ion exchange and physical adsorption. Typically, metals form complexes with pulp functional groups, such as carboxylic and phenolic groups. Their sorption is specific, although slightly predictable by coordination chemistry (Granholm et al., 2010; Södö et al., 2007). A study of transition metals' affinity to hardwood kraft pulp showed that monovalent ions are weakly bounded, while trivalent and bivalent ions, especially iron (Fe^{3+}), lead (Pb^{2+}), and cooper (Cu^{2+}), are more strongly bounded to the pulp as indicated by the following series (Södö et al., 2007):

$$Fe^{3+}>>Pb^{2+}>>Cu^{2+}>>Cd^{2+}>Zn^{2+}>Ba^{2+}>Ca^{2+}>Mn^{2+}>Fe^{2+}>Sr^{2+}>Mg^{2+}>K^{+}>Rb^{+}>Na^{+}$$

The chelation stage is usually performed at a medium pulp consistency, a temperature between 50°C and 70°C, and a retention time from 30min to 1h, using EDTA or DTPA at 0.2% to 0.4% (calculated per dry pulp) (Ghasemi et al., 2010; Granholm et al., 2010; Sixta, 2006).

2.2.3. Pulp Specifications

As a raw material for regenerated cellulose fibers production, dissolving grade pulps must fulfill certain requirements to be considered high-quality pulp, which is proper for the application field. Many methods for evaluating pulp quality have been established over the decades; however, cellulose characterization, as a scientific method, requires the evaluation of the relationship between the cellulosic material structure, chemical composition, and behavior as a complex system (Sixta, 2006). Table 2.3 summarizes the fundamental properties evaluated to classify a high-quality dissolving pulp.

One of the key dissolving pulp properties mentioned earlier is the high alpha-cellulose content (>90%) (Chen et al., 2016; Jiang et al., 2020; Sixta, 2006). Cellulose can be divided into three types: alpha (α), beta (β), and gamma (γ) cellulose. Alpha-cellulose is the undegraded portion of cellulose, with molecules of higher molecular weights, insoluble in an alkaline media; the beta and gamma-cellulose are defined as the short-chain carbohydrates resulting from cellulose degradation. The beta-cellulose is the precipitated formed upon acidification of the alkaline solution, while de gamma-cellulose comprises the carbohydrate residue that remains in the solution (Sixta, 2006).

In RCF applications, alpha-cellulose content is directly correlated to fiber mechanical properties, such as tenacity and elongation capacity (Jiang et al., 2020; Sixta, 2006). The lyocell process does not require an extremely high alpha-cellulose content, generally around 92%. Even though hemicelluloses are soluble in NMMO, their percentage must be controlled because it can affect fiber mechanical strength (Jiang et al., 2020). In the viscose process, hemicelluloses can also affect the filterability and xanthation of the fiber (Chen et al., 2016; Köpcke, 2010).

The residual lignin content in dissolving pulps, typically <0.05%, reflects the pulp brightness (Bajpai, 2018a; Sixta, 2006). Lignin structure contributes to final product yellowing; however, optical properties are not the sole parameter of concern for dissolving pulps. The pulp delignification by pulping treatments and bleaching improves the pulp reactivity and prevents lignin precipitation, affecting some dissolution and regeneration processes (Sixta, 2006). An ISO brightness of over 90% is indicated for high-quality dissolving pulps (Mendes et al., 2021).

The processability of pulp, given by its reactivity to chemicals, is one of the most critical parameters. The accessibility of the OH groups in the pulp is related to the cellulose supramolecular structure and involves an extensive characterization, from its morphology to the molecular level, considering its crystallinity, pore structure, degree of polymerization, fibril aggregations, and more (Chen et al., 2016; Mendes et al., 2021; Sixta, 2006). The pulp reactivity is commonly obtained by the reference methodology, the Fock Test (Fock, 1959). Generally, it is considered that dissolving grade pulps should show a reactivity of over 50% (Mendes et al., 2021); however, commercial dissolving pulps has a reactivity of around 65% (Köpcke, 2010) and a value of almost 63% have been reported for recycled paper dissolving pulp (Asikainen et al., 2014).

An intermediate degree of polymerization (DP) is expected for dissolving pulps (Sixta, 2006) once short-chain molecules represent weaker parts of the regenerated fiber, and extremely high DP, despite the expected improved mechanical strength, may cause a cellulose solubility reduction and an increased viscosity of the spinning dope, affecting the processability of the fiber (Jiang et al., 2020). Notwithstanding, it is common consent that a uniform molecular weight distribution (MWD) is a critical property. The more regular the MWD, the more cost-effective the process for obtaining fibers with better strength properties (Sixta, 2006).

Generally, the intrinsic viscosity indicated for dissolving pulps is between 400 and 600 mL/g (Chen et al., 2016). For lyocell fibers, a DP between 650-750 and an intrinsic viscosity from 280 to 350 mL/g are considered (Jiang et al., 2020; Mendes et al., 2021; Zhang et al., 2018), while for the viscose process, the optimum intrinsic viscosity is around 200 to 250mL/g (Chen et al., 2016; Duan et al., 2015).

Dissolving-grade pulps require a high degree of purity, especially in terms of their metal ion profile and ash content (Bajpai, 2018a; Jiang et al., 2020). The presence of transition metals, such as Fe, Cu, Mn, etc., is a well-known challenge for pulp bleaching in the paper industry once they catalyze the degradation of the oxidizing agent (hydrogen peroxide). A chelation stage is applied, using typically ethylenediaminetetraacetic acid (EDTA) or diethyleneaminepentaacetic acid (DTPA), where the metal ions are complexed and removed by pulp washing (Pinto et al., 2015).

These same transition metals can also cause detrimental effects on RCF production by affecting pulp dissolution, the filterability, and spinnability of the dope (mainly in viscose and lyocell fibers production), causing yellowing in the final product, and reduction of fiber strength (Christoffersson, 2005; Gong et al., 2022; Guo et al., 2021; Jiang et al., 2020; Sixta, 2006). Those metals (especially iron ions) are even more critical in the lyocell process. The occurrence of undesired side reactions and formation of byproducts in the NMMO/H_2O/cellulose system cause,

among other effects, the discoloration of the resulting fibers, cellulose, and NMMO degradation, thus compromising the solvent recovery, the most attractive environmental claim of lyocell process (Guo et al., 2021; Jiang et al., 2020; Rosenau et al., 2001, 2002). The NMMO degradation will be discussed in detail further.

The most common method applied for ash and metal ion removal in dissolving pulps is the acid wash treatment (Asikainen et al., 2014; Gong et al., 2022; Wang et al., 2018), reported as effective in reducing the ash content to the recommended level of <0.1% and iron of <5 mg/L for lyocell applications (Jiang et al., 2020).

Table 2.3. Properties of a high-quality dissolving pulp.

Property	**Typical Value**	**Property**	**Typical Value**
alpha-cellulose content[a]	>90%	Intrinsic Viscosity[a]	400-600 mL/g
Lignin content[b]	<0.05%	Reactivity[c]	>50%
Hemicellulose content[b]	<4%	Ash content[d]	<0.1%
ISO Brightness[c]	>90%	Iron content[d]	<5 mg/L

a. (Chen et al., 2016)

b. (Bajpai, 2018a)

c. (Mendes et al., 2021)

d. (Jiang et al., 2020)

2.3. Cellulose Dissolution

2.3.1. Supramolecular Structure

As expected, polysaccharides display various shapes and arrangements (Zugenmaier, 1998). Cellulose, as a regular homopolymer, has a simple molecular structure (Rosenau et al., 2019). Nevertheless, its supramolecular structure has been the target of extensive investigation, revealing complexity in terms of interactions, conformational arrangements, accessibility, and dissolution behavior (Glasser et al., 2012; Lindman et al., 2010; Medronho et al., 2012).

The insolubility of cellulose in water and typical organic solvents is attributed to its potential to form intramolecular (within the molecule/cellulose chain) and intermolecular (between different molecules/cellulose chain) hydrogen bonds, as described in Figure 2.6 (Lindman et al., 2010; Rosenau et al., 2019). The intramolecular interactions are responsible for chain stiffness, while the intermolecular hydrogen bonds allow the formation of fibrillar structures (like microfibrils) by creating linear biopolymer multilayers parallel to the equatorial planes (Bruel et al., 2019; Medronho & Lindman, 2014a; Rosenau et al., 2019). Beyond the OH-O hydrogen bonds, weaker interactions such as CH-O and van der Waals represent the cohesive forces of cellulose chains (Bruel et al., 2019).

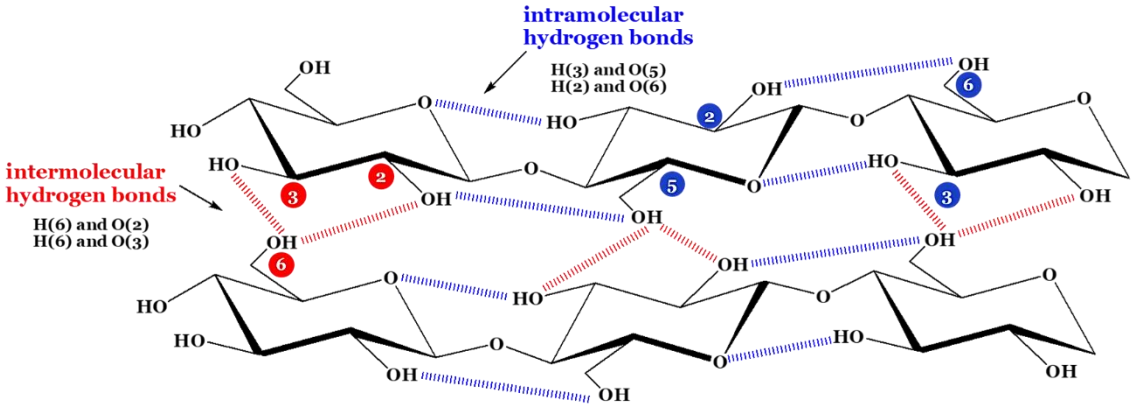

Figure 2.6. Representation of hydrogen bond network in cellulose, showing intramolecular (in blue) and intermolecular (in red) interactions (Adapted from (Medronho & Lindman, 2014a; Rosenau et al., 2019)). Developed at ChemDraw Ultra 8.0 by Cambridge Soft Corp.

The hydrogen bond network is responsible not only for the polymer's physical-chemical properties, stability, and strength but also for the formation of cellulose allomorphs shown in Figure 2.7 These forms differ in hydrogen bonds disposition, determining the degree of order of

cellulose chains and their geometry (Nishiyama et al., 2003; Rosenau et al., 2019). Amorphous or paracrystalline regions of low order coexist with higher-order crystalline domains in cellulose, making it a semi-crystalline polymer (Medronho & Lindman, 2014a). The principal crystalline phases are cellulose I, the naturally occurring form, divided into two subgroups I_α and I_β; and cellulose II, which shows the anti-parallel arrangement adopted by regenerated or mercerized cellulose. Other allomorphs are obtained under special conditions (Biermann et al., 2001; Medronho & Lindman, 2014b; Rosenau et al., 2019).

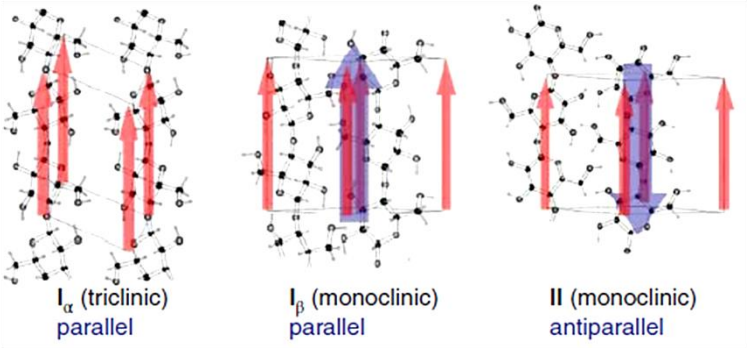

Figure 2.7. Cellulose allomorphs and solid-state structure of cellulose I (I_α and I_β) and cellulose II (Rosenau et al., 2019).

The understanding of the bonds involved in the initial crystallization steps follows the model in which two-dimensional sheets are formed by hydrogen-bonded chains (with different conformations) and associated by van der Waals forces to form microfibrils (Brown et al., 1982; Cousins & Brown, 1995). However, in a packed regular crystal lattice, hydrophobic interaction is also considered the driving force for sheet association (Bergenstråhle et al., 2010; Cousins & Brown, 1995; Medronho et al., 2012).

The early 2010s brought to the scientific community the development of hypotheses and debates based on cellulose amphiphilicity and hydrophobic molecular interactions (Bergenstråhle et al., 2010; Glasser et al., 2012; Medronho et al., 2012). Intending to rationalize the insolubility of cellulose in water and its selective solubility in a class of solvents with no apparent correlation, studies showed a solid supramolecular structure analysis beyond the well-established hydrogen bonds network and cellulose crystallinity (Medronho et al., 2012).

An amphiphilic compound is defined as one in which the molecule shows hydrophilic (polar) and hydrophobic (non-polar) sides or groups (Medronho et al., 2012). Cellulose, as a homopolymer, had its amphiphilicity neglected for a long time until the construction of its structure by computer simulations (Biermann et al., 2001; Yamane et al., 2006).

In a chair configuration, the hydroxyl groups of the molecule are in an equatorial position of the ring. The high density of hydroxyl groups results in the formation of a hydrophilic surface. On the other hand, the hydrogen atoms of C-H bonds are axial, conferring a hydrophobic character to the plane (Bruel et al., 2019; Medronho et al., 2012; Yamane et al., 2006).

Figure 2.8 shows a schematic representation of cellulose molecules with their hydrophilic and hydrophobic areas. This intrinsic structural anisotropy of cellulose molecules creates planes of opposite polarities, which may considerably affect its interactions and solubility from a micro and macroscopic perspective (Bergenstråhle et al., 2010; Medronho et al., 2012).

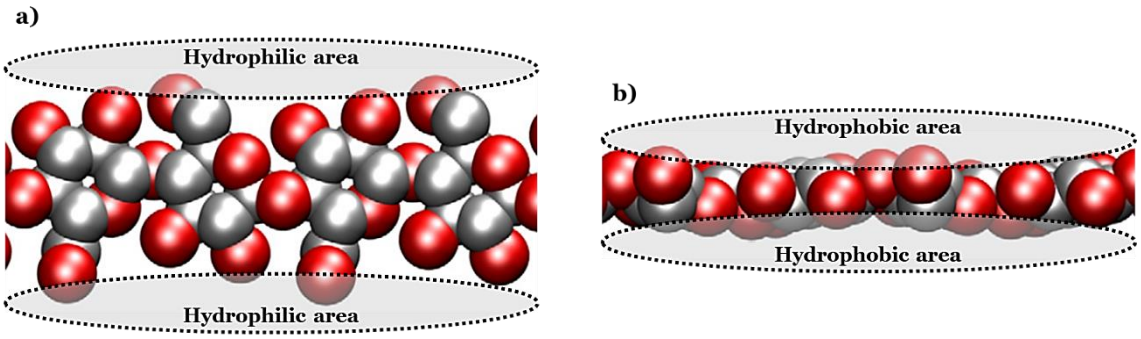

Figure 2.8. Van der Waals surface representation of the cellulose chain, a) 'above' view and b) side view, with oxygen atoms colored red and the non-polar carbon atoms shaded gray. Hydrogen atoms are not represented for clarity (Adapted from Bergenstråhle et al., 2010; Yamane et al., 2006).

Comprehending cellulose supramolecular structure, i.e., crystallographic structures, bonding, and interaction arrangements, provides important insights into cellulose stability and reactivity (Nishiyama et al., 2003). The balance between intra and intermolecular interactions (in this case, hydrogen bonds), van der Waals, and hydrophobic associations need to be considered to understand the behavior and properties of a complex system such as cellulose (Medronho et al., 2012).

2.3.2. Reactivity and Accessibility of Cellulose

In the cellulose complex network structure discussed earlier, with its fibrillar aggregations, interchain forces, and elementary crystallites, limited accessibility to reactive agents is observed (Krässig, 1993). From the reactivity point of view, cellulose accessibility is a critical factor (Christoffersson, 2005), which leads to alternations of interactions between reagents and the functional groups and fibrillar strands (Krässig, 1993).

Cellulose accessibility has been strongly associated with its structure and morphology, especially the degree of crystallinity. However, not only amorphous regions are predominately accessible to chemical reactions. Accessibility has been proven to be affected by the crystal size distribution and variation, which indicates that molecules in the regions between crystallites, on fibrillar interstices, and those on the surface of the elementary fibrils are also accessible to reagents (Köpcke, 2010; Krässig, 1993). In line with that statement, it has also been asserted that the reactivity of cellulose is more closely linked to the extension of fibril agglomerations and the capacity of the reagent to dissociate them (Fahmy & Mobarak, 1971).

Chemical bonds play an essential role in accessibility. Intermolecular hydrogen bonds involving the functional hydroxyl groups and oxygen atoms (Figure 2.6), hydrophobic, dipoles, and van der Waals interactions keep cellulose chains together and bind the microfibrils, limiting the access of solvents and reagents (Christoffersson, 2005; Köpcke, 2010; Krässig, 1993; Lindman et al., 2010).

Hornification, a structural change phenomenon occurring in pulp fibers upon drying, also affects the reactivity of cellulose (Fernandes Diniz et al., 2004; Köpcke, 2010; Krässig, 1993). The presence of pores and their size in the fiber ultrastructure is crucial for the sorption of reactive agents and the establishment of interactions. When fibers are dried, their internal volume shrinks, and those pores tend to irreversibly collapse, reducing the surface area of the pulp and the fiber accessibility (Fernandes Diniz et al., 2004; Henniges et al., 2014; Krässig, 1993).

Dissolution of cellulose is a challenging task. For this reason, it needs to be "activated" and become accessible to solvents and other reagents (Celine Cuissinat & Navard, 2006). To increase the accessibility of pulps, some activation treatments are employed, such as degradative (hydrolysis, oxidation, enzymatic, etc.), mechanical (milling, freeze drying, steam explosion, etc.), and swelling/chemical treatments (inter and intrafibrillar) (Henniges et al., 2014; Krässig, 1993). These methods aim to open the interfibrillar interstices, disrupt fibrillar aggregations, disturb the crystalline order, and change the chemical bond network to improve the reactivity of fiber and the way it behaves in terms of interactions with chemicals (Krässig, 1993).

2.3.3. Swelling of Cellulose

Swelling of cellulose is an important initial step for several processes, considered an activation stage to increase cellulose accessibility and reactivity (Fidale et al., 2008; Köpcke, 2010). Different from dissolution, swelling is, in some extension, a reversible process where the solvent molecules penetrate the polymer structure, causing the disruption of cellulose supramolecular structure to a certain extent (Fidale et al., 2008; Henniges et al., 2014; Medronho & Lindman, 2014a).

On the mechanism of cellulose swelling, the solvent/solute interaction occurs with OH-6 and OH-2 (Figure 2.5), while OH-3 bonds remain largely unaffected. This results in the cleavage of 75% of OH-6 and OH-2 intra and intermolecular hydrogen bonds in a highly swollen state (Henniges et al., 2014; Rosenau et al., 2019). The extension of those interactions and the degree of swelling of a pulp depend on the cellulose supramolecular structure, precisely its degree of polymerization, alpha-cellulose content, and crystallinity index. The intercrystalline swelling tends to decrease as those properties increase, i.e., it shows an inverse proportionality (Fidale et al., 2008; Köpcke, 2010).

The fiber activation by swelling can be performed with inorganic acids (sulfuric, phosphoric, nitric, and others), inorganic salts (mainly from Zn^{2+} and Li^{+}), amines and their complexes (ammonia, mono, and diamines, etc.), and alkali metal hydroxides (NaOH, LiOH, etc.). Swelling in a water-free organic solvent followed by a solvent exchange is one of the most effective treatments applied (Krässig, 1993). The swelling agent must show the ability to interact with cellulose by hydrogen bonds. Notwithstanding, characteristics of the solvent, such as molar volume, polarity, and its behavior as a proton acceptor or donor, among others, have influence over those interactions and the swelling extension (Fidale et al., 2008; Krässig, 1993).

The swelling capability of organic solvents has been assigned to a number of its properties, such as their molar volume (V_m), Hildebrand's (δ) and Hansen's (δ_D, δ_P, and δ_H) solubility parameters, Kamlet–Taft solvatochromic parameters (α, β, π^*), and Gutmann's acceptor (AN) and donor (DN) numbers (Fidale et al., 2008; Hansen & Björkman, 1998; Spange et al., 2003). This demonstrates that the understanding of swelling behavior cannot be predicted nor described by a single property (Fidale et al., 2008; Köpcke, 2010).

Hansen's solubility parameters

Hansen's solubility parameters (HSP) are the most used model to quantify solvent–polymer compatibility (Hansen & Björkman, 1998; Venkatram et al., 2019). Hansen model was developed as an improvement of the Hildebrand model, which utilizes a single parameter (δ), the square root of the cohesive energy density (i.e., the molar potential energy of the liquid divided by its molar volume) (Hansen, 1967; Venkatram et al., 2019).

The total cohesion energy (E) of a liquid, which is equal to its energy of vaporization, can be divided into three significant modes of interaction (Equation 2.2) attributable to nonpolar or dispersion forces (London), E_D, permanent dipole or polar interactions, E_P, and hydrogen bonding interactions, E_H (Hansen, 1967; Hansen & Björkman, 1998).

$$E = E_D + E_P + E_H \qquad Equation\ 2.2$$

Dividing Equation 2.2 by the molar volume (V_m) gives the cohesion energy densities for the respective energy types (Equation 2.3), where δ is the Hildebrand's solubility parameter, and δ_D, δ_P, and δ_H are the Hansen's solubility parameters, which represent the effects of the dispersion forces, polar forces, and hydrogen bonding forces, respectively. The units of solubility parameters are $MPa^{½}$ (Hansen, 1967; Hansen & Björkman, 1998; Venkatram et al., 2019).

$$\delta^2 = \delta_D^2 + \delta_P^2 + \delta_H^2 \qquad Equation\ 2.3$$

By Equation 2.3, each solvent is located within a three-dimensional system, where its solubility parameters can be considered a vector with Hansen's parameters as coordinates. These parameters can also be used to define the HSP distance (R_a) between two molecules (Equation 2.4), considering how alike they are. The smaller R_a, the less the difference in the solubility parameters, and the more likely they are to be compatible (Hansen, 1967; Hansen & Björkman, 1998).

$$R_a^2 = 4(\delta_{Dp} - \delta_{Ds})^2 + (\delta_{Pp} - \delta_{Ps})^2 + (\delta_{Hp} - \delta_{Hs})^2 \qquad Equation\ 2.4^*$$

*The subscripts "p" indicates the solute/polymer parameters, and "s" the solvent parameters.

The HSP model also allows to classify "good" or "bad" solvents by plotting a hypothetical sphere of radius R_o, centered on the solute's δ_D, δ_P, and δ_H values, called Hansen sphere. The magnitude of the radius of the sphere is given by experimental evaluation of a solute with several solvents of known HSPs (de los Ríos & Ramos, 2020; Hansen & Björkman, 1998). Figure 2.9 shows a Hansen sphere of R_o=8 $MPa^{1/2}$ determined based on empirical considerations in the critical assessment of Hansen's model by Venkatram et al., 2019. Solvents and non-solvents fall within or outside the sphere, respectively (Venkatram et al., 2019).

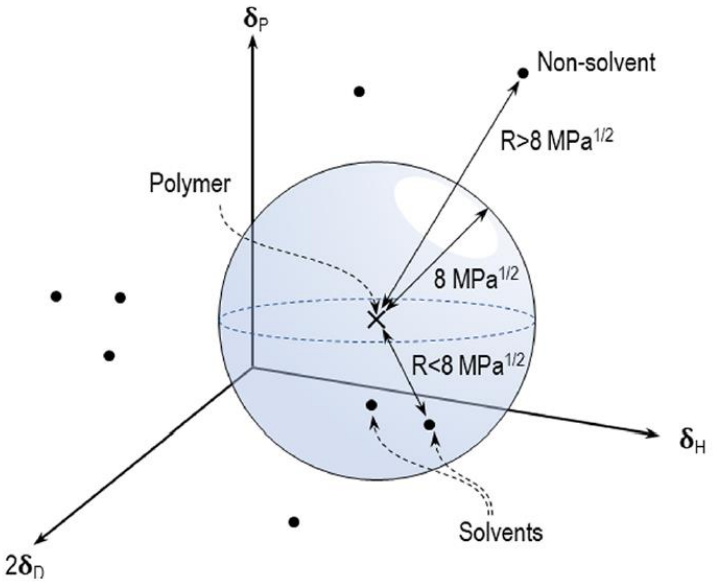

Figure 2.9. HSP sphere given by the Hansen's solubility model, where the three axes represent δ_D, δ_P, and δ_H components (Venkatram et al., 2019).

2.3.4. Dissolution Mechanism

From a thermodynamic point of view, the dissolution of a polymer, such as cellulose, is governed by the Gibbs free energy of mixing (ΔG_{mix}), composed of a usually positive enthalpic (ΔH_{mix}) term, dependent on intermolecular interactions and an entropic (ΔS_{mix}) term (Equation 2.5). The process occurs spontaneously when ΔG_{mix} is negative; however, the higher the molecular weight of a polymer, the lower the entropy term tends to be, and the more difficult to dissolve the polymer. In this scenario, the enthalpy term becomes crucial to the sign of Gibbs' free energy of mixing (Lindman et al., 2010; Medronho & Lindman, 2014a). ΔH_{mix} is given by the energy of mixing of the solvated polymer molecules with solvent in an infinitely diluted solution, which is usually an exothermic term (Ramos et al., 2005).

$$\Delta G_{mix} = \Delta H_{mix} - T\Delta S_{mix} \qquad Equation\ 2.5$$

An appropriate solvent must overcome the low entropy through its interactions with the polymer, typically promoting conformational changes in the cellulose supramolecular structure (Lindman et al., 2010; Medronho & Lindman, 2014a). Notwithstanding, the crystallinity of the polymer may be a relevant factor for its solubility understanding. Higher-order crystalline regions have lower energy, in terms of entropy than amorphous domains, which indicates that the higher the number

of crystalline regions in a polymer, the stronger the inter-chain interactions and more difficult its dissolution (Bergenstråhle et al., 2010; Lindman et al., 2010; Medronho et al., 2012).

Cellulose can be dissolved by derivative and non-derivative processes (Jiang et al., 2020). In the derivatizing process, such as cellulose acetate, cellulose nitrite, and viscose, the chemical structure of cellulose is changed, and an intermediate compound is formed (Sayyed et al., 2019). For viscose production, the most produced man-made fiber, an alkali cellulose intermediate, is formed by the diffusion of alkali ions from NaOH on cellulose structure, resulting in a morphological change from cellulose I to cellulose II. This irreversible swelling is followed by a xanthation, which involves the reaction of the intermediate with CS_2, producing the viscose spinning dope of sodium cellulose xanthate (Jiang et al., 2020; Sayyed et al., 2019). In the non-derivatizing process, cellulose is directly dissolved in the solvent system, such as salts dissolved in organic solvents (LiCl/N,N-dimethylacetamide), ionic liquids (ILs), N-methylmorpholine-N-oxide (NMMO), aqueous alkali systems (NaOH/urea or thiourea, NaOH/ZnO), aqueous inorganic complexes (cuprammonium hydroxide), concentrated salt solutions (zinc chloride, ammonium, etc.), non-aqueous solvents, etc. (Jiang et al., 2020; Lindman et al., 2010; Medronho & Lindman, 2014b; Sayyed et al., 2019).

Regarding the cellulose dissolution mechanism, it is widely accepted as an irreversible process where a solvent shows the ability to break inter- and intramolecular hydrogen bonds among cellulose molecules and establish new interactions, resulting in the formation of a homogeneous solution (Henniges et al., 2014; Medronho & Lindman, 2014a). Dissolution is considered an "extension" of swelling, involving the cleavage of OH-3 (Figure 2.6) hydrogen bonds, prior kept almost unaffected. The break of those bonds is crucial in the biopolymer dissolution mechanism (Henniges et al., 2014; Rosenau et al., 2019).

However, the understanding of cellulose dissolution behavior shows itself as a more complex topic, which involves the balance between different interactions beyond the hydrogen bonding, i.e., van der Waals and hydrophobic interactions (Medronho et al., 2012). Considering cellulose an amphiphilic molecule, its intrinsic structural anisotropy suggests that hydrophobic interactions are significant in the governance of cellulose solubility. Following this hypothesis, besides the capacity to effectively break the interchain hydrogen bonds in cellulose, a solvent needs to overcome those hydrophobic interactions that contribute to the biopolymer crystalline structure and low accessibility and solubility (Medronho et al., 2012; Medronho & Lindman, 2014b).

2.4 Regenerated Cellulose

Regenerated cellulose materials are classified as those that resulted from the conversion of native cellulose (cellulose I) into a soluble cellulosic system and its subsequent regeneration (cellulose II) to produce materials with a wide range of applications (Niaounakis, 2017), such as fibers (like viscose and lyocell) (Felgueiras et al., 2021), films (Liu et al., 2020), hydrogels (Huang & Wang, 2022), aerogels (Wan et al., 2019), and composites (Sharma et al., 2019).

2.4.1. Lyocell Process

The first studies on cellulose dissolution in tertiary amine oxides are dated from 1939 but only 30 years later Eastman Kodak Company patented the solvent system based on cyclic amine oxides, specifically N-methylmorpholine N-oxide (NMMO) (Figure 2.10) (Fink et al., 2001; Graenacher & Sallmann, 1939; Johnson, 1969; Zhang et al., 2018). The first industrial production of regenerated cellulose using NMMO as a solvent occurred in 1982, and later developed as the known environmentally friendly technology "lyocell". Since 2004, Lenzing Group is the leader of lyocell fiber-making technology under the brand Tencel™ (Ciechańska et al., 2009; A. J. Sayyed et al., 2019; S. Zhang et al., 2018). In comparison to other man-made fibers like Viscose® and Modal®, Tencel™ Lyocell represents a lower environmental impact, particularly in terms of energy, water, and chemical consumption, green-house gases emission (CO_2 and SO_2) and ecotoxicity (Shen & Patel, 2010).

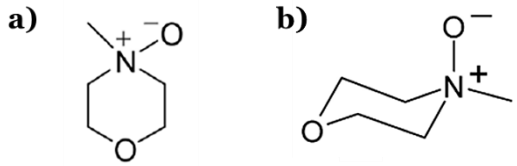

Figure 2.10. NMMO chemical structure in a) front view, and b) lower energy chair conformation (Rosenau et al., 2002, 2003).

The manufacturing process is summarized in five main steps (Figure 2.11) (Fink et al., 2001; Rosenau et al., 2001; Zhang et al., 2018):

1. Dissolution: formation of a NMMO/H2O/cellulose slurry and further dissolution to form a high-viscosity dope with a typical composition of 14% cellulose, 10% water, and 76% NMMO. The process occurs in temperatures between 80-130°C and under vacuum conditions for water removal;

2. Filtration: foreign and insoluble compounds removal;
3. Spinning: extrusion of the dope through an air gap into a coagulation bath (cellulose regeneration);
4. Washing: the lyocell fibers are washed, and the NMMO is recovered and recycled;
5. Finishing: drying and post-treatment of the fibers.

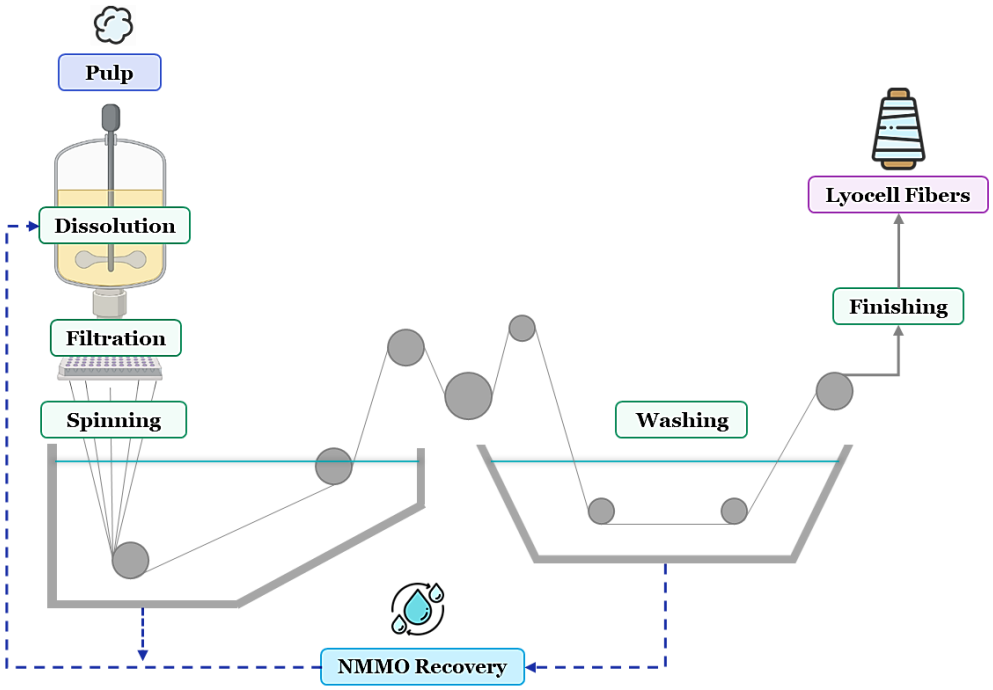

Figure 2.11. Lyocell manufacturing process (Adapted from Fink et al., 2001; Rosenau et al., 2001; Zhang et al., 2018).

Lyocell fibers exhibit excellent mechanical properties, high tensile strength, high tenacity, and lower elongation, especially when compared to viscose. The wearing comfort, similar to natural fibers such as cotton, is given by the high degree of orientation of the fibrils, which confers high elastic modulus and fibrillation capability to the filament (Ciechańska et al., 2009; Haule et al., 2016; Ingildeev et al., 2013). Those properties increase the range of applications for lyocell fibers in textiles, consumer goods, and industrial products (Zhang et al., 2018).

2.4.2. The system NMMO/Water/Cellulose

Lyocell is characterized as a direct cellulose dissolution process in an organic and aprotic solvent (NMMO), without the formation of derivative compounds (Ingildeev et al., 2013; Jiang et al., 2020; A. J. Sayyed et al., 2019). Cellulose swelling is a critical step for the lyocell process once it

allows the solvent to penetrate the polymer crystalline structure and swell the pulp fibers (Bruel et al., 2019; Fink et al., 2001). The slurry formed in the swelling step of cellulose dissolution in NMMO is indicated in the ternary phase diagram of the NMMO/water/cellulose system described in Figure 2.12. The water is extracted from the slurry at high temperature and reduced pressure until the dissolution region indicated, forming the dope with around 13-15% of water. The homogeneous concentrated cellulose solution passes through a coagulation bath, where the cellulose is extracted from the NMMO/water solvent system during the spinning and dried to result in the final product: the lyocell fiber (Fink et al., 2001; Jadhav et al., 2021). The NMMO is then recovered in a system consisting of two purification steps (air flotation and ion exchange), and one concentration step, namely the evaporation (Guo et al., 2021).

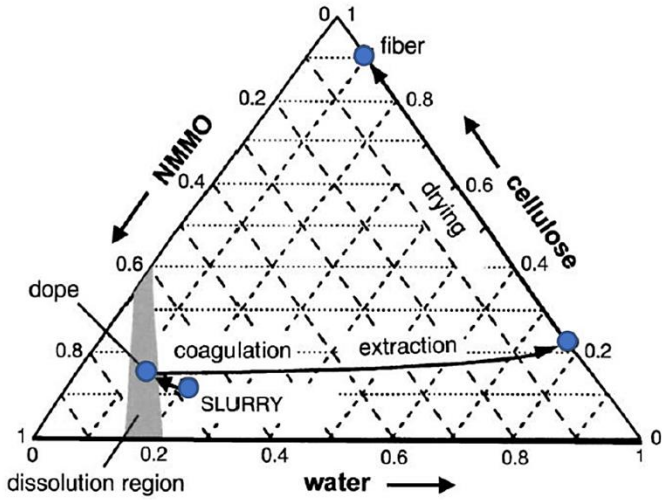

Figure 2.12. Phase diagram of system NMMO/H_2O/cellulose (Adapted from Fink et al., 2001).

The mechanism proposed for dissolution (Figure 2.13) involves the cleavage of cellulose intermolecular hydrogen bonds and the formation of stronger H-bonds between the active and high-polar N-O group from NMMO and the hydroxyl groups in the equatorial position of cellulose (Bruel et al., 2019; Medronho & Lindman, 2014b; Rosenau et al., 2001; Sayyed et al., 2019).

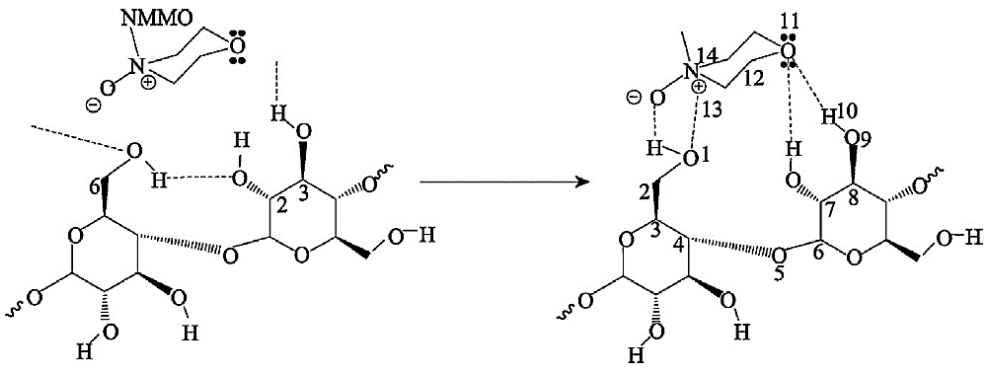

Figure 2.13. Mechanism of cellulose dissolution in the solvent system NMMO/H_2O (Jiang et al., 2020).

NMMO is a biodegradable and non-toxic solvent that has a recovery rate greater than 99% (Guo et al., 2021; Jiang et al., 2020). Nevertheless, the solvent has some disadvantages concerning degradation/decomposition reactions above 100°C, especially in the presence of heavy metals, which requires the use of stabilizers such as propyl gallate to avoid solvent degradation, depletion on NMMO recyclability, pulp degradation, i.e. degree of polymerization (DP) loss, among other effects described in summary in the Figure 2.14 (Ingildeev et al., 2013; Rosenau et al., 2001, 2002).

The degradation of NMMO by homolytic (formation of a radical) or heterolytic (non-radical) processes is thermally induced and catalyzed by transition metals or reducing agents. The cleavage of the N-O bond induces a cascade of side reactions by the formation of aminyl radical and other intermediates that causes solvent and cellulose degradation. In general, transition metals affect the stability of NMMO by acting as reductant agents in the first step of the degradation radical chain reactions. Iron and Copper are the main metals studied in the chemistry of the lyocell process since they represent the main influence on NMMO recovery rate depletion. Their presence in pulp, even in small concentrations, can decrease the temperature of the decomposition reactions and potentialize the degradation of cellulose under elevated temperatures (Rosenau et al., 2001).

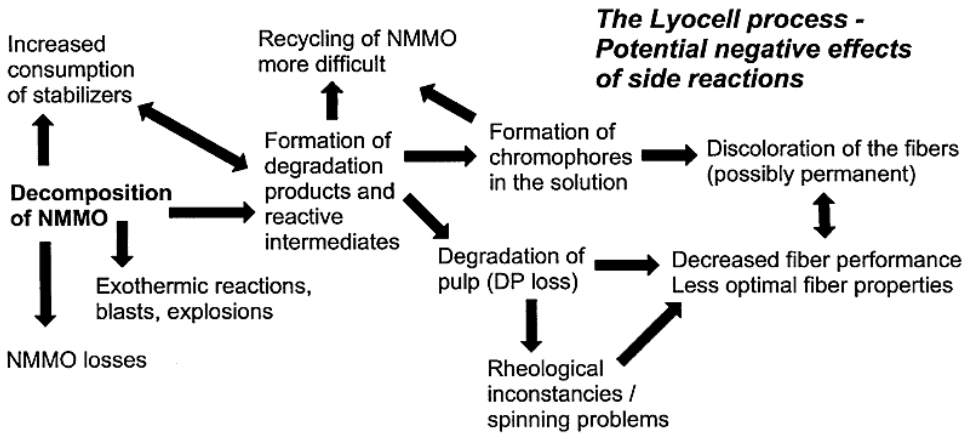

Figure 2.14. Potential negative effects of side reactions and byproducts formation in the lyocell system (Rosenau et al., 2001).

Chapter 3: Materials and Methods

3.1. Materials

3.1.1. Dissolving Wood Pulps (DWP)

Eucalyptus globulus wood chips (3-4mm of thickness) provided by Biotek (Empresa de Celulose do Tejo SA) were treated in different prehydrolysis kraft conditions, in a flow-through (FTR) and batch reaction systems, as described in section 3.2.1. Pulping Treatments.

A sample of commercial dissolving wood pulp was obtained in the market and used as a reference for comparison of properties with the dissolving pulps produced in the studies shown in this thesis.

3.1.2. Recycled Paper Pulp (RPP)

The recycled paper pulp was provided by an industrial partner (Papeleira Coreboard SA) and washed in a pulp washer machine for contaminants removals, such as plastics, inorganic salts, pigmented fibers, and foreign materials. This initial sample was named "RPP Original", with a Kappa number of 49.9. Thereafter, the washed material was submitted to PHK pulping treatments in different conditions, as part of an extensive study to ensure pulp properties that met the requirements for a high-quality dissolving pulp and improve pulp reactivity for textile applications such as the lyocell process.

3.1.3. Chemicals

Methanol (PA), sodium hydroxide (PA), and sulfuric acid (95-97%) were provided by LabChem; acetic acid (glacial), potassium iodide (99.5%), and sodium sulfide trihydrate (61%) were provided by VWR Chemicals; ethylenediamine (>98%), ferrous ammonium sulfate (FAS) (≥99%), lithium chloride (≥99%), potassium dichromate (99.9%), potassium permanganate (≥99%), and sodium thiosulfate (≥99.5%) were provided by Merck; cupri-ethylenediamine (CED) (1M) was provided by Scharlau; carbon disulfide (≥99%), dimethylacetamide (DMAc) (HPLC grade, ≥98%), dimethyl sulfoxide (DMSO) (≥99.9%), EDTA (≥99%), N-methyl-morpholine-N-oxide (NMMO) (50% v/v), and propyl gallate (≥98%) were provided by Sigma-Aldrich.

The reagents were used as received, or otherwise used to prepare solutions following the requirements of the standard methods adopted.

3.2. Methods

The methods applied for the studies are divided into three different sections directly correlated to the objectives of this project: Pulping Treatments; Pulp Characterization; and Dissolution Analysis.

3.2.1. Pulping Treatments

Figure 3.1 shows a schematic summary of the chemical pulping treatments applied in a batch reactor, and the chemical concepts involved in each step, i.e., hemicellulose removal in the pre-hydrolysis and delignification during the kraft cooking.

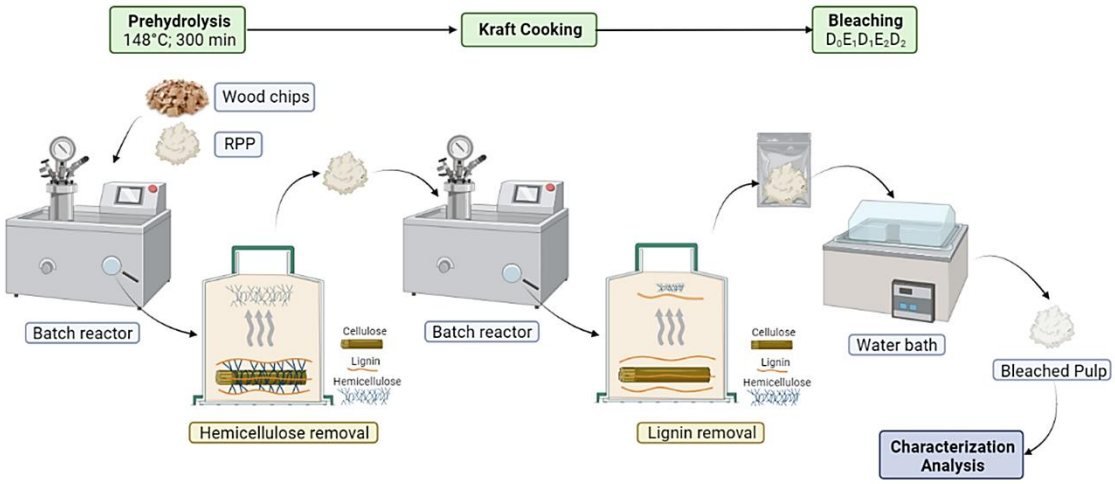

Figure 3.1. Schematic representation of pulping treatments applied. Developed at BioRender© platform.

3.2.1.1. Prehydrolysis

Batch hydrolysis was conducted in steel reactors with a 150 mL total volume attached to a mechanical rotating shaft, enabling the vessel to emerge in an oil bath with temperature control. This system allows the slow increase in temperature to facilitate the impregnation of the wood chips, resulting in uniform treatment.

The wood chip samples were impregnated overnight with distilled water at room temperature to achieve a more uniform liquor diffusion during the hydrolysis. After that, 20g (oven-dry base) was added to each reactor with an L/W ratio of 5:1 (w/w), the liquid phase of distilled water. A heating ramp of 90 minutes was set until it reached the final temperature of 148°C. The treatment

continued for 210 minutes (148ºC), after which the reactor was cooled in flowing water to stop the reaction. The final pH of the resulting liquor was about 3.5 due to acetic and formic acid production during the treatment.

For recycled paper pulps, the auto-hydrolysis proceeded by adding 8,3g of pulp (oven-dry base) in the steel reactor with an L/W ratio of 15:1 (w/w). The hydrolysis conditions in terms of time and temperature applied were the same used for wood chips samples: 148ºC for 300min as the total reaction time.

The flow-through (FTR) reactor (Figure 3.2) comprises a more complex system, where a membrane pump is used to ensure the optimum flow rate of 25 mL/min of the aqueous solution of acetic acid (pH 3.5), which aims to mimic the reaction medium in a batch system. A metal coil and the reactor immersion in a thermostatic oil bath ensure the solution and the reactor temperature maintenance. In the FTR reaction system, 40g of wood chips (oven-dry base) were added to the reactor, and the same time/temperature profile of the batch system was applied (148ºC/300min).

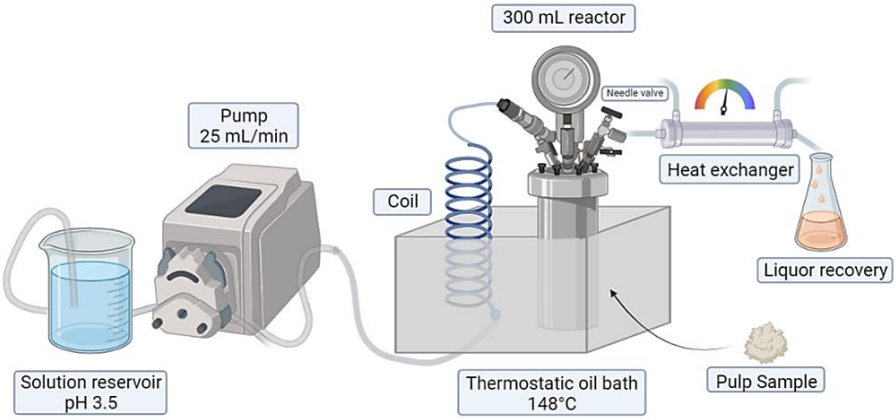

Figure 3.2. Schematic diagram of the flow-through reactor. Developed at BioRender© platform (Adapted from Cunha & Simões, 2023).

3.2.1.2. Kraft Cooking

The kraft cooking occurred in the same 150 mL batch reactor used for pre-hydrolysis treatments of recycled paper pulp and wood pulp batch samples, as shown in Figure 3.2. Table 3.1 summarizes the pulping conditions for each sample. Wood pulp samples shared the same cooking conditions, while an extensive study (shown in detail in the next section) resulted in the improved

kraft cooking parameters expressed for recycled paper pulp. Figure 3.3 shows a sequence of photos of DWP, from the wood chips to bleached PHK pulp.

Table 3.1. Pulping treatments conditions of wood pulps and recycled paper samples.

Sample	Prehydrolysis	Kraft	Bleaching
DWP FTR	Acid-hydrolysis (pH~3.5); 148 °C; 300 min	L:S= 5:1; 24% AA; 30% sulfidity; 148 °C; 270 min H-factor: ~400	$D_0E_1D_1E_2D_2$
DWP Batch	Auto-hydrolysis; 148 °C; 300 min		
Recycled Paper Pulp	Auto-hydrolysis; 148 °C; 300 min	L:S= 15:1; 24% AA; 30% sulfidity; 170 °C; 210 min H-factor: ~2000	

L:S = Liquid:Solid proportion

The white liquor was prepared with NaOH and Na_2S as active chemicals in a concentration to reach 24% of active alkali (AA) charge, 20.4% of effective alkali (EA), and a sulfidity of 30%. The active alkali comprises the active ingredients in the pulping process, i.e., NaOH + Na_2S (both reported as NaOH), while EA considers compounds that will produce alkali under pulping conditions (EA= NaOH + ½ Na_2S, as NaOH). The sulfidity of the liquor is the ratio of Na_2S in the AA, expressed as a percent. The rate of delignification is directly related to this parameter, the higher the sulfidity, the higher the nucleophilic action of the hydrosulfide anion (HS^-) and the cleavage of lignin β-arylether linkages and methoxy groups (Bajpai, 2018b).

3.2.1.3. Bleaching

The same ECF bleaching treatment was applied to the samples, considering their initial Kappa number. The bleaching sequence applied, $D_0E_1D_1E_2D_2$, consisted of an initial dioxide chlorine delignification (D_0) at 45°C for 30 minutes, followed by an alkali extraction with sodium hydroxide (E) at 70°C for 60 minutes and $D_1E_2D_2$ bleaching stages. The percentage of active chlorine in the D_0 step is given in terms of the pulp lignin content (Equation 3.1), and the charges of the remaining stages (D_n) are calculated as 75% of the previous charge (Equation 3.2). The charge of NaOH is given in terms of the active chlorine, expressed by Equation 3.3.

$$D_0 = 0.2 \times Kappa\ number \qquad Equation\ 3.1$$

$$D_n = D_{n-1} \times 0.75 \qquad Equation\ 3.2$$

$$E_n = D_{n-1} + 0.15 \qquad Equation\ 3.3$$

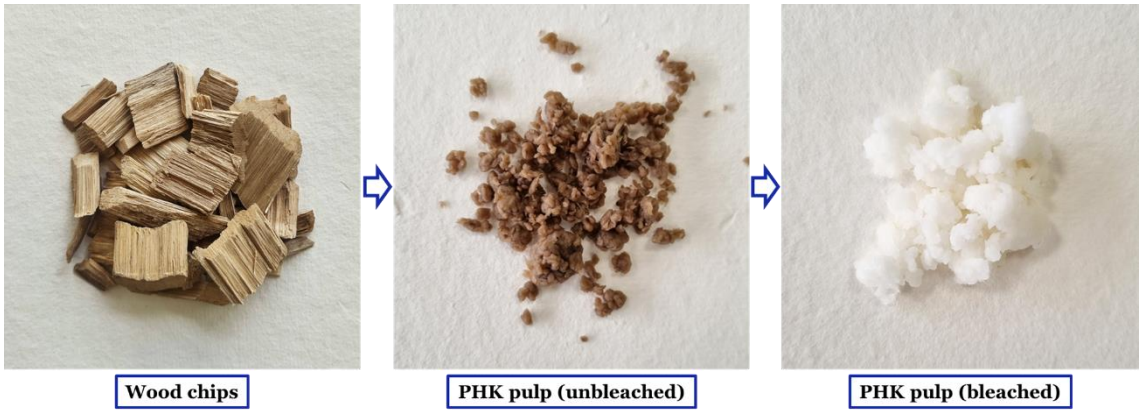

Figure 3.3. Material transformation sequence: from *Eucalyptus globulus* wood chips to bleached prehydrolyzed-kraft (PHK) pulp.

3.2.1.4. Optimization of recycled paper pulp treatments

The recycled paper pulp used for this study can be classified as an ordinary grade recovered paper, i.e., a mixture of various grades of paper and board, including newspapers and magazines, without a shortage of fiber content (Scott, 2011). Those composition variations cause a challenging raw material heterogeneity affecting cellulose recovery and dissolution to produce cellulose derivatives (Bajpai, 2014b).

An extensive study of the cooking conditions was developed to improve the pulp quality and its reactivity. The samples of recycled paper pulps (RPP) A1 and A2 were cooked considering the same H-factor, changing the active alkali to understand its effect on pulp delignification. Sample RPP B shows an extreme trial at H-factor around 3000 to identify the effects of a high delignification extent on pulp properties. Finally, RPP C_1, C_2, and C_3 show a study of pulp characteristics at the same H-factor and different cooking temperatures and times.

The specification of pulping process conditions applied (namely alkali charge, sulfidity, time, temperature, and H-factor), bleaching conditions, and Kappa number obtained are listed in Table 3.2. The selected sample for characterization analysis and further tests, C_3, is indicated. Figure 3.4 shows all the RPP samples produced for this study.

The original sample of recycled paper pulp showed an elevated ash content (>10%), which indicated the need for a metal ion removal treatment to improve the raw material's suitability for RCF processes. Initially, samples C_1 and C_3 were submitted to screening trials to identify the

treatment with higher efficacy. A chelation with EDTA 0.3% (oven-dry pulp base) showed a reduction of 31% of the ash content of sample C_3. Meanwhile, the acid washing with a solution of sulfuric acid pH~2.5 showed better performance by reducing over 46% of the ash content of the sample at the first washing cycle. A second step of acid washing was executed to improve the metal ion removal, resulting in a decrease of over 79% of ashes in C_3. From these preliminary trials and considering the environmental footprint of the process, the acid-washing method was selected for the purification treatment of the recycled paper pulp. The treatments conditions are described in detail in Table 3.3, and the acid method selected is highlighted.

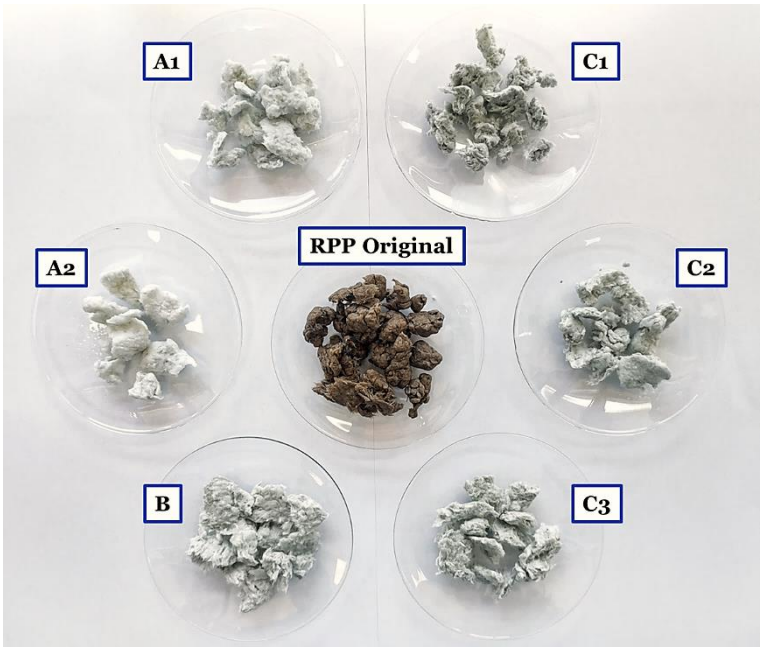

Figure 3.4. Recycled Paper Pulp (RPP) samples produced for the study of optimization of fiber reactivity by prehydrolysis-kraft cooking.

Table 3.2. Specification of Recycled Paper pulping conditions used for this study.

Sample	Prehydrolysis	Kraft	Bleaching	Kappa number
RPP Original	-	-	-	49.9
RPP A1	148 °C; 300 min	L:S= 15:1; 24% AA; 30% sulfidity; 148 °C; 270 min; H-factor: ~400	$D_0E_1D_1E_2D_2$	4.7
RPP A2		L:S= 15:1; 48% AA; 30% sulfidity; 148 °C; 270 min; H-factor: ~400		4.7
RPP B		L:S=15:1; 24% AA; 30% sulfidity; 170 °C; 270 min; H-factor: ~3000		2.5
RPP C1		L:S=15:1; 24% AA; 30% sulfidity; 160 °C; 375 min; H-factor: ~2000		1.8
RPP C2		L:S=15:1; 24% AA; 30% sulfidity; 165 °C; 270 min; H-factor: ~2000		1.9
RPP C3		L:S=15:1; 24% AA; 30% sulfidity; 170 °C; 210 min; H-factor: ~2000		1.3

L:S = Liquid:Solid proportion

Table 3.3. Purification treatments applied for metal ion removal from recycled paper pulp.

Treatment	Agent	Conditions	Performance
Chelation	EDTA 0.3% (oven-dry pulp base)	Pulp consistency: 2% Temperature: 70°C Retention time: 1h	31% of reduction in ash content
Acid Washing*	Sulfuric acid pH~2.5		79% of reduction in ash content

*Performed two times in sequence to improve the metal ion removal from pulp

3.2.2. Pulp Characterization

The experimental analysis performed for pulps characterization are listed in the scheme of Figure 3.5. This section aims to identify the critical pulp properties that may affect fiber dissolution and its suitability for lyocell process application.

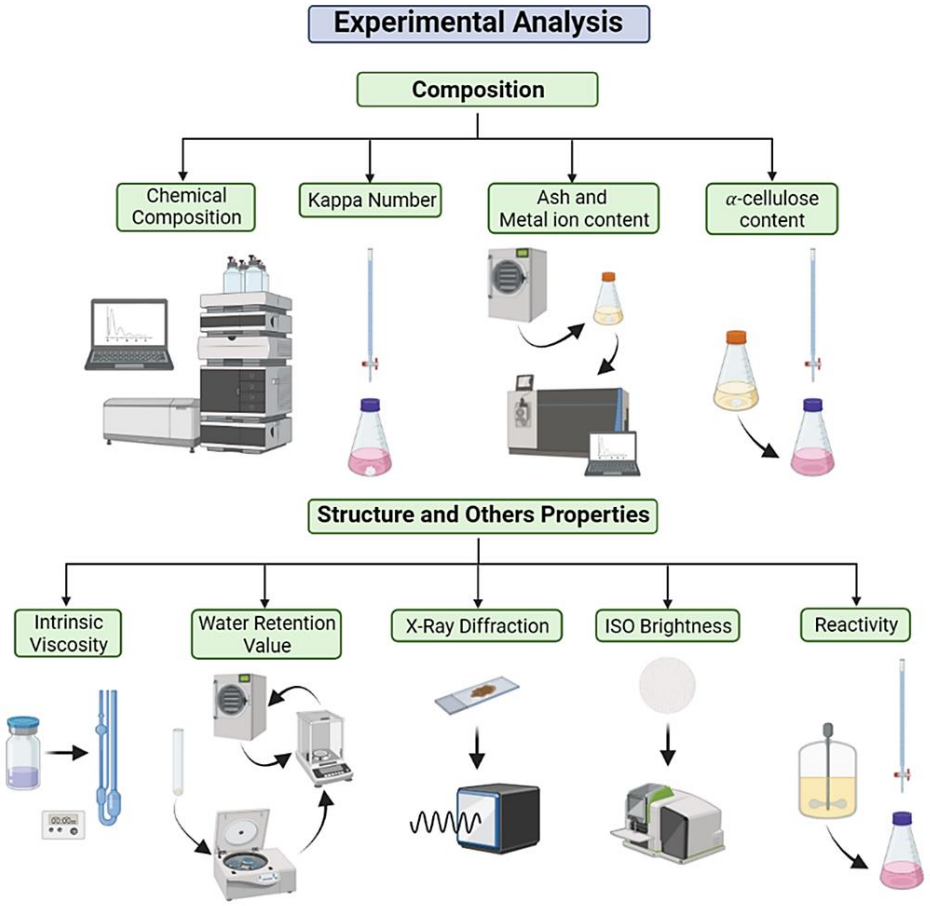

Figure 3.5. Schematic diagram of the characterization analysis performed. Developed at BioRender© platform.

3.2.2.1. Chemical Composition

Sample hydrolysis followed TAPPI standard method T222 om-02: "Acid-insoluble lignin in wood and pulp", by a two-step acid hydrolysis with 72% and 4% sulfuric acid. The first step consists of the pulp dissolution in sulphuric acid at 72% at room temperature in an ultrasound bath. The last hydrolysis was completed by autoclaving the sample at 121 ºC for 60 minutes in a Tuttnauer™ autoclave (2540 mL capacity), following the standard method NREL/TP-510: "Determination of Structural Carbohydrates and Lignin in Biomass". The acid-insoluble material (lignin and contaminants) was determined gravimetrically after filtering the hydrolyzate through a filter crucible (DURAN, filter crucible, 50 mL, porosity 2).

Subsequently, the supernatant samples were filtered (0,45 µm Nylon syringe filter by Kinesis®) and analyzed for monosaccharides, oligosaccharides, and degradation by-products with High-Pressure Liquid Chromatography (HPLC), using a refractive index (RI) detector (RefractoMax 520) and a photodiode array (Accela PDA detector (80 Hz) from Thermo Scientific™, EUA). The compounds were separated using a Rezex™ ROA-Organic Acid H+ (8%) column in an acid medium to identify the acids and the sugar monomer (0.005N H_2SO_4, 300 µL/min at 70 ºC). The compounds analyzed were quantified using calibration curves from purchased standards ranging from 0.1 to 3 g/L.

The hydrolysis of lignocellulosic biomass leads to a series of degradation products, which are the compounds identified in the chromatogram. Figure 3.6 brings a scheme indicating the main formation routes of those degradation products. The hydrolyzed cellulose product is glucose, while hemicellulose usually degrades to compounds such as pentoses (xylose and arabinose) and hexoses sugars (glucose, mannose, and galactose), and acetic acid. The furan aldehydes, 5-hydroxymethylfurfural (HMF), and furfural (F) are sub-products formed by the degradation of hexoses and pentoses, respectively. Sugar acids and aliphatic acids (such as formic and levulinic acids), and phenolic compounds are also formed from HMF and furfural, lignin, and other extractives (Andary et al., 2021; Jönsson et al., 2013). However, these by-products are not identified by the methodology developed in this work.

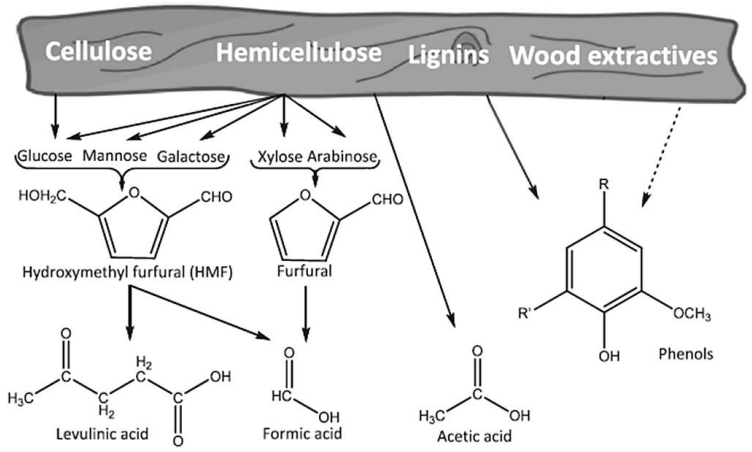

Figure 3.6. Scheme of lignocellulosic biomass degradation products by acid-catalyzed hydrolysis (Adapted from Jönsson et al., 2013).

3.2.2.2. Kappa Number

The determination of the Kappa number of the samples was obtained following the standard method ISO 302:2015: "Pulps — Determination of Kappa number". The Kappa number indicates the lignin content of the pulp based on the consumption of potassium permanganate, a strong oxidizing agent. In this study, the Kappa number was used to verify the effect of the pulping treatments (kraft cooking and bleaching) applied for pulp delignification.

In this method, 200mL of water is added to around 0.3g of sample (depending on the expected Kappa number for each pulp), then 25mL of H_2SO_4 2M and 25mL of $KMnO_4$ 0.02M are added and left under stirring for 10 min. Before the titration with sodium thiosulphate ($Na_2S_2O_3$) 0.2M, and 2g/L amide as an indicator, 10mL of 1M potassium iodide (KI) solution is added to the Erlenmeyer to stop the reaction. The exceeding potassium permanganate reacts with iodide (I^-) to iodine (I_2), titrated with sodium thiosulfate. The Kappa number (X) is calculated considering Equations 3.4 and 3.5.

$$V_1 = \frac{(V_2 - V_3)c}{0.02 \times 5} \qquad Equation\ 3.4$$

$$X = \frac{V_1 d}{m}[1 + 0.013(25 - t)] \qquad Equation\ 3.5$$

Where: V_1 is the volume (mL) of $KMnO_4$; V_2 is the volume (mL) of $Na_2S_2O_3$ consumed during the blank test; V_3 is the volume (mL) of $Na_2S_2O_3$ consumed during the sample test; c is the

concentration of $Na_2S_2O_3$ (mol/L); *d* is correction factor, expressed as a function of V_1; *m* is the sample mass (g); *t* is the current temperature during test.

3.2.2.3. Ash and Metal ion content

The ashes in the samples under study were determined according to the TAPPI standard method T 211 om-85: "Ash in wood and pulp". In the present procedure, the material is weighed (oven-dry basis) and allowed to ignite at 575±25°C for 3h, and the mass of the remaining ashes are determined after cooling in a desiccator. The percentage of ash content is calculated by the quotient of the final ash weight, the initial sample weight, and the final ash weight.

The metal ion content determination was performed by an external laboratory. Initially, samples were digested with nitric acid and hydrochloric acid and let stand overnight at room temperature. The digestions were submitted to a temperature program in a DigiPrep MS heating block (SCP Science, Canada), heating to 75°C during 5 minutes, increasing to 85°C for 10 minutes, and finally to 95°C for 20 minutes. Digestions were cooled to a temperature below 40°C, and the previous heating program was repeated. The digestion was diluted to 50 mL with ultrapure pure water. Sample digestions were analyzed by ICP-MS (Agilent 7700 ICP-MS equipped with an octopole reaction system (ORS) collision/reaction cell technology to minimize spectral interferences) using Germanium (^{72}Ge), Rhodium (^{103}Rh) and Iridium (^{193}Ir) as internal standards.

3.2.2.4. Alpha-cellulose content

Among the three classes of cellulose, alpha-cellulose consists of the non-degraded fraction of high molecular weight, with a higher degree of polymerization and stability than the β and γ fractions. The alpha-cellulose content in the samples under study was determined according to the TAPPI standard method T 203 om-88: "Alpha-, beta- and gamma-cellulose in pulp", described in detail in Figure 3.7.

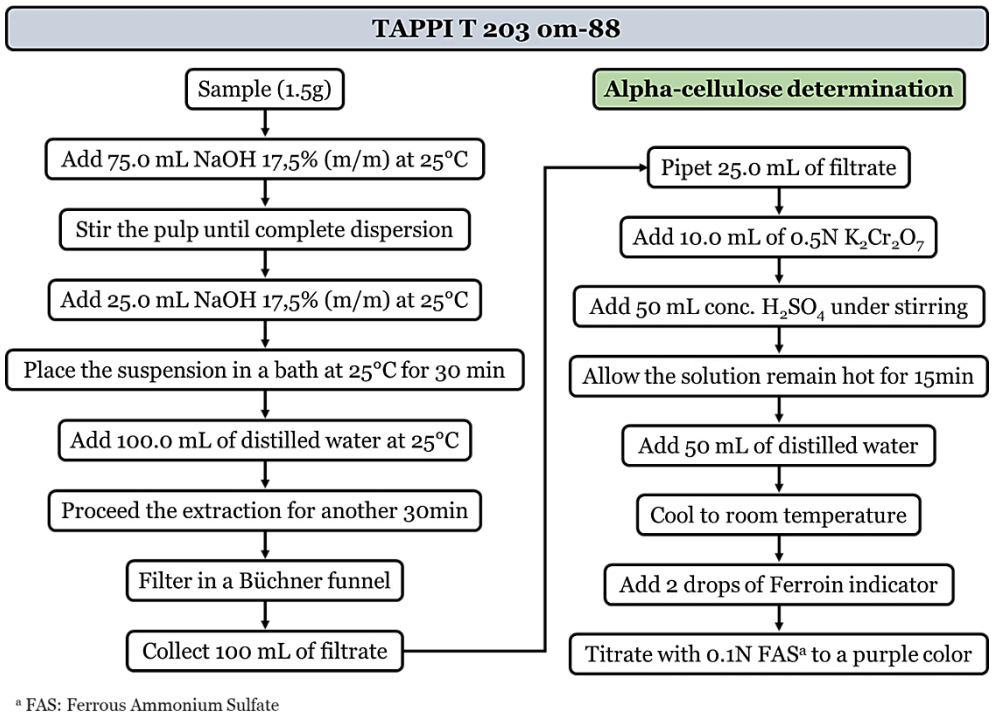

Figure 3.7. TAPPI T 203 om-88 standard method flowchart.

Equation 3.6, described in the preferred method, was used to calculate the percentage of alpha-cellulose content in pulps samples.

$$alpha - cellulose\ (\%) = 100 - \frac{6.85(V_2 - V_1) \times N \times 20}{A \times W} \qquad Equation\ 3.6$$

Where: V_1 is the volume (mL) of FAS consumed during titration; V_2 is the volume (mL) of blank titration; N is the FAS normality; A is the volume (mL) of filtrate; and W is the oven-dry weight of pulp (g).

3.2.2.5. Intrinsic Viscosity

Samples' intrinsic viscosity was determined by the standard method UNE 57039-1:1992: "Cellulose in dilute solutions. Determination of limiting viscosity number in cupri-ethylenediamine (CED) solution". This method consists of the prior disintegration of 0.05-0.1g of sample in 25mL of distilled water for 30min, then proceeding to a second step of fiber dissolution in 25mL of CED 1.00±0.02M, shaking the bottle for 30min (until complete dissolution) in an inert atmosphere. The solution bottle is placed in a water bath at 25°C to reach thermal equilibrium, then the solution of dissolved pulp in CED is inserted in a capillarity viscosimeter, and the efflux

time is determined. The relative viscosity (η_r) is obtained by Equation 3.7, which compares the efflux time of the sample solution (t) and the efflux time of pure solvent (t_o). The intrinsic viscosity, [η] ($cm^3.g^{-1}$), i.e., the limiting value of the viscosity number at infinite dilution is obtained by Equation 3.8, where *c* is the concentration of the pulp solution in CED ($g.cm^{-3}$), and the term (η.c) is given (fixed values indicated by the method) as a function of η_r.

$$\eta_r = \frac{t}{t_0} \qquad Equation\ 3.7$$

$$[\eta] = \frac{(\eta . c)}{c} \qquad Equation\ 3.8$$

Intrinsic viscosity is one of the typical properties used to characterize a dissolving pulp (Christoffersson, 2005) and its potential applications. The present method also shows Equation 3.9 as an estimation of the sample's average degree of polymerization (DP), another important property considered for dissolving pulps (Christoffersson, 2005; Evans & Wallis, 1989).

$$DP^{0.905} = 0.805 \times [\eta] \qquad Equation\ 3.9$$

The desired intrinsic viscosity for dissolving pulp may vary depending on the intended application. However, the average values between 400 and 600 mL/g are reported in the literature (Duan et al., 2015). For the lyocell process, an intrinsic viscosity between 280 and 350 mL/g and a DP from 650 to 750 have been described (Jiang et al., 2020; Mendes et al., 2021; Zhang et al., 2018).

3.2.2.6. Water Retention Value (WRV)

The water retention value is an empirical measure of the capacity of fibers to hold water, which may correlate to solvent diffusion through microfibrils and the fiber dissolution profile. The analysis followed the standard method ISO 23714:2014: "Pulps — Determination of water retention value (WRV)".

The pulp samples (around 0.9g oven-dry base) were let under distilled water overnight to allow complete swelling. The next step was to generate small pulp sheets in a sheet former Lorentzen & Wettre using a plastic mold. Each rolled sheet was inserted in an acrylic tube allowing excess water drainage, and the samples were submitted to centrifugation at 3000g of centrifugal force for 30 min in a Kubota KN-70 centrifuge (R=130mm). The sheets' mass was determined immediately after centrifugation (m_1) and after drying at 105±2°C for 24h (m_2). The WRV was determined by Equation 3.10.

$$WRV(\%) = \frac{(m_1 - m_2)}{m_2} \times 100 \qquad Equation\ 3.10$$

3.2.2.7. X-Ray Diffraction (XRD)

The characterization of cellulosic fiber materials by X-ray diffraction is a crucial tool for the understanding of its crystallographic structure, the determination of the proportion of crystalline and amorphous regions, and the dissolution behavior of natural cellulose fibers (Manimaran et al., 2019; Segal et al., 1959). The crystallinity index (CI), obtained by Equation 3.11, is given by the intensities of the amorphous pick (I_{AM}), 2θ=18°, and the pick of the crystalline plane 002 (I_{002}), where 2θ=22.4°, as showed in Figure 3.8 (Segal et al., 1959).

$$CI = \frac{(I_{002} - I_{AM})}{I_{002}} \times 100 \qquad Equation\ 3.11$$

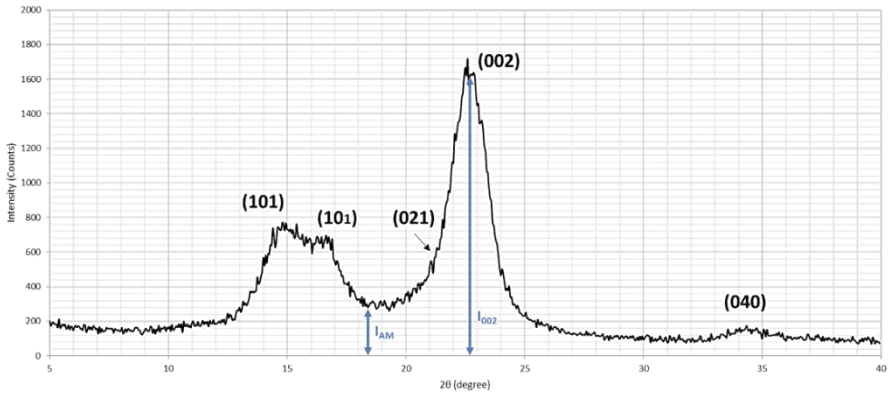

Figure 3.8. Indication of the picks used for crystallinity index determination (Source: original data from this study).

The samples were processed in a ball mill Retsch CryoMill for 2 min at a 25 (1/s) frequency. The analysis proceeded in a Rigaku DMAX III/C X-ray diffractometer. The intensity of Cu Kα radiation (wave-length of 0.1542 nm, 40 kV e 30 mA) was measured in a 2θ range between 5° and 40°, at a velocity of 2°/min.

3.2.2.8. ISO Brightness

The pulp sheets were prepared following the ISO 3688:2022: "Pulps — Preparation of laboratory sheets for the measurement of optical properties", where the amount of pulp to produce sheets of (225 ± 25) g/m² was disintegrated (30,000 revolutions), filtered in a Büchner funnel, pressed (0.3 MPa), and dried in an air-conditioning room.

The pulps brightness was determined according to the ISO standard method 2470-1:2016: "Paper, board, and pulps — Measurement of diffuse blue reflectance factor". The testing equipment used was a Color Touch 2 (Model ISO) by Technidyne, effective wavelength of 457 nm and standard illuminant D65.

3.2.2.9. Reactivity (Fock Test)

Dissolving pulp reactivity (also referred to as accessibility) is widely used as a quality parameter for assessing the processability of pulp by the reactivity of hydroxyl groups of the glucose unit in cellulose to carbon disulfide (Tian et al., 2013). The most popular test method, the Fock test, was described in 1959 (Fock, 1959), where the cellulose xanthation and subsequent regeneration are promoted to quantify the percentage of reacted cellulose. The method used in this study was adapted from Tian et al., 2013 and Köpcke, 2010 (Köpcke, 2010; Tian et al., 2013).

Around 0.50 g of pulp sample (oven-dry) was placed in a 50 mL reactor. 50 ml of 10% (w/w) NaOH solution was added, stirring for homogenization. Then, 1.3 ml of CS_2 was added, the reactor was sealed, and the mixture was stirred with a magnetic stirrer for 3h at 15°C. After the reaction time, distilled water was added to give the solution a total weight of 100 g. The mixture was shaken and transferred to a falcon tube and centrifuged at 4500 rpm (approx. 3400g) for 15 min to separate the cellulose xanthate from the undissolved cellulose. An aliquot of 10 mL of the supernatant was pipetted into a 100 mL Erlenmeyer and neutralized with 3 mL sulfuric acid of 20% (w/w). The solution shifts from yellow to transparent.

Degasification to remove carbon disulfide (CS_2) occurred overnight in a fume hood, where the solution was left to settle. For the next step, 20 mL sulfuric acid (H_2SO_4) (68% w/w) was added, and the solution and stirred with a magnetic stirrer for 1h. Thereafter, 10 mL of $K_2Cr_2O_7$ solution (1/6 M) was added, and the mixture was refluxed for 1h to oxidize the regenerated cellulose. The mixture was cooled to room temperature and diluted to 100 mL. 40 mL of this solution was transferred into a 250 mL Erlenmeyer, 5 mL of KI (10% w/w) was added, and the solution was titrated with sodium thiosulfate (0.1 N) using starch as the indicator. After the titration, the final

solution resulted in a pale blue color. The percentage of dissolved cellulose is given by Equation 3.12 below.

$$Dissolved\ Cellulose\ (\%) = \frac{\{v_1 c_1 - (v_2 c_2 \times {}^{100}/_{40}) \times {}^{1}/_{6}\} \times M \times {}^{1}/_{4} \times {}^{100}/_{10.4}}{m} \times 100 \qquad Equation\ 3.12$$

Where υ_1 is the volume of added (0.01 L); c_1 is the concentration of $K_2Cr_2O_7$ solution (1/6 M); υ_2 is the volume (L) of consumed $Na_2S_2O_3$; c_2 is the concentration of $Na_2S_2O_3$ solution (0.1 N); M is the molecule weight of glucose unit (162 g.mol^{-1}); m is the oven-dry weight of pulp tested (g); (100/40) is the dilution of the 40 mL sample to 100 mL; (1/6) corresponds to each dichromate ion that consumes six thiosulfate ions, (1/4) means each glucose unit consumes four dichromate ions, and (100/10.4) is the 10 mL aliquot (equal to 10.4 g) taken out from the 100 g viscose liquid.

3.2.3. Dissolution Analysis

The analysis in this section aims to study the accessibility and dissolution behavior of the fibers and establish a relation between pulp physico-chemical properties and their performance in different solvent systems (LiCl/DMAc and NMMO/H_2O).

3.2.3.1. Fiber activation by solvent exchange

The activation process is crucial for opening the crystalline structure of cellulose in order to increase solvent diffusion (Dupont, 2003). Two different activation methods were tested using the solvent exchange technique with three different solvents: N,N-dimethylacetamide (DMAc), dimethyl sulfoxide (DMSO), and ethylene diamine (EDA) for subsequent dissolution of the cellulose fibers in the system lithium chloride/N,N-dimethylacetamide (LiCl/DMAc). The methods performed contemplate adaptations of the processes developed by Dupont, 2003 (DMAc), Siller et al., 2014 (DMSO), and Ono & Isogai, 2021 (EDA). Figure 3.9 shows a flowchart of the processes applied: H2O→Methanol→DMAc, H2O→Methanol→DMSO, and EDA→Methanol→DMAc (Dupont, 2003; Ono & Isogai, 2021; Siller et al., 2014).

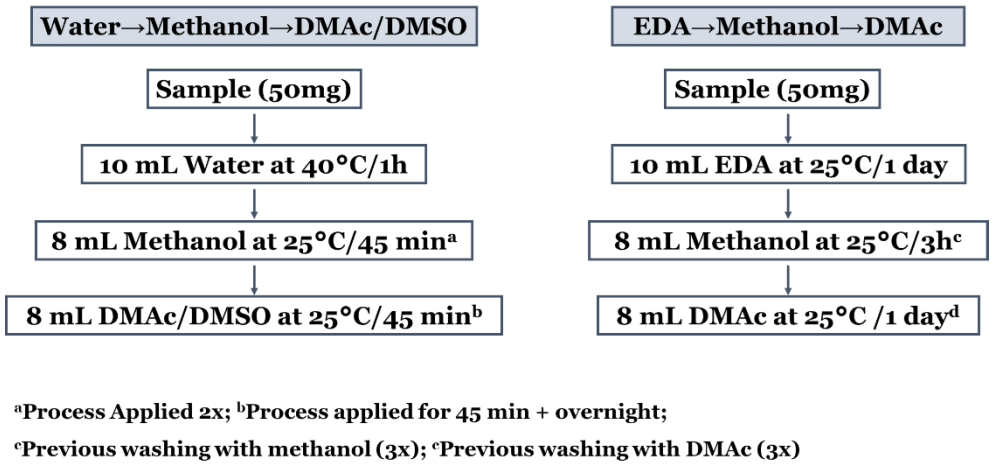

Figure 3.9. Schematic flowchart of solvent exchange methodologies. Left: description of the activation process for DMAc and DMSO; Right: process with EDA (Adapted from Dupont, 2003; Ono & Isogai, 2021; Siller et al., 2014).

The effect of the solvent exchange was evaluated by the WRV of untreated fibers compared with the WRV after the activation pretreatment. Besides that, microscopic analysis was carried out to examine the swelling behavior of fibers in different activation processes.

The images were generated in an optical Nikon Microscope, using high power objective lens (40x), and Leica MC190HD coupled camera. The fiber diameter was measured and analyzed with LAS-X Core software, version 4.13.

3.2.3.2. Pulp dissolution in LiCl/DMAc

The pretreated fibers by the solvent exchange were submitted to dissolution in the solvent system LiCl/DMAc. The lithium chloride was oven-dried and left to cool to room temperature in a desiccator before weighing. The LiCl (8% w/w) was dissolved in anhydrous N, N – dimethylacetamide at 40°C under magnetic stirring. Around 0.05g of activated fiber was dissolved in 5 mL of 8% LiCl/DMAc solution at 25°C for 15 hours. After that period, the temperature was reduced to 4°C. Following the study by Dupont, 2003, 48h is the dissolution time of cellulose in the referred solvent system and pulp consistency of 1% (Dupont, 2003). The dissolution extension was evaluated after the indicated 48h by optical microscopy.

3.2.3.3. Pulp dissolution in NMMO

The process of dissolving cellulose in NMMO by the evaporation method can be divided into two steps: swelling and dissolution. The slurry formation occurs in the first step, where the solvent (NMMO/H_2O) penetrates the cellulose supramolecular structure. Subsequently, water from the system cellulose-NMMO-H_2O is removed under vacuum application until reaching the proportions indicated in the dissolution zone (Figure 2.7 of section 2.5.1.1), where the mixture must have approximately 76% NMMO and 13% cellulose (Jadhav et al., 2021). The resulting dope has a clear brown appearance and contains around 13-15% water (Fink et al., 2001).

Initially, the original NMMO 50% (v/v) solution was concentrated by rotary evaporation at 65-70°C and 92 mbar, up to 65% NMMO (v/v). Then, 0.3% (m/v) of propyl gallate (PG) (≥98% assay) was added to avoid solvent degradation. The process conditions used in each of the stages of the dissolution by evaporation, adapted from the study carried out by Jadhav et al., 2021, are shown in Figure 3.10 (Jadhav et al., 2021). The dissolution system was developed as an alternative on a laboratory scale to the industrial equipment suggested in the literature. After the level of removed water at step 2 was reached, the vacuum was turned off, and the agitation was increased from 7,000 to around 15,000 rpm to promote greater shearing and mass transfer. The dissolution process was considered completed after being verified by optical microscopy in the samples taken during the reaction time.

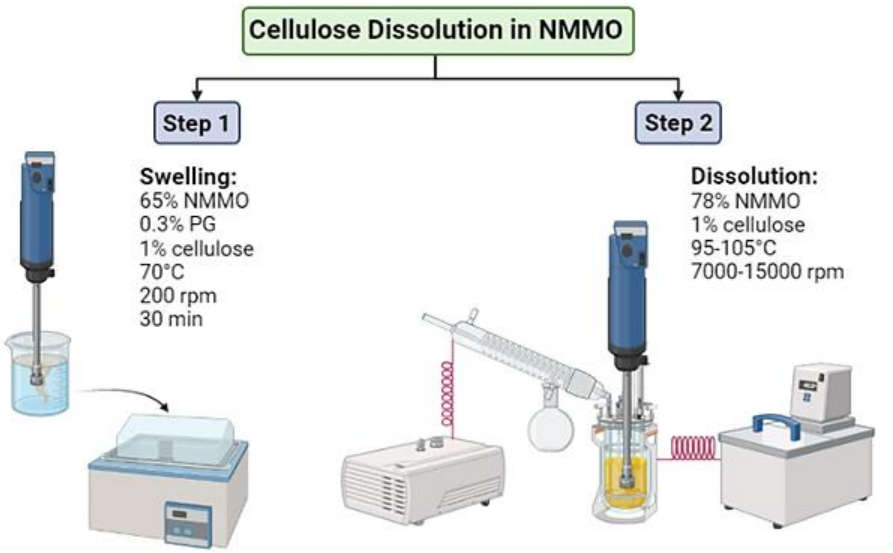

Figure 3.10. Schematic representation of pulp dissolution process in NMMO by the evaporation method. Developed at BioRender© platform.

As an additional step, a regeneration set-up (Figure 3.11) was developed to evaluate the effectiveness of the dissolution and the dope regeneration capability. The preliminary trials of lyocell fibers production were performed by adding the dope at 80°C in a warm steel syringe. The cellulose/NMMO/H_2O solution was pumped through a mesh until the regeneration water bath, where the fibers were pulled and stretched. The resulting RCFs were later analyzed by optical microscopy.

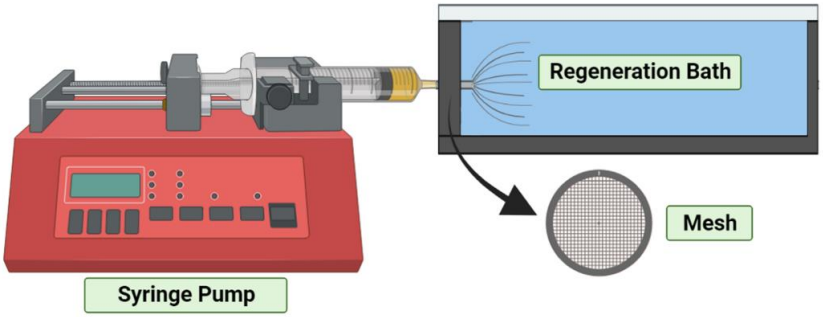

Figure 3.11. Schematic representation of regeneration process developed. Developed at BioRender© platform.

Chapter 4: Results and Discussion

4.1. Effects of pulping treatments

This work broadly assessed the effects on pulp properties caused by variations in pulping processes. Table 4.1 summarizes the characterization results obtained in the experimental analysis based on the dissolving pulp requirements listed in section 2.2.3. These results are discussed below, divided by source: wood chips and recycled paper.

The average values, their respective standard deviations, and additional metal ions results are described in Appendix A.

Table 4.1. General results of pulps' characterization analysis.

	DWP FTR	**DWP Batch**	**DWP Commercial**	**RPP Original**	**RPP C3**
Cellulose (%)	93.4	90.8	96.5	56.7	88.9
Hemicellulose (%)	3.8	4.9	2.9	7.8	4.9
Insoluble matter (%)	2.8	4.3	0.6	35.5	6.2
Kappa Number	1.2	2.0	< 1.0[c]	49.9	1.3
alpha-cellulose (%)	88.1	90.9	78.0	74.3	70.2
ISO Brightness	85.9	87.8	88.6	29.0	75.5
Viscosity (cm^3/g)	549	874	474	669	414
DP[a]	838	1400	713	1042	612
CI[b] (%)	51.4	53.7	16.7	67.1	41.9
Reactivity (%)	71.2	57.1	91.5	45.6	84.1
Ash content (%)	0.3	0.3	<0.1[c]	10.1	1.2
Iron content (ppm)	55	32	-	681	183

a. Degree of Polymerization
b. Crystallinity Index
c. Values below the precision indicated in the methods.

4.1.1. Dissolving Wood Pulps

Hardwood (*Eucalyptus globulus*) chips were subjected to two different prehydrolysis treatments, and the effect on pulp key properties, such as chemical composition, viscosity, crystallinity index, etc., was studied. The DWP samples (FTR and Batch) resulted from an extensive study (Cunha & Simões, 2022, 2023) from our research group, which identified the optimum flow rate and reaction time in the prehydrolysis flow-through system to recover high molecular weight xylooligosaccharides (XOs), promoting the valorization of the hydrolyzate byproducts, and implementing a biorefinery strategy to DWP production. The understanding of the effects of different prehydrolysis treatments on pulps dissolution performance is crucial to connect their application to the sustainable biorefinery concept.

The effect of an acid-prehydrolysis over pulps' chemical composition can be observed in Figure 4.1. The acid prehydrolysis carried out under the flow-through (FTR) method demonstrated better performance on hemicellulose removal than the corresponding treatment carried out under batch mode. The pulp produced by the FTR mode (DWP-FTR) showed a hemicellulose content around 22% lower than DWP-Batch. The value of 3.8% obtained for the DWP-FTR is closer to the reference DWP-Commercial pulp (2.9%) and of the range defined as required for a high-quality dissolving pulp (less than 4% of hemicellulose). Even so, the hemicellulose content in the DWP-Batch may not affect its dissolution performance in NMMO.

The prehydrolysis was demonstrated to be an essential process to improve pulps' cellulose content and to increase the delignification extent. As per Table 4.1, DWP-FTR showed a lower insoluble matter content and kappa number, despite the slightly lower ISO brightness. The decreasing of CI (Appendix D), albeit discrete, suggest that flow-through pre-treatment can be responsible for cellulose supramolecular structure disruption to some extent, which contributes to its accessibility during the kraft cooking, and the removal of lignin and other insoluble matters.

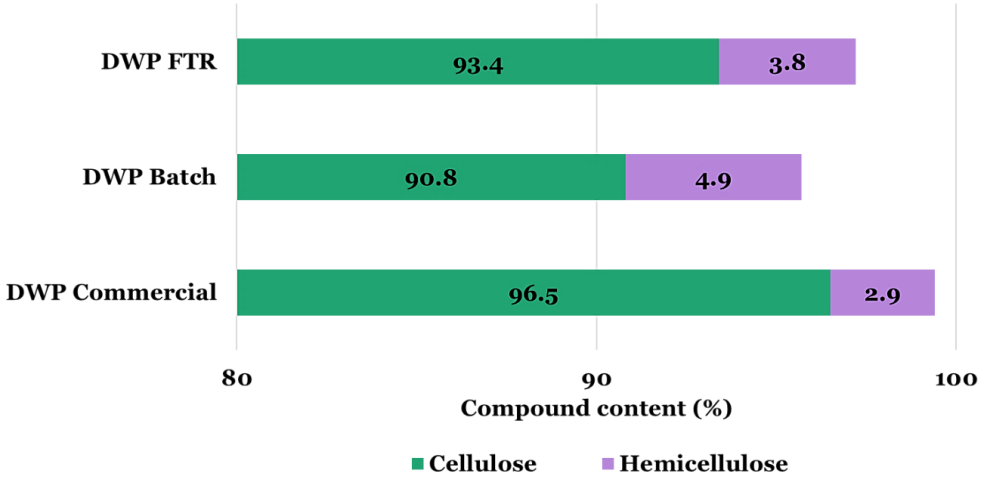

Figure 4.1. Chemical composition of dissolving wood pulps.

Comparing the results for the final pulps (Table 4.1) obtained with prehydrolysis treatments under FTR and batch modes, we can speculate the FTR prehydrolysis contributed to the penetration of the chemicals in the fiber structure due to a significantly lower intrinsic viscosity and an alpha-cellulose content slightly lower than the corresponding batch pulp. The reduction of the alpha-cellulose content caused by an acid-hydrolysis, when compared to autohydrolysis, indicates some level of degradation of cellulose since the alpha-cellulose represents the undegraded portion of cellulose of high molecular weight.

In summary, the intrinsic viscosity (Table 4.1) is, by far, the most evident difference between DWP-FTR and DWP-Batch, with a reduction of over 37% of the pulp's intrinsic viscosity and DP. To investigate the relationship between the intrinsic viscosity, or the corresponding cellulose degree of polymerization, and their aptitude to dissolving pulp, Figure 4.2 shows pulp DP and percentage of reacted cellulose, evaluated by the Fock test.

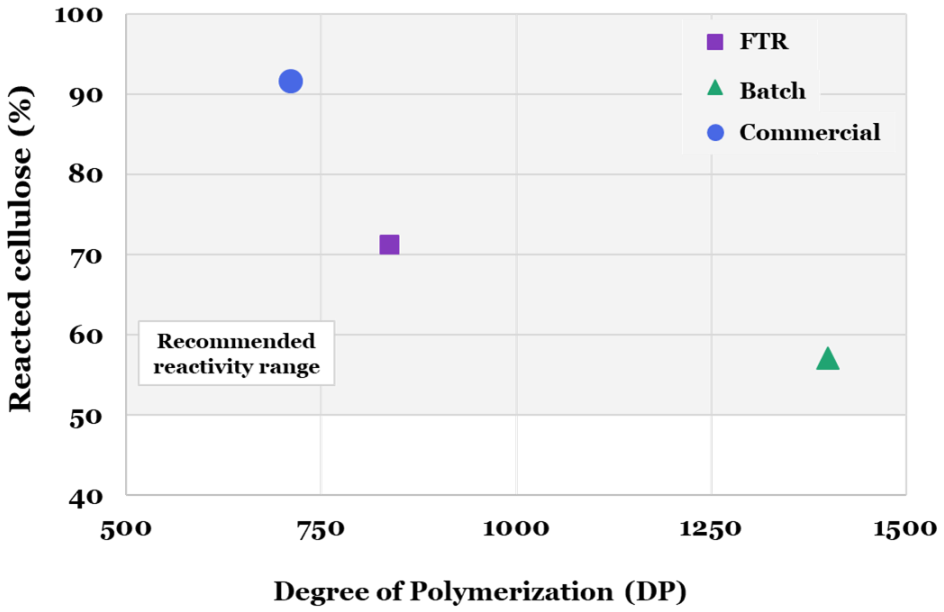

Figure 4.2. Correlation between the percentage of reacted cellulose (Fock reactivity) and pulps' DP for DWPs. The reactivity range recommended (>50%) for high-quality dissolving pulps is indicated in light grey.

The Batch pulp, with higher DP, exhibits lower reactivity, while pulps of lower DP (FTR and Commercial) show higher values of reacted cellulose. These results evidenced an adverse effect of pulp DP on cellulose reactivity, suggesting an inverse relation between them, i.e., the lower the viscosity, the higher the Fock reactivity. The extremely high reactivity of the DWP-Commercial should be highlighted and related to the low cellulose degree of polymerization and extremely low crystallinity index (16.7%).

4.1.2. Recycled Paper Pulp

In the paper industry, the physical properties of the materials are among the most valuable characteristics for paper production to ensure processability performance and product quality in terms of strength and resistance. Paper products can be produced in different pulp grades, from hardwood or softwood, chemical or mechanical pulps. The ordinary-grade recycled paper pulp used in this work contains a mixture of papers (such as office paper, newspapers, and magazines), and a large proportion of cardboard.

Cardboard, especially, requires a pulp with high quantities of hemicelluloses and lignin, which is indicated not only by the RPP visual aspect and ISO brightness but also by its initial kappa number

of 49.9 (representing a high lignin content) and acid-insoluble matter of 35.5%, accompanied by a significative content of hemicellulose (7.8%). At the end of the paper recycling cycle, these cellulose-based materials can be used to recover the cellulose. To do this, the removal of hemicelluloses, lignin, and other non-cellulose materials should be carried out. In this way, the recycled paper was subjected to prehydrolysis kraft cooking to remove hemicelluloses and lignin.

4.1.2.1. Effects of prehydrolysis

While the acid-prehydrolysis demonstrated the capacity to better remove hemicelluloses from wood, the application of this procedure would be expected. However, this pre-treatment caused a viscosity decrease of 37% comparing DWP-FTR and DWP-Batch, which was a relevant factor for RPP processing selection, considering the heterogeneity of the recovered paper and its evident degraded fibers.

An auto-hydrolysis was applied to the RPP using operating conditions close to those applied in the treatment of *E. globulus* wood chips (148ºC for 300 minutes in the batch reactor). Table 4.2 shows the effect of the prehydrolysis treatment on the process yield, the chemical composition (based on 100g of initial recycled paper pulp), and other properties of the recycled paper pulp.

Table 4.2. Effect of pulping treatments in RPP composition (based on 100g of initial RPP) and viscosity.

	Recycled Paper Pulp			
	Original	PH	C_3 unbleached	C_3 bleached
Global Yield (%)	100.0	88.1	65.5	59.4
Cellulose (%)	56.7	56.4	50.3	52.8
Hemicellulose (%)	7.8	8.0	2.7	2.9
Insoluble matter (%)	35.5	25.1	12.0	3.6
Intrinsic Viscosity (cm^3/g)	669	554	517	414

The yield along the different processing stages and the corresponding chemical composition were evaluated. The chemical composition was conjugated with the yield to give the evolution of the main components along the process chain reported in Table 4.2. The results show that the prehydrolyzed (PH) stage had a marginal effect on the cellulose and hemicellulose amounts. In

particular, the auto-hydrolysis was non-effective for hemicellulose removal, despite the reduction of the final pH of the auto-hydrolysis solution (3.6). The acidification of the medium could suggest the release of acetic and glucuronic acid from hemicelluloses; however, the amount of hemicellulose remained unchanged (the variation observed can be linked to the methodology applied). However, effective hemicellulose removal was evidenced in the next step of chemical pulping, the kraft cooking, which will be discussed later.

Although the PH stage showed a good performance in removing biomass impurities, decreasing from 35.5 g (based on 100 g of initial pulp) to 25.1 g (100g of initial pulp), a reduction of almost 30% of insoluble matter content (material not hydrolyzed in the procedure of sugar composition determination, involving successive treatment of sulfuric acid at 72% and 4% (m/m)).

Despite the low temperature of the treatment, a lower viscosity value is observed for RPP PH samples (Table 4.2) in contrast with the original raw material, suggesting some extent of cellulose hydrolysis, which did not affect the overall cellulose yield in PH pulp. The ideal viscosity for dissolving pulp varies with the process used; however, the average values are between 400 and 600 cm^3/g (Chen et al., 2016). The reduction obtained in the prehydrolysis positively affects attaining quality dissolving pulp. Still, the following process conditions must be managed to avoid fiber degradation and a pronounced reduction in pulp viscosity.

The compounds usually released during prehydrolysis are mainly sugars and can be reused in different applications in a biorefinery strategy (mainly for energy generation by incineration). Some studies use the sugar-rich hydrolyzate samples to produce bioethanol by fermentation (Erdei et al., 2012) or as a growth medium for yeasts (Lapeña et al., 2020). Recently, another field of valorization of the liquor byproducts has been widely discussed in the literature, involving the production of xylooligosaccharides with probiotic potential and their application in food products (Costa et al., 2019; Cunha & Simões, 2022; Henriques et al., 2021; Poletto et al., 2020). However, considering the presence of contaminants in the referred RPP, energy production can be suggested as a viable option for the hydrolyzate liquor, which enhances the potential of this process in a circular economy scenario.

4.1.2.2. Effects of kraft cooking and ECF bleaching

Recycled paper can have multiple grades and sources (softwood and hardwood, including chemical and mechanical pulps), and optimizing the cooking conditions is a must to obtain the desired results. For example, pine wood needs higher temperatures to reach the same delignification level as the *Eucalyptus globulus*. Based on the different sources of the recycled paper, the overall effects and delignification extent promoted by the kraft cooking process were assessed with distinct processing conditions, varying cooking temperatures, and alkali charges. The differences were evaluated, mainly by kappa number, viscosity, and chemical composition results. This study was divided into two phases: 1) A_1, A_2, and B samples; and 2) C_1, C_2, and C_3 samples.

The kappa number (KN) describes the amount of lignin that remains in the pulp after cooking; the higher the number, the more residual lignin there is. Dissolving pulp requires very low residual lignin values to achieve a good dissolving profile (Sixta, 2006). In this way, Figure 4.3.a shows the kappa number of the RPPs, unbleached and bleached, by the ECF bleaching sequence. Appendix B contains the results expressed in Figure 4.3 and their respective standard deviations.

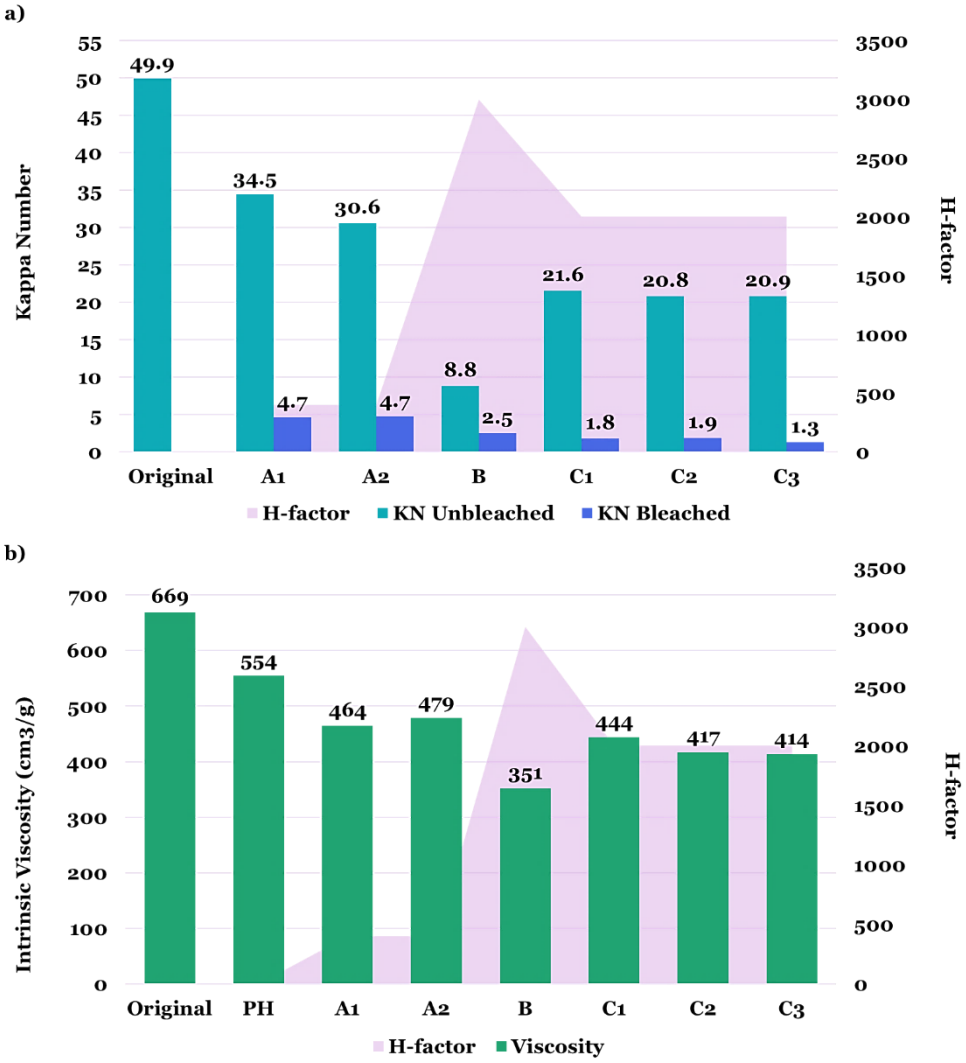

Figure 4.3. Effect of kraft cooking conditions (regarding the H-factor) and bleaching on RPPs properties a) kappa number; b) intrinsic viscosity.

Pulps of phase 1, at H-factor about 400 (A_1 and A_2), and H-factor ~3,000 (B) have significant differences in kappa number. The 2-fold increase of alkali charge at 148 ºC, from 24% (A_1) to 48% (A_2), only resulted in a slight reduction of KN, from 34.5 to 30.6. Moreover, after the cooking process, the black liquor of A_2 had a very high residual alkali (elevated pH), showing that the delignification was occurring mildly despite the quantities of NaOH and Na_2S. To further enhance delignification, a higher temperature (170ºC) was assessed (sample B), keeping the initial alkali charge of 24% and cooking time, which increased the H-factor to about 3,000. The unbleached pulp from this assay achieved an 8.8 kappa number, a decrease of 75% from the lower temperature assays.

This preliminary result proves the delignification kinetic model, which directly correlates the temperature with the lignin removal rate (Equation 2.1) and demonstrates the need for a higher H-factor to promote the delignification of recycled paper when compared with the production of dissolving pulp from *Eucalyptus globulus*, where a H-factor of approximately 400 and temperature of 148°C were enough to attain a good delignification extent. The conditions used in the kraft process for samples A_1, A_2, and B, particularly the temperature, significantly impact the conversion of recycled paper to a pulp with dissolving potential. Although, the delignification extent cannot be considered as a single parameter for dissolving pulp production and other parameters should be considered.

Figure 4.3.b shows the intrinsic viscosity obtained for RPPs. The sharp viscosity reduction for sample B indicates pulp degradation at an elevated H-factor (~3,000), which is not desired for the pretending applications. Viscosity is a crucial component of pulp properties since it is related to the average molecular weight of the cellulose molecules. Too high viscosity can and will affect the dissolution process by limiting the homogeneity of the process. Additionally, some problems can appear when regenerating the fiber due to dope viscosity, resulting in heterogeneous fibers with more fragilities. On the other hand, too low viscosity pulps show lower stabilization, affecting regenerated cellulose fibers' strength.

Taking into consideration the results of phase 1, the second part of this study was conducted in an intermediate H-factor of around 2,000, with cooking temperatures of 160°C (C_1), 165°C (C_2), and 170°C (C_3). Samples from phase 2 showed similar kappa numbers (Figure 4.3.a) after kraft cooking, which was expected following the delignification theory, and even lower values for bleached samples (compared with samples of phase 1). In matters of viscosity, the same behavior was observed (Figure 4.3.b). The slight difference between phase 2 samples was not considered relevant considering their standard deviations (Appendix B), and the methodology applied for intrinsic viscosity determination, which does not allow high levels of precision.

Afterward, all samples showed good potential for dissolving pulp regarding residual lignin content and viscosity (still in the recommended optimum range), demonstrating the effectiveness of the processing developed. RPP C_3 was selected as the reference sample for further analysis due to its properties (Appendix B), and lower residence time in kraft cooking, which is a relevant factor from an industrial perspective.

The effect of cooking process conditions should be analyzed under two different perspectives: (1) process and components yield; and (2) materials' chemical composition. The first one is related to the quantity, and the second one with the quality of the materials. Figure 4.4 shows the global

and components yield along the processing steps. The global yield of the several processing steps to obtain the bleached pulp from the initial recycled paper pulp was 59.4%. Regarding product quality, i.e., its chemical composition, the final pulp has 88.9% of cellulose, 4.9% of hemicellulose, and 6.2% of other compounds, including residual lignin.

Appendix C exposes the reference chromatograms for chemical composition analysis (HPLC) of the materials in the different processing stages.

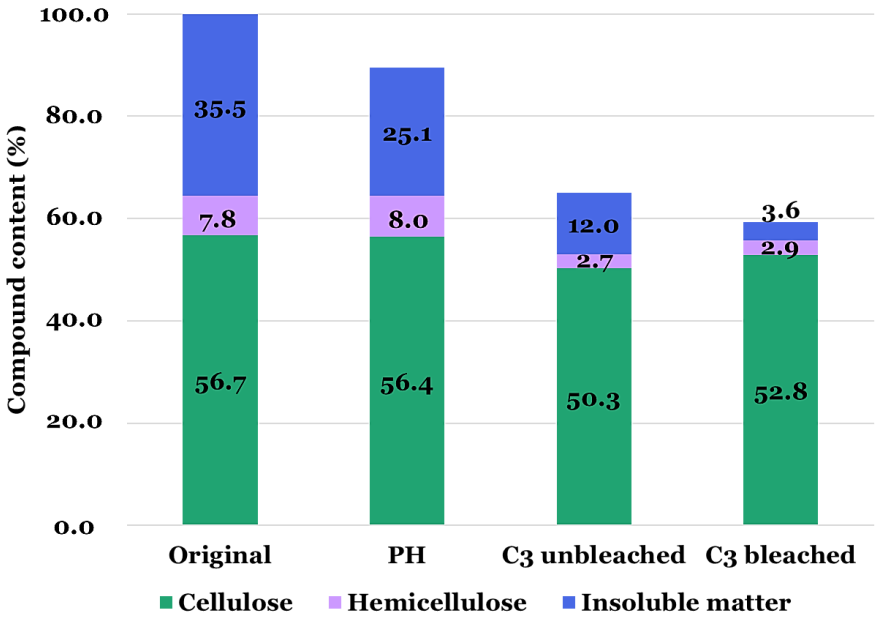

Figure 4.4. Yield of cellulose and hemicellulose content and insoluble matter throughout the pulping treatments applied to RPP.

Assessing the hemicellulose yield of the pulp, no apparent significant changes were observed during the prehydrolysis, as discussed earlier. However, after the kraft cooking, an expressive reduction was obtained from 8.0 g (100g of initial pulp) in RPP prehydrolyzed to 2.7 g (100g of initial pulp) in RPP C_3 unbleached. The overall decrease in hemicellulose yield corresponds to almost 63% of the initial amount (from 7.8% to 2.9%).

In terms of insoluble matters (lignin and impurities), kraft cooking achieved a reduction from 25.1 g to 12 g. The highest removal of insolubles (70%), represented in Figure 4.4 above, was obtained during the bleaching, where the residual lignin degraded in kraft cooking is finally taken from the pulp.

The reduction of hemicellulose and insolubles observed in this stage (kraft cooking) proves the theory exposed earlier. The prehydrolysis is responsible for opening the cellulose supramolecular structure, improving its accessibility to the white liquor, promoting fiber delignification, and removing residual hemicellulose from PH treatment.

An unfavorable outcome of this extensive process was the significant cellulose degradation, identified by cellulose yield losses (>10%), from 56.7 g (100g of initial pulp) to 52.8 g (100g of initial pulp). Notwithstanding, when comparing the chemical composition of the initial (original) RPP and the final product (C_3 bleached) (Figure 4.5), became evident the effectiveness of the pulping and bleaching processes applied to achieve a pulp composition with high amounts of cellulose and low content of hemicellulose and insolubles.

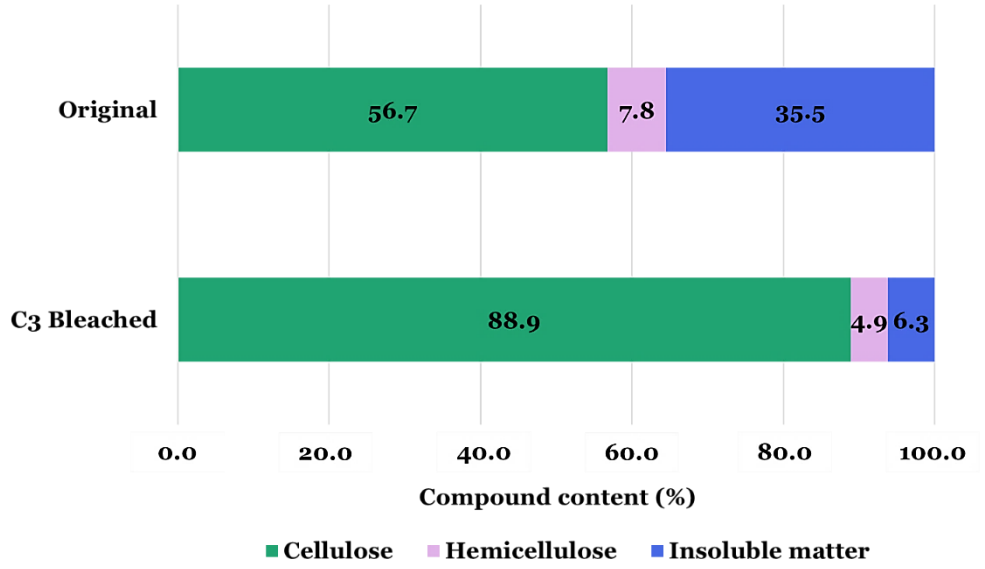

Figure 4.5. Chemical composition of RPPs (as the total amount of identified compounds).

The improvement in cellulose content (from 56.7% to 88.9%), as well as the reduction in the amount of hemicellulose (from 7.8% to 4.9%), can be correlated to the pronounced reduction of insoluble matters (>82%), i.e., lignin, impurities, and foreign materials, increasing the overall cellulose and hemicellulose content. The chemical composition reached after PHK and ECF bleaching meets the requirements for a high-quality dissolving pulp. Despite the hemicellulose content still above 4%, this amount may not affect pulp dissolution.

4.1.2.3. Improvements in RPP general properties

The pulping treatments' main objective was to produce a high-quality dissolving pulp from wastepaper, developing an innovative process to promote a new potential application. Besides the already mentioned improvements on pulp chemical composition and the effects over its viscosity, the PHK promoted considerable changes in pulp properties, considered key for dissolving pulps.

The detrimental effects of metal ions on the regenerated cellulose fibers process have been discussed earlier, which led to the importance of their removal from the pulp. Recycled materials, especially RPP, have high amounts of ashes and metal ions; therefore, a study of the better washing procedure to remove metal ions was performed. Figure 4.6 shows the ash content results for RPP-Original, and RPP C_1 and C_3, considering their initial values and the outcomes after the washing treatments with EDTA and acid washing (one and two stages in sequence).

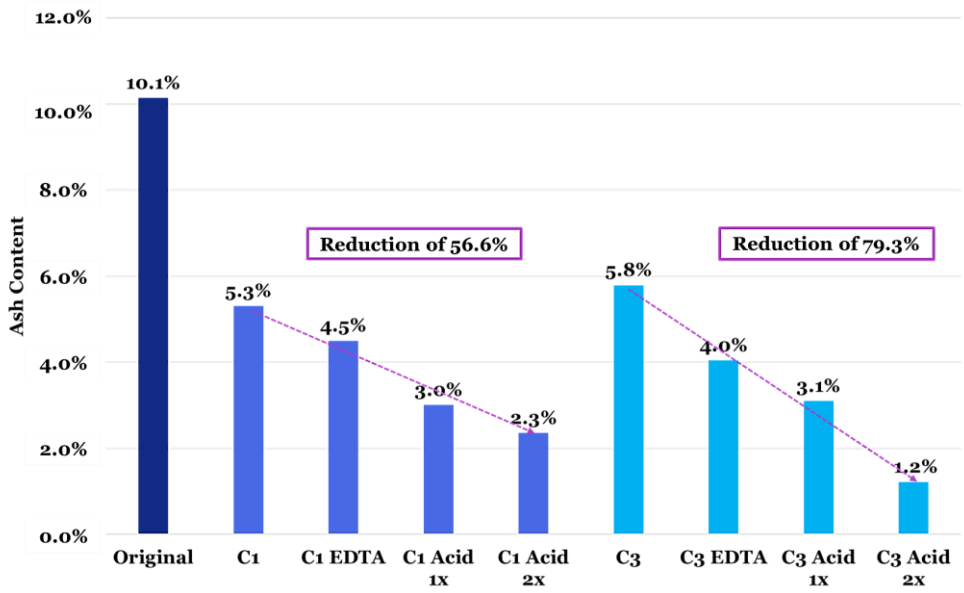

Figure 4.6. Ash content of RPPs, before and after washing treatments.

The PHK caused a reduction of more than 40% in pulps ash contents, considering the initial value of 10.1% of RPP-Original. The acid-washing showed a better removal extent when comparing the first washing cycle with EDTA and sulfuric acid (pH~2.5). Taking into consideration this preliminary result, and the environmental impact related to chelating agents usage, acid-washing was considered the adequate method, and a second cycle of washing was performed, reaching the 1.2% of ash content for the selected sample RPP-C_3.

The metal ions content, given in ppm, is presented in Table 4.3, where the iron content must be highlighted since it is the most critical metal ion for the lyocell process, compromising the NMMO recovery.

Table 4.3. Metal ions content of RPPs.

Analyte Symbol	Original	C_1	C_1 Acid 2x	C_3	C_3 Acid 2x
Na (ppm)	103	115	70	117	49
Mg (ppm)	781	674	128	606	163
Al (ppm)	4616	769	261	1909	441
P (ppm)	80	47	8	31	9
K (ppm)	170	47	22	92	22
Ca (ppm)	32385	19402	821	19603	2541
Mn (ppm)	22	20	4	15	4
Fe (ppm)	**681**	**536**	**193**	**414**	**183**
Co (ppm)	1	0	0	0	0
Ni (ppm)	3	4	3	3	2
Cu (ppm)	117	56	18	47	25
Sr (ppm)	39	22	1	21	3
Ba (ppm)	24	38	3	11	4
Pb (ppm)	9	8	3	8	4

The levels of metal ions are still quite above those recommended for dissolving pulps; however, considering the origin of the raw material, a significant improvement was achieved, especially regarding the most strongly bonded ions to pulp: Fe, Pb, and Cu, with a reduction of almost 74% of these metals content in RPP C_3. Nevertheless, additional treatment and optimization should be done before the industrial scale-up trial.

ISO brightness (Figure 4.7) is another important property of dissolving pulps. Although highly enhanced, from 29% to more than 75%, the pulp brightness is still far from the 90% indicated. An additional treatment to promote chromophores oxidation could be applied, but fiber degradation should be considered for the chosen method, avoiding an even more pronounced viscosity and alpha-cellulose content reduction.

Figure 4.7. Sheets of RPP-Original (left), and RPP-C_3 (right) used for ISO brightness analysis.

In terms of pulp accessibility, the depletion of the crystallinity index from 67.1% in the RPP-Original to 41.9% after the PHK (RPP-C_3) was unexpected since kraft pulping leads to preferential removal of the less ordered carbohydrates (Monrroy et al., 2012). The first stage of cooking alkaline degradation consists of hydrolysis of glycosidic bonds at reducing end groups of the cellulose chain. This cleavage generates sites for additional degradation reactions. Hemicelluloses are more extensively degraded due to their amorphous character and lower DP (De Souza et al., 2002; Gustavsson, 2006). Since the less ordered cellulose fractions are removed, an increase in the relative crystalline cellulose in the pulp is expected (Gümüskaya et al., 2003).

Some authors have reported an increase between 1-5% in crystallinity of *Eucalyptus globulus* kraft pulps in different cooking and hydrolysis conditions (Monrroy et al., 2012; Shevchenko et al., 2023). Otherwise, for *Pinus radiata*, a constant increase in the degree of crystallinity was observed as the kraft cooking proceeded (Evans et al., 1995). However, a reduction in kraft pulps CI has been presented before (De Souza et al., 2002; Gümüskaya et al., 2003), explained by a less-discussed cellulose degradation reaction.

Considering the cellulose elemental fibril structure, the crystalline regions are interrupted by non-crystalline amorphous regions, more easily accessed and degraded. A random cleavage may occur in the crystalline regions that present defects (kinks or folds), leading to more accessible chains, which can then be considered amorphous. This structural change caused by this degradation may increase the total amorphous character of the cellulose, decreasing its relative degree of crystallinity (De Souza et al., 2002). Considering this observed behavior and the expected high number of kinks in the recycled fibers due to the recycling process, some sort of crystallite

degradation due to cellulose chain defects can be presumed. The diffractograms are presented in Appendix D for comparison.

The improvement of pulp chemical composition, by reducing the insoluble compounds from 35.5% to 6.3%, alongside the enhanced accessibility (lower CI), and the reduction of pulp viscosity, resulted in an outstanding increase in pulp's reactivity when compared with the original recycled paper (Figure 4.8), or even with the dissolving wood pulps produced (FTR and batch).

The Fock reactivity of 84,1% obtained is far beyond the recommended of over 50% for dissolving pulps.

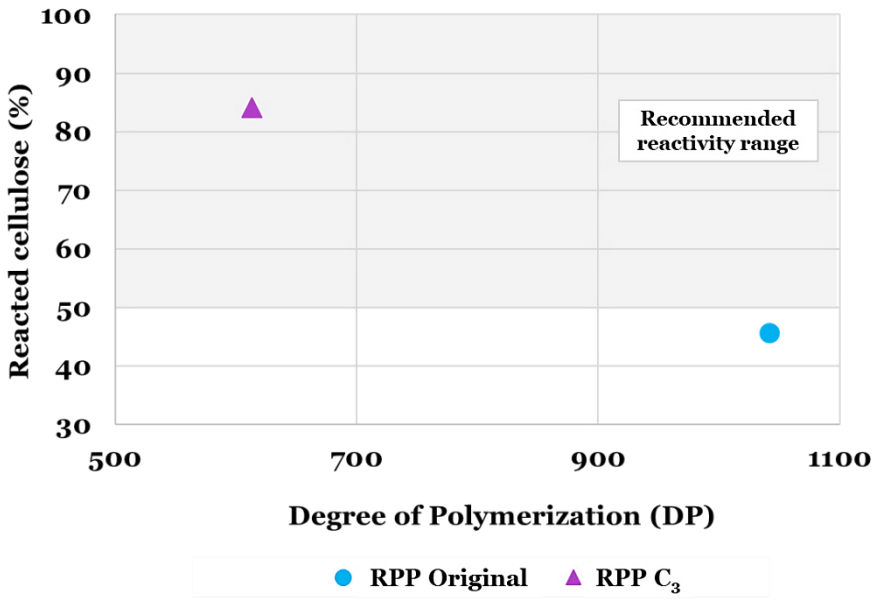

Figure 4.8. Relation between pulp DP and Fock reactivity, given by the percentage of reacted cellulose for RPPs. The reactivity range recommended (>50%) for high-quality dissolving pulps is indicated in light grey.

4.2. Effects of pulps properties on their dissolution behavior

4.2.1. Solvent Exchange Activation

The fibers swelling was promoted by a solvent exchange activation process as a preliminary step for samples' direct dissolution in 8%LiCl/DMAc. This solvent system was discovered as a non-derivatizing system in the '80s and was further used with commercial proposes for synthetic fibers production (Hearle et al., 2001; Sayyed et al., 2019). Nowadays, LiCl/DMAc is widely used for size exclusion chromatography (SEC), or gel permeation chromatography (GPC), for molar mass distribution (MMD) determination of lignocellulosic materials (Siller et al., 2014). The activation step is essential to cause the disruption of polymer supramolecular structure, improving the accessibility of solvent molecules to packed crystalline regions (Dupont, 2003; Fidale et al., 2008).

An extensive study was conducted to evaluate the extent of fiber structure deconstruction by solvent exchange and to understand solvent/cellulose interactions. The water retention value measurement, before and after the activation treatments, and optical microscopic observation were used. The WRV is an indication of the ability of a fiber to retain water, which can be related to its porosity and crystallinity and, in terms of this study, can indicate the effectiveness of an activation process. Figure 4.9 shows the results of WRV for DWPs (FTR and Batch) and RPP-Original pulps, before and after the solvent exchange treatment. The results will be discussed later.

Additionally, an evaluation of fiber swelling performance was conducted by the measurement of fibers' diameter by optical microscopy images. Figure 4.10 illustrates the method for DWP-FTR samples, and Figure 4.11 shows graphically the results, also expressed in Table 4.4.

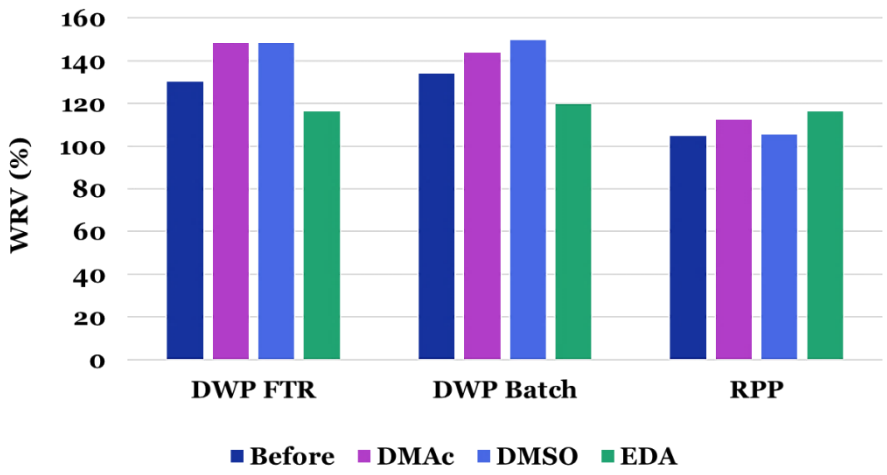

Figure 4.9. Water Retention Values for dissolving wood pulps samples (FTR and Batch), and RPP-Original, before and after the solvent exchange activation processes, indicated by DMAc: H2O→Methanol→DMAc; DMSO: H2O→Methanol→DMSO; and EDA: EDA→Methanol→DMAc.

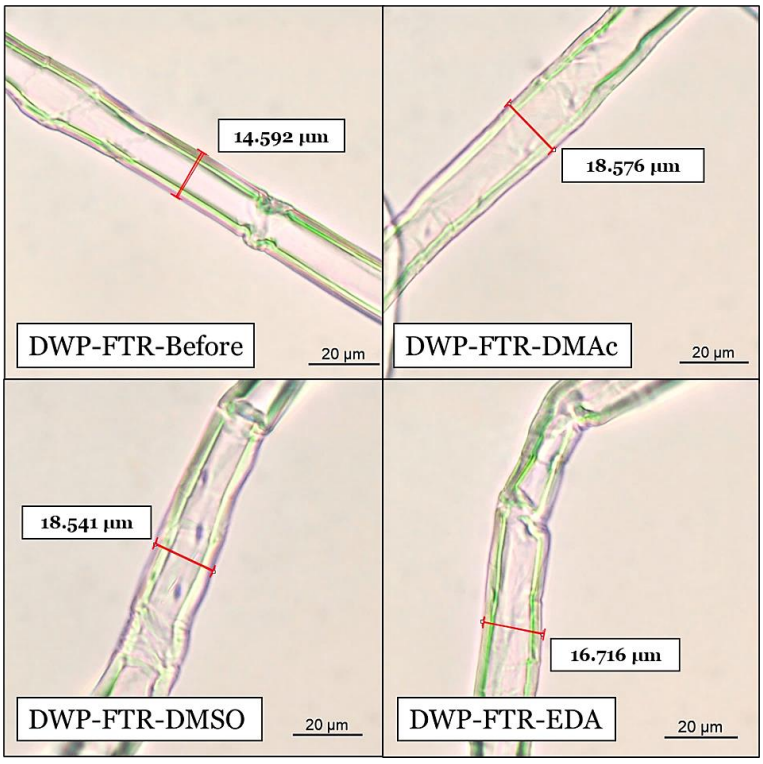

Figure 4.10. Demonstration of the methodology adopted to measure fiber diameters. Only DWP-FTR samples are represented for each activation process.

Table 4.4. Fiber diameter results before and after solvent exchange activation, and the percentage of increment obtained.

Sample			Before	DMAc	DMSO	EDA
DWP FTR	Fiber diameter (µm)	Average	14.390	18.542	18.434	16.221
		Std Dev	3.655	2.621	2.868	2.766
		Increment	-	29%	28%	13%
DWP Batch		Average	14.570	19.453	20.169	16.739
		Std Dev	2.646	3.066	2.230	2.258
		Increment	-	34%	38%	15%
RPP		Average	18.319	22.804	21.176	24.429
		Std Dev	5.260	6.287	5.408	6.519
		Increment	-	24%	16%	33%

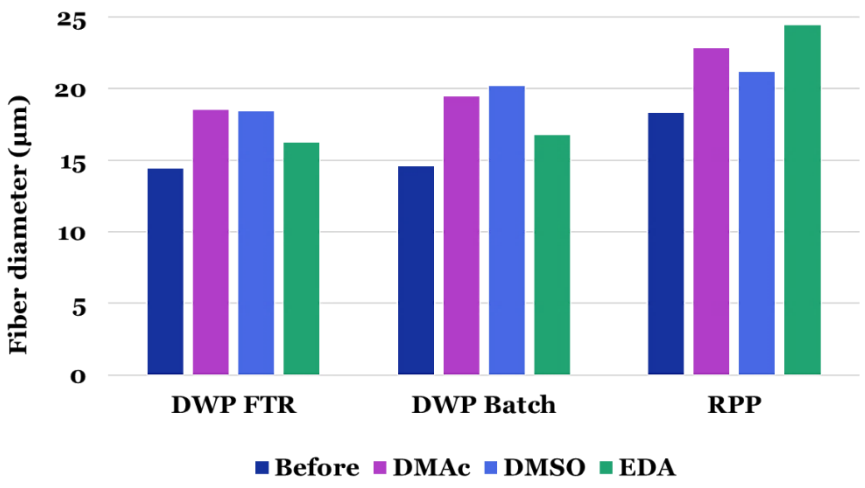

Figure 4.11. Results of fiber diameter before and after activation treatments.

The results obtained for WRV and fiber diameter increasing are coincident. In terms of improvement of pulp water retention value, both wood pulps showed better results for DMAc and DMSO treatments, while EDA was more effective for recycled pulps. For DWP-FTR, DMAc and DMSO activations resulted in an improvement of around 14% of fibers WRV. The best result was obtained with DMSO (almost 12%) for DWP-Batch. EDA activation was more effective for recycled paper pulps, increasing the WRV from 104% to 116%.

The same behavior was observed in the increment of fibers' diameter, with a slightly better performance in DMSO for DWPs, and a significant swelling for RPP fibers. The percentage of improvement caused by the activation treatments is indicated in Table 4.4. To rationalize these results, we elucidate over solvents' physicochemical properties listed in Table 4.5, Hansen's solubility parameters (δ_D, δ_P, δ_H), and molar volume (V_m).

Table 4.5. List of properties for the selected solvents for activation treatment. NMMO is additionally included for comparison as the main solvent for the lyocell process.

Solvent	DMAc[b]	DMSO[b]	EDA[c]	NMMO[d]
V_m	92.5	71.3	67.3	97.6
δ_T[a]	22.8	26.7	25.3	26.9
δ_D	16.8	18.4	16.6	19
δ_P	11.5	16.5	8.8	16.1
δ_H	10.2	10.2	17.0	10.2
R_a (Polar)	10.6	6.4	12.1	6.9
R_a (Apolar)	7.7	12.4	11.3	12.3

a. δ_T is the Hildebrand's parameter, given by Equation 2.3.
b. (Hansen, 2007; Islam et al., 2020; Kamlet & Abboud, 1975)
c. (Hansen, 2007; Stenutz, 2020)
d. (Hansen & Björkman, 1998; Leipner, 2002)

Empirical parameters of cellulose crystalline units lattice plans (Figure 4.12) (Bruel et al., 2019) are listed in Table 4.6.

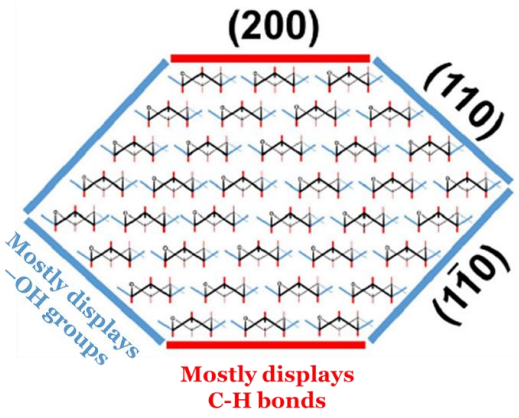

Figure 4.12. Lattice planes (110), (1$\bar{1}$0), and (200) of cellulose crystalline unit (Adapted from Bruel et al., 2019).

Table 4.6. Solubility parameters for cellulosic lattice plans (Bruel et al., 2019).

	Solubility Parameters			
Cellulose Lattice Plan	**δ_D**	**δ_P**	**δ_H**	**R_o**
(110) and (1$\bar{1}$0)	18.1	20.4	15.3	7.8
(200)	17.4	4.8	6.5	2.1

The structural amphiphilicity of cellulose, as mentioned before, shows hydrophilic planes (110) and (1$\bar{1}$0), where the hydroxyl groups are oriented in equatorial positions, also nominated as polar planes. The hydrophobic (apolar) plane (200) of lower surface energy, parallel to the sheets plane, is formed by the hydrogen atoms of C-H bonds in the axial position, as shown in Figure 4.12 (Bruel et al., 2019). According to Hansen's theory, the solubility parameters of those planes (Table 4.6) were used as coordinates in a 3-dimensional graph, generating Hansen's spheres of radius R_o for polar and apolar planes of cellulose (Figure 4.13). HSP values of solvents used in the activation processes and NMMO were also considered in the plotting to indicate their affinity to the polymer.

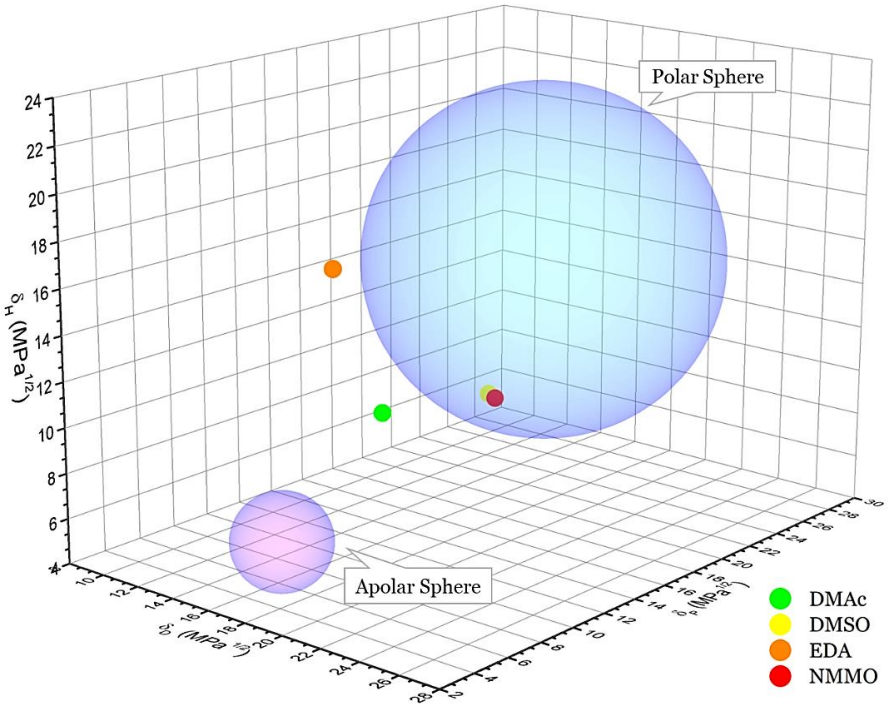

Figure 4.13. Hansens' spheres for polar and apolar cellulose planes, and HSP of solvents are represented as coordinates. Developed at Origin®9.

As mentioned before, the HSP model allows the indication of "good" or "bad" solvents quantitatively by the HSP distance, R_a. The values of R_a calculated for each solvent and plane are listed in Table 4.5 and agree with the results in Figure 4.13. The solvents inside the polar sphere, DMSO and NMMO, are the only ones in which the R_a values are smaller than R_o (the sphere's radius).

Despite the DMSO solubility parameters being in the range of those calculated for cellulose, its direct dissolution in this specific solvent is not thermodynamically favorable (Hearle et al., 2001). DMSO tends to form hydrogen bonds with cellulose hydroxyl groups, which, combined with its high dipole moment and relatively small volume, may enhance the swelling efficiency of the solvent (Fidale et al., 2008). These aspects, alongside the HSP theory, can justify the results in comparison with another aprotic solvent (DMAc) for wood pulps; still, the differences are not significant. Although, none of these properties explain the outstanding result for EDA activation in RPPs. In this case, the molar volume of the solvent seems to govern its penetrating capability and swelling performance. RPP-Original has a more crystalline structure than the studied DWPs (Figure 4.14), which can be related to structural changes caused by recycling operations. The smaller volume of ethylenediamine implies better permeability through cellulose's packed structure and acts as an amphiphilic cosolute, able to weak hydrophobic interactions (Medronho et al., 2012).

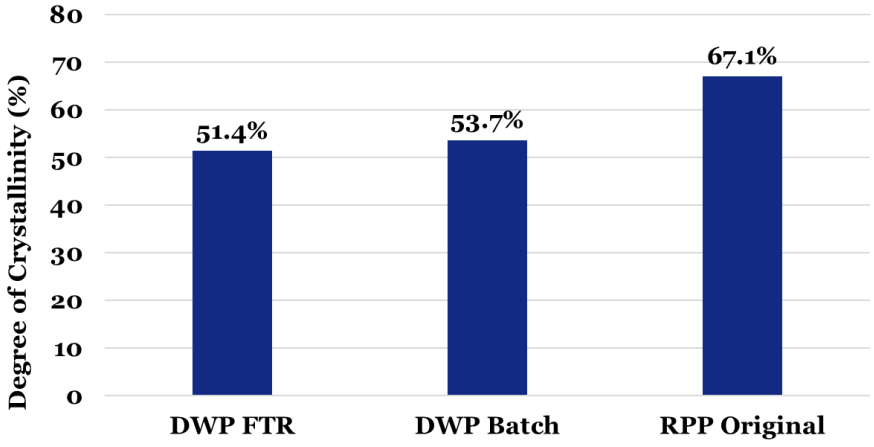

Figure 4.14. Degree of crystallinity of studied samples: DWP-FTR, DWP-Batch, and RPP-Original.

According to our experimental data, the synergetic contribution of the frequently neglected interactions (dispersion forces and dipolar interactions) was evidenced in the prediction of solvent–polymer compatibility by Hansen's solubility parameters theory. Moreover, the molar

volume of a solvent showed as a determinant factor of its swelling performance, especially in a crystalline structure, contributing to the disruption of hydrophobic interaction in the intrinsic anisotropic structure of cellulose. For structures with large voids, in this case, high initial WRV and higher amount of amorphous regions, the high molar volume of the solvent is not detrimental to swelling since it is able to establish interactions with cellulose molecules. These results are, somehow, in line with those obtained in the reference study by Philipp and Schleucher, 1973, mainly in terms of the role of polar interactions and the significance of solvent molar volume and cellulose structure (Philipp & Schleicher, 1973). However, the study considers a strong dependence of swelling performance on the hydrogen bond interactions (δ_H), which was not observed as a relevant parameter (when taken as a single variable) for the samples analyzed in our work.

4.2.2. Pulp Dissolution

4.2.2.1. Dissolution in LiCl/DMAc

DMAc can dissolve cellulose only when it is conjugated with lithium chloride (Sayyed et al., 2019). In this system, the most accepted dissolution mechanism involves a polyelectrolyte effect, where the Li^+ ions, complexed as Li-DMAc, interact with oxygen electrons from cellulose, while the strong negative Cl^- ions interact with hydroxyl groups (Figure 4.15). The charge repulsion causes the disruption of the bonds between cellulose molecules, resulting in its dissolution (El-Kafrawy, 1982; Hearle et al., 2001; Medronho & Lindman, 2014a).

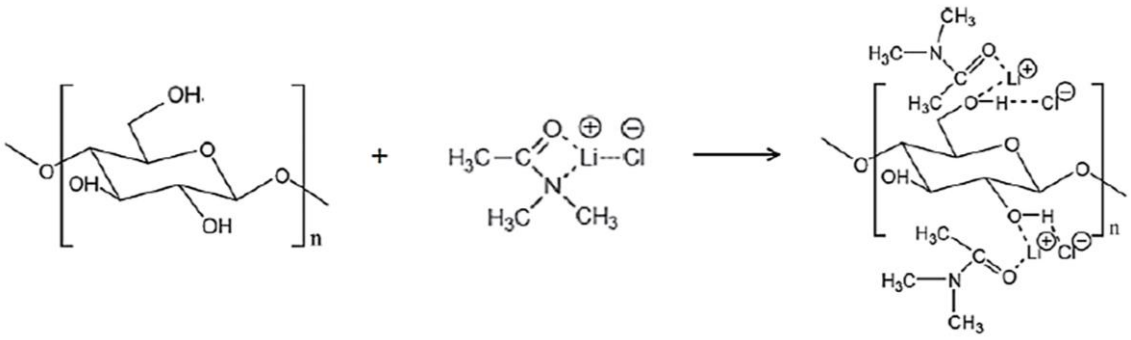

Figure 4.15. Proposed mechanism for the cellulose dissolution in the LiCl/DMAc solvent system, and the formation of the intermediate LiCl/DMAc/cellulose complex (El-Kafrawy, 1982; Medronho & Lindman, 2014a)

As a trial of pulps dissolution performance, before the NMMO process, samples were activated by solvent exchange processes and submitted to dissolution at the solvent system LiCl/DMAc. The

optical microscopy images of Figure 4.16 show the dissolution extension of samples after six weeks in 8%LiCl/DMAc. Only images of better performance among all pre-treatments applied are considered. The dissolution extension images for each activation process can be found in Appendix E.

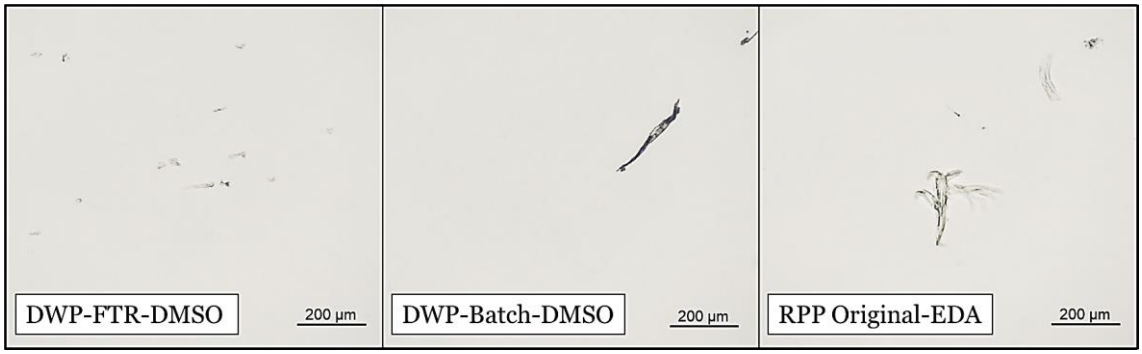

Figure 4.16. Microscopy images (40x) of pre-activated samples for dissolution extension evaluation at 8%LiCl/DMAc solvent system.

The visual evaluation of the dissolution extension aimed to examine the solutions qualitatively, identify the profile and morphology of the undissolved fibers, and quantify the unsoluble matter by determining the degree of dissolution (as a percentage).

For the DWPs (FTR and Batch), all systems showed a dissolution greater than 90%, with a more pronounced apparent dissolution for the H2O→Methanol→DMSO system. RPP-Original showed a higher dissolution rate in pretreated samples with EDA (>70%). These results are aligned with the outcomes from the fiber activation study presented earlier, which indicate the effectiveness of the pretreatments applied to convert the more crystalline domains of cellulose into more accessible regions, improving its solubility.

The dissolution extension for RPP-Original is in accordance with the expected since the insoluble matter (lignin and foreign materials) represents over 35% of pulp content (oven-dry weight). To all samples, the undissolved fibers, as seen in Figure 4.16, suggest a certain degree of hornification, which may explain their non-dissolution.

A curious effect of nonregular swelling along the fiber (Figure 4.17) was observed for RPP, where the disruption of cellulose macrofibrils can be observed. This phenomenon, known as ballooning, is commonly observed in native cellulose fibers such as wood and cotton (Cuissinat et al., 2008). The ballon formation evidence a non-homogeneous diffusion of the solvent between the crystalline (unswollen sections) and amorphous (balloons) phases of the pulp (Figure 4.17.a). The

amorphous regions are more easily accessed due to their higher free energy, so this differential swelling behavior is observed (Medronho & Lindman, 2014b).

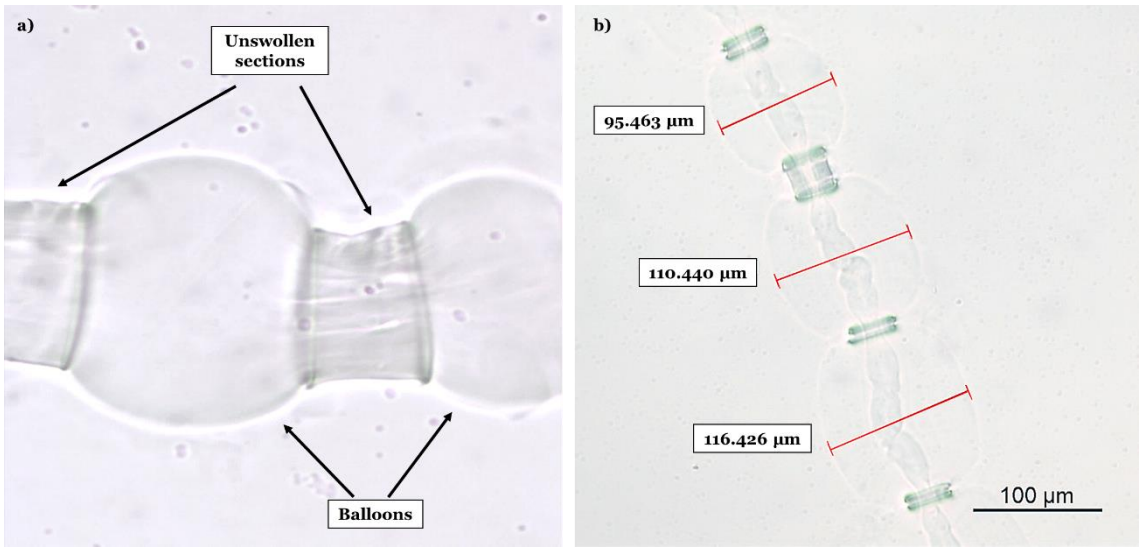

Figure 4.17. The ballooning effect observed for the RPP-Original sample after 1 hour in 8%LiCl/DMAc. Solvent exchange activation by a) DMSO and b) DMAc.

Ballooning is part of the dissolution mechanism, composed of four phases: 1) the solvent penetrates the fiber in some specific zones, forming the balloon; 2) the balloon diameter increase (Figure 4.17.b) until it bursts, releasing the cellulose solution inside its membrane; 3) the unswollen zones, now dispersed as rings in the solution, are dissolved; 4) dissolution of balloon membrane scraps (Cuissinat et al., 2008). This phenomenon indicates LiCl/DMAc as a mild solvent for RPP, while for DWPs, no balloons were observed, which indicates higher compatibility of DWP cellulose fibers to the solvent, once good solvents tend to disintegrate the fiber into fragments and dissolve them rapidly (Cuissinat et al., 2008; Cuissinat & Navard, 2006). A fiber's swelling and dissolution mechanisms can be related to its origin and arrangement (Cuissinat & Navard, 2006). The origin of the ordinary grade RPP can vary in hardwood/softwood content, considering its heterogeneity. Also, the material degradation caused by papermaking operations, evident high rate of hornificated fibers, and higher crystallinity index can be considered important factors for this distinct affinity with the solvent system.

The samples were dissolved in the 8% LiCl/DMAc system after activation by solvent exchange (EDA→Methanol→DMAc) to evaluate the influence of different cooking conditions on the dissolution behavior of the recycled paper pulp. The resulting solution for sample B (H-factor

~3,000) had a considerably lower viscosity, in agreement with the lowest pulp intrinsic viscosity values obtained.

Through Figure 4.18, a slight difference can be noticed between the samples submitted to different alkali charge conditions (A_1 and A_2). The three upper images show some residues of cellulose fibers, where a) presents insoluble fibers with more significant swelling. Meanwhile, b) and c) allow the analysis of a dissolution profile greater than 90%, where c) (sample B) can be considered a more homogeneous environment. The three lower images (d, e, and f) show the solutions from samples in which kraft cooking was performed with an H-factor of around 2,000. Despite the high observed dissolution extension (>90%), no significant difference was observed between samples, which can be justified by their similar lignin and insoluble matter content.

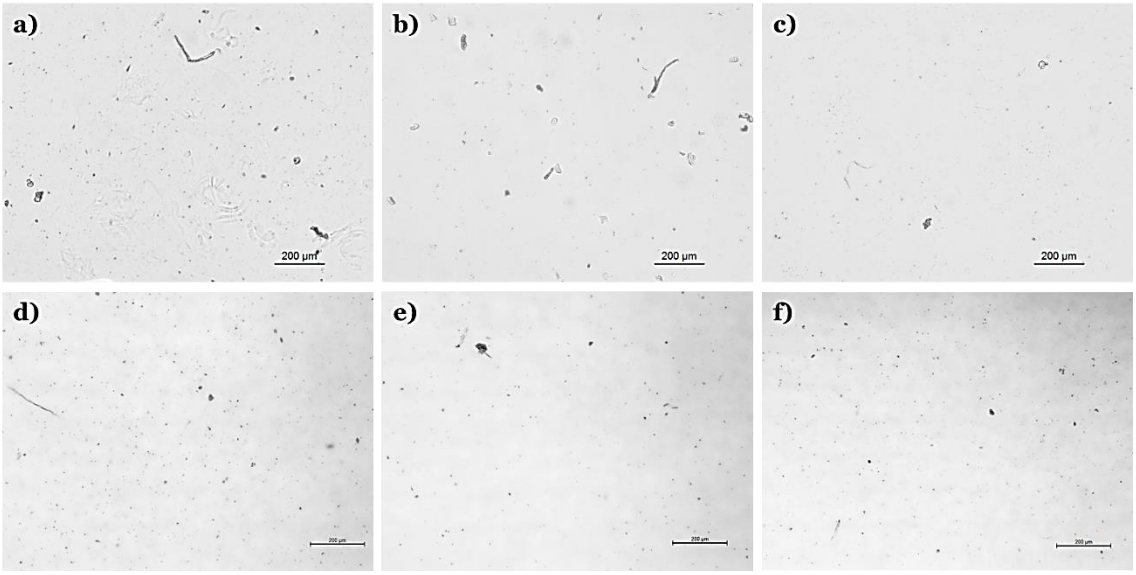

Figure 4.18. Microscopy images (40x) of PHK bleached recycled paper pulps a) A_1; b) A_2; c) B; d) C_1; e) C_2; and f) C_3 for dissolution extension evaluation at 8%LiCl/DMAc solvent system.

4.2.2.2. Dissolution in NMMO

The dissolution in NMMO was carried out under a pulp consistency of 1%, w/w, and their time for completion and identified mechanism are shown in Table 4.7.

The evolution of pulp dissolution was observed by microscopy images of dope samples taken during the process. From these images, a dissolution mechanism was observed, divided into five phases: 1) swelling of fibers; 2) balloons formation; 3) rupture of fibers or balloons bursting; 4)

formation of fibers fragments; and 5) dissolution of the remaining fragments, indicated as the end of the dissolving process.

Table 4.7. The dissolution profile of DWP and RPP samples concerning time and mechanism.

	DWP FTR	**DWP Batch**	**DWP Commercial**	**RPP C_3**
Viscosity (cm^3/g)	549	874	474	414
CI (%)	51.4	53.7	16.7	41.9
Reactivity (%)	71.2	57.1	91.5	84.1
Time (min)	105	105	60	60
Mechanism	Ballooning	Ballooning	Rupture	Rupture

The dissolution profile of the produced dissolving wood pulps was quite different from that of the commercial sample (and the PHK recycled paper pulp) concerning the dissolution time and mechanism. The dissolving pulp properties, intrinsic viscosity, crystallinity index, and reactivity presented above (Table 4.7) can be correlated with the dissolving mechanism and extension. Samples DWP-FTR and Batch showed a higher viscosity than DWP-Commercial and RPP-C_3, and exhibited a more difficult dissolution process in NMMO. These observations suggest a relation between pulp viscosity (or DP) and time for dissolution, which is in line with the observed through Fock's reactivity results. The higher the DP of a pulp, the less accessible its structure becomes, and the more complicated the solvent diffusion to establish interactions able to dissolve the cellulose chain. However, the DWP-FTR pulp has a relatively low intrinsic viscosity and exhibits a low dissolution tendency, which suggests that other pulp properties influence the dissolution in NMMO, such as the crystallinity index.

Figure 4.19 shows the time required for the different pulps to reach the different dissolution phases. For the DWP-FTR fibers (Figure 4.20), the ballooning phase only appears after 45 minutes of treatment (figure 4.21), whereas the DWP-Batch reaches this phase after 30 minutes. As shown in Figure 4.20, no ballooning was observed after 30 minutes at 70°C, but an extensive and homogeneous swelling was noted (Figure 4.21), followed by ballooning at 45 minutes. The rupture of fibers was only identified by the fragments (60 min) since it may have occurred faster. DWP-Batch, in turn, had all the steps well defined, allowing their identification throughout the dissolution (Appendix F).

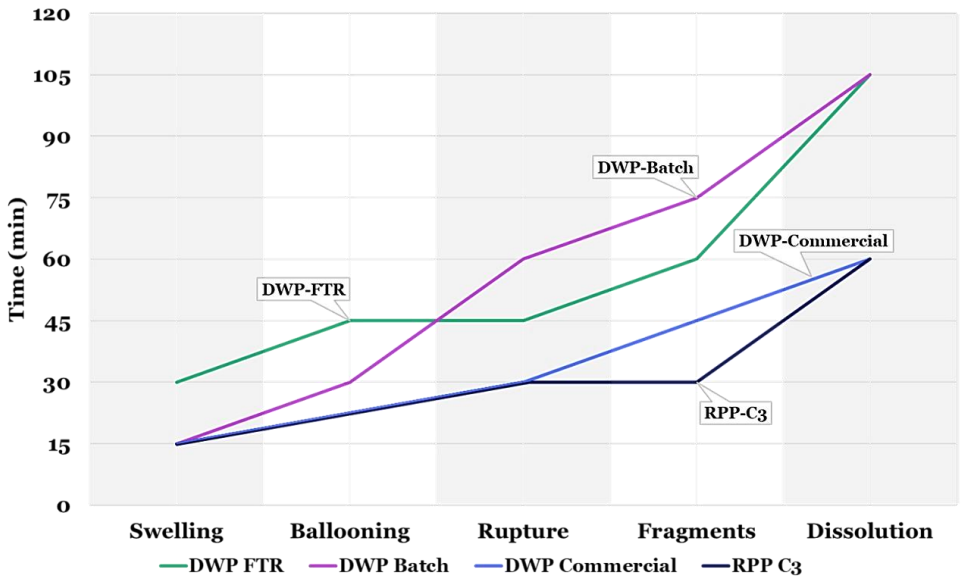

Figure 4.19. Dissolution development of pulps observed by microscopy images separated into phases: fiber swelling, balloon formation, fiber rupture, fiber fragments, and dissolution.

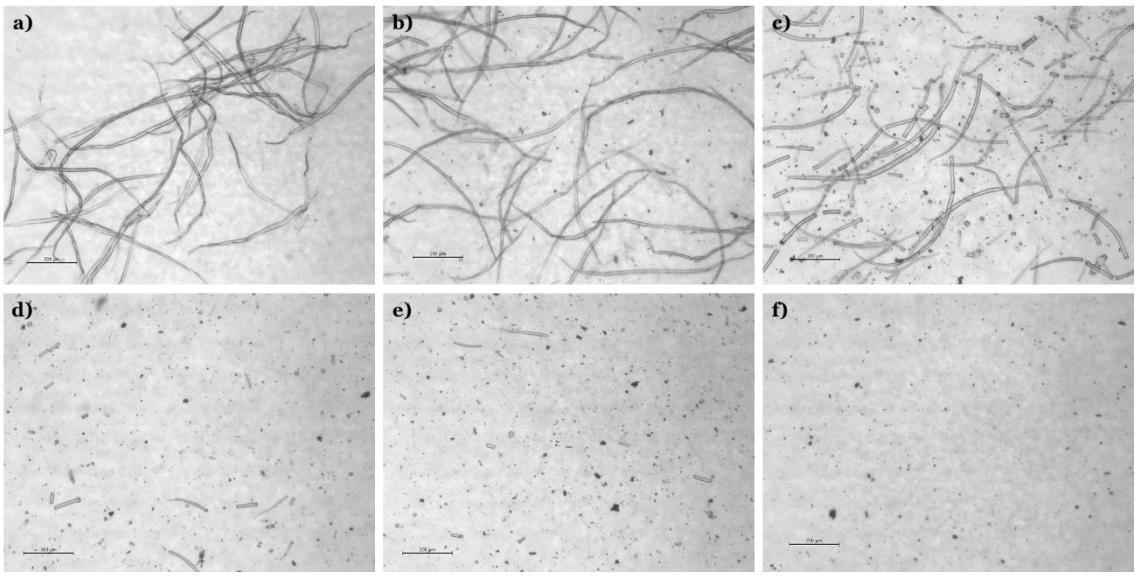

Figure 4.20. Images (40x amplified) of the dissolution progress of DWP-FTR in NMMO/H_2O after a) swelling; b) 15 min; c) 45 min; d) 60 min; e) 90 minutes; and f) 105 min.

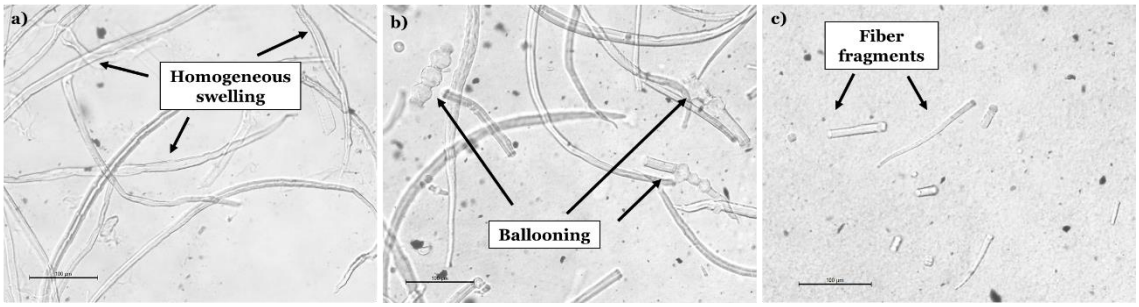

Figure 4.21. Images of the critical point of the dissolution development of DWP-FTR between a) 30 min; b) 45 min; and c) 60 min. Indications of the evidenced mechanism, from the homogeneous swelling, and balloons formation, to the remained fiber fragments.

DWP-Commercial and RPP-C3 showed the same dissolution profile in the first 30 minutes, from swelling to fibers rupture. DWP-Commercial had a named "critical point of dissolution" at 30 to 60 minutes, going from the rupture to the complete dissolution with almost no fragments observed in between (images available in Appendix F). For RPP-C3 (Figure 4.22), fragments and broken fibers were observed from 30 to 45 minutes, allowing the observation of fiber surface disruption and dissolved cellulose release into the solvent media (Figure 4.23).

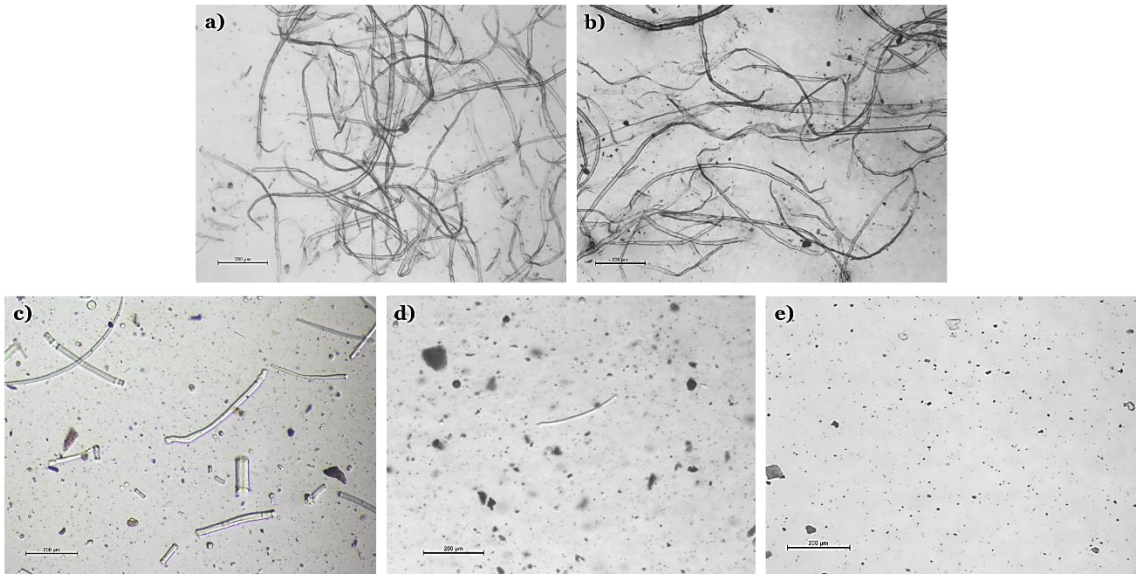

Figure 4.22. Images of the evolution of RPP C_3 dissolution in NMMO/H2O in the stages: a) after swelling (40x amplified); at dissolution time of b) 15 min (100x amplified); c) 30 min (40x amplified); d) 45 min (40x amplified); and e) 60 min (40x amplified).

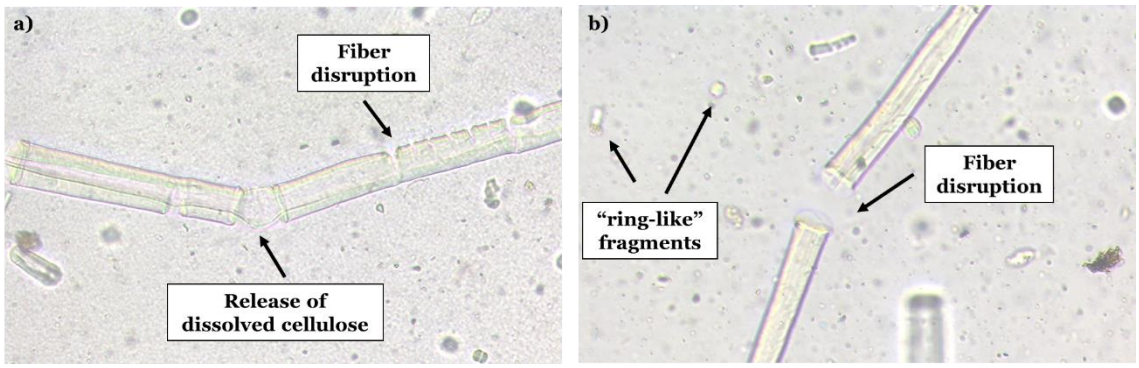

Figure 4.23. Dissolution mechanism of RPP C_3 in NMMO/H_2O after 30 min (100x amplified).

The principal difference observed refers to the intermediary phase of dissolution, where DWP-FTR and DWP-Batch fibers show balloons formations, while DWP-Commercial and RPP-C3 fibers undergo a direct rupture in the first 30 minutes. The mechanism of dissolution, as discussed before through the theory exposed by Cuissinat et al., 2008, shows the existence of better compatibility between the more reactive samples (DWP-Commercial and RPP C_3) and the solvent system (NMMO/H_2O). This compatibility is indicated by the disintegration of the fibers into fragments without evidence of an intermediate ballooning stage.

Figure 4.24 shows regenerated cellulose fibers (lyocell) produced from the dissolution of RPP-C_3 (left), and DWP-Batch (right), with surface characteristics close to the observed in synthetic fibers. The first trials with RPP-C_3 resulted in fibers with an average diameter of 100 µm, while a second test with DWP-Batch produced fibers of width between 35-50 µm, closer to commercial lyocell fibers, which show diameters in the order of 20µm (Cui et al., 2022). This indicates that the process of regeneration developed still needs additional improvements. Nevertheless, the proven regeneration capability is an excellent outcome as the actual application of the pulps produced through this study.

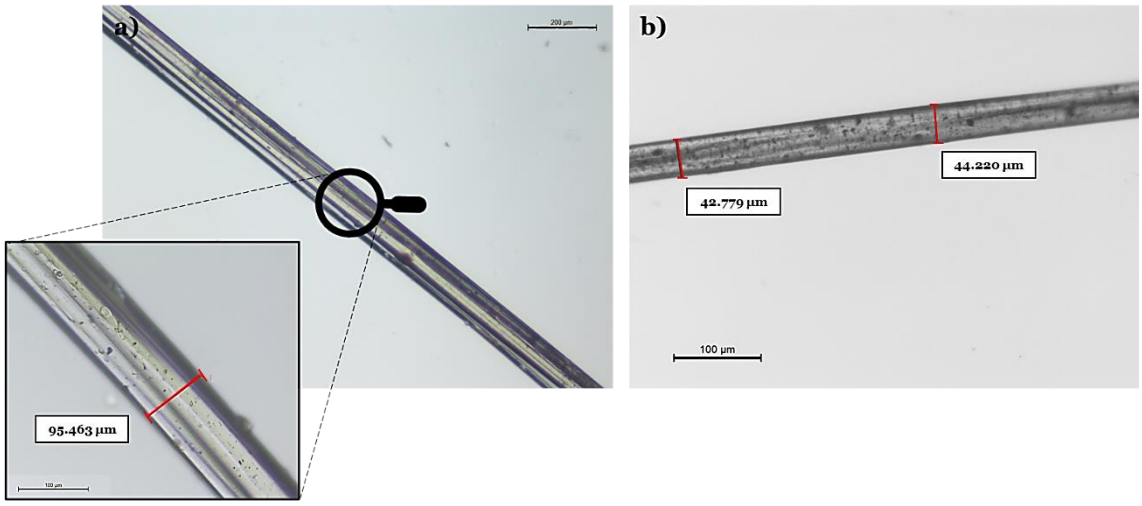

Figure 4.24. Regenerated fibers from a) RPP amplified 40x and zoom-in (100x), and b) DWP-Batch amplified 100x.

Chapter 5: Conclusions

This work has demonstrated that prehydrolysis kraft processes can be manipulated and optimized to produce dissolving-grade pulps from *Eucalyptus globulus* and recycled paper. The effect of the prehydrolysis applied in different conditions was studied, demonstrating the flow-through (FTR) acid-hydrolysis as the more effective for producing dissolving wood pulps (DWP) with better characteristics and potential for textile applications. The FTR liquid operation mode enabled a higher hemicellulose and lignin removal extent, in combination with a higher alpha-cellulose content (91%) and cellulose reactivity (>71%). The reduction of pulp viscosity was also considered a positive outcome in attaining the required dissolving pulp quality.

An innovative processing was developed to improve cellulose dissolution from recycled paper, promoting a new field of applications for a disposable material. The auto-hydrolysis, followed by a kraft cooking (H-factor around 2,000), was considered the optimum process conditions to produce a dissolving-grade pulp with an outstanding reactivity of 84.1%, and a cellulose content of almost 89%. Despite the excellent properties achieved, such as the intermediate DP (613) and lower residual lignin content (kappa number of 1.3), additional treatments will be required to improve pulp purity regarding metal ions content.

Through our experimental results for fiber activation by solvent exchange, to predict the compatibility of a polymer with a solvent, the consideration of at least three parameters is needed beyond the hydrogen bonding-related interactions, i.e., (1) the dispersive (δ_D) and polar (δ_P) interactions; (2) the molar volume (V_m) of the solvent; (3) the cellulose supramolecular structure in term of its crystallinity and anisotropy.

The dissolution extension of the studied pulps in 8% LiCl/DMAc proved the effectiveness of the solvent exchange treatment and the PHK processes applied to RPPs. The dissolution behavior observed in the solvent system NMMO/H_2O demonstrated a better solvent compatibility with the reference DWP sample (DWP-Commercial) and the PHK-processed RPP. These observations, alongside the results of Fock's reactivities, allow a relationship to be established between the fiber supramolecular structure, mainly the degree of polymerization, and the pulp's dissolution profile.

References

Almeida, R. O., Maloney, T. C., & Gamelas, J. A. F. (2023). Production of functionalized nanocelluloses from different sources using deep eutectic solvents and their applications. *Industrial Crops and Products*, *199*, 116583. https://doi.org/10.1016/j.indcrop.2023.116583

Andary, J., Maalouly, J., Ouaini, R., Chebib, H., Rutledge, D. N., & Ouaini, N. (2021). Stability study of furans, glucose and xylose under overliming conditions: Effect of sugar degradation products. *Bioresource Technology Reports*, *15*(March), 100722. https://doi.org/10.1016/j.biteb.2021.100722

Araújo, J. D. (2008). *Production of vanillin from lignin present in the Kraft black liquor of the pulp and paper industry* [University of Porto]. http://repositorio-aberto.up.pt/handle/10216/11944

Asif, M. (2009). Sustainability of timber, wood and bamboo in construction. In *Sustainability of Construction Materials*. Woodhead Publishing Limited. https://doi.org/10.1533/9781845695842.31

Asikainen, S., Määttänen, M., Harlin, A. and, & Sivonen, E. (2014). *Method of producing dissolving pulp and use of method* (Patent No. WO 2014/041251 A1).

Asikainen, S., Määttänen, M., Harlin, A., Valta, K. and, & Sivonen, E. (2015). *Method of producing dissolving pulp, dissolving pulp and use of method* (Patent No. US 2015 / 0225901 A1).

Bajpai, P. (2005). ECF and TCF bleaching. In *Environmentally Benign Approaches for Pulp Bleaching* (pp. 177–192). Elsevier. https://doi.org/10.1016/B978-044451724-1/50005-8

Bajpai, P. (2014a). Industrial Applications of Xylanases. In P. Bajpai (Ed.), *Xylanolytic Enzymes* (pp. 69–104). Academic Press. https://doi.org/10.1016/b978-0-12-801020-4.00008-1

Bajpai, P. (2014b). Recycling and Deinking of Recovered Paper. In *Recovered Paper* (pp. 1–19). Elsevier Inc. https://doi.org/10.1016/b978-0-12-416998-2.00001-5

Bajpai, P. (2018a). Production of Dissolving Grade Pulp. *Biermann's Handbook of Pulp and Paper*, 375–388. https://doi.org/10.1016/b978-0-12-814240-0.00014-8

Bajpai, P. (2018b). Pulping Fundamentals. In *Biermann's Handbook of Pulp and Paper*. https://doi.org/10.1016/b978-0-12-814240-0.00012-4

Bajpai, P. (2018c). Wood and Fiber Fundamentals. In *Biermann's Handbook of Pulp and Paper*. https://doi.org/10.1016/b978-0-12-814240-0.00002-1

Bergenstråhle, M., Wohlert, J., Himmel, M. E., & Brady, J. W. (2010). Simulation studies of the insolubility of cellulose. *Carbohydrate Research Journal*, *345*, 2060–2066. https://doi.org/10.1016/j.carres.2010.06.017

Bertella, S., & Luterbacher, J. S. (2020). Lignin Functionalization for the Production of Novel Materials. *Trends in Chemistry*, *2*(5), 440–453. https://doi.org/10.1016/j.trechm.2020.03.001

Bi, R., Khatri, V., Chandra, R., Takada, M., Figueroa, D. V., Zhou, H., Wu, J., Charron, D., & Saddler, J. (2021). Enhancing Kraft based dissolving pulp production by integrating green liquor neutralization. *Carbohydrate Polymer Technologies and Applications*, *2*, 100034. https://doi.org/10.1016/j.carpta.2021.100034

Biermann, O., Hädicke, E., Koltzenburg, S., & Müller-plathe, F. (2001). Hydrophilicity and Lipophilicity of Cellulose Crystal Surfaces. *Angewandte Chemie*, *40*(20), 2–5. https://doi.org/10.1002/1521-3773(20011015)40:20%3C3822::AID-ANIE3822%3E3.0.CO;2-V

Björquist, S., Aronsson, J., Henriksson, G., & Persson, A. (2018). Textile qualities of regenerated cellulose fibers from cotton waste pulp. *Textile Research Journal*, *88*(21), 2485–2492. https://doi.org/10.1177/0040517517723021

Brown, R. M., Haigler, C., & Cooper, K. (1982). Experimental Induction of Altered Nonmicrofibrillar Cellulose. *Science*, *6*, 1141–1142. https://doi.org/10.1126/science.218.4577.1141

Bruel, C., Tavares, J. R., Carreau, P. J., & Heuzey, M. C. (2019). The structural amphiphilicity of cellulose nanocrystals characterized from their cohesion parameters. *Carbohydrate Polymers*, *205*(July 2018), 184–191. https://doi.org/10.1016/j.carbpol.2018.10.026

Ceccherini, S., Ståhl, M., Sawada, D., Hummel, M., & Maloney, T. C. (2021). Effect of Enzymatic Depolymerization of Cellulose and Hemicelluloses on the Direct Dissolution of

Prehydrolysis Kraft Dissolving Pulp. *Biomacromolecules*, *22*(11), 4805–4813. https://doi.org/10.1021/acs.biomac.1c01102

Çetinkol, Ö. P., Smith-Moritz, A. M., Cheng, G., Lao, J., George, A., Hong, K., Henry, R., Simmons, B. A., Heazlewood, J. L., & Holmes, B. M. (2012). Structural and Chemical Characterization of Hardwood from Tree Species with Applications as Bioenergy Feedstocks. *PLoS ONE*, *7*(12). https://doi.org/10.1371/journal.pone.0052820

Chen, C., Duan, C., Li, J., Liu, Y., Ma, X., Zheng, L., Stavik, J., & Ni, Y. (2016). Cellulose (Dissolving Pulp) Manufacturing Processes and Properties: A Mini-Review. *BioResources*, *11*(2), 5553–5564. https://doi.org/10.15376/biores.11.4.5553-5564

Christoffersson, K. E. (2005). *Dissolving pulp: Multivariate Characterisation and Analysis of Reactivity and Spectroscopic Properties*. Umeå University.

Ciechańska, D., Wesołowska, E., & Wawro, D. (2009). An introduction to cellulosic fibres. In *Handbook of Textile Fibre Structure* (Volume 2, pp. 3–61). Elsevier. https://doi.org/10.1533/9781845697310.1.3

Costa, J. R., Tonon, R. V., Gottschalk, L. M. F., Santiago, M. C. de A., Mellinger-Silva, C., Pastrana, L., Pintado, M. M., & Cabral, L. M. C. (2019). Enzymatic production of xylooligosaccharides from Brazilian Syrah grape pomace flour: a green alternative to conventional methods for adding value to agricultural by- products. *Journal of the Science of Food and Agriculture*, *99*(3), 1250–1257. https://doi.org/10.1002/jsfa.9297

Cousins, S. K., & Brown, R. M. (1995). Cellulose I microfibril assembly: computational molecular mechanics energy analysis favours bonding by van der Waals forces as the initial step in crystallization. *Polymer*, *36*(20), 3885–3888. https://doi.org/10.1016/0032-3861(95)99782-P

Cui, S., Zhang, Y., Liu, C., Lou, S., Zhang, Y., Zhang, Y., & Wang, H. (2022). The influence of the multi-level structure under high drawing on the preparation of high strength Lyocell fiber. *Cellulose*, *29*(2), 751–762. https://doi.org/10.1007/s10570-021-04364-x

Cuissinat, Celine, & Navard, P. (2006). Swelling and Dissolution of Cellulose Part 1: Free Floating Cotton and Wood Fibres in N-Methylmorpholine-N-oxide–Water Mixtures. *Macromolecular Symposia*, *244*(1), 1–18. https://doi.org/10.1002/masy.200651201

Cuissinat, Céline, Navard, P., & Heinze, T. (2008). Swelling and dissolution of cellulose. Part IV: Free floating cotton and wood fibres in ionic liquids. *Carbohydrate Polymers*, *72*(4), 590–596. https://doi.org/10.1016/j.carbpol.2007.09.029

Cunha, A. and, & Simões, R. (2022). Effect of Pre-Hydrolysis Reaction Conditions on Xylooligosaccharides Extraction in Eucalyptus Globulus. *KnE Materials Science*, *2022*, 8–14. https://doi.org/10.18502/kms.v7i1.11603

Cunha, A. and, & Simões, R. (2023). Dissolving Kraft Pulp Production and Xylooligosaccharide Coproduction: Effect of Pre-Hydrolysis Conditions. *ACS Omega*. https://doi.org/10.1021/acsomega.2c07594

de los Ríos, M. D., & Ramos, E. H. (2020). Determination of the Hansen solubility parameters and the Hansen sphere radius with the aid of the solver add-in of Microsoft Excel. *SN Applied Sciences*, *2*(4), 1–7. https://doi.org/10.1007/s42452-020-2512-y

de Oliveira, C. R. S., da Silva Júnior, A. H., Mulinari, J., & Immich, A. P. S. (2021). Textile Re-Engineering: Eco-responsible solutions for a more sustainable industry. *Sustainable Production and Consumption*, *28*, 1232–1248. https://doi.org/10.1016/j.spc.2021.08.001

De Souza, I. J., Bouchard, J., Méthot, M., Berry, R., & Argyropoulos, D. S. (2002). Carbohydrates in oxygen delignification Part I: Changes in cellulose crystallinity. *Journal of Pulp and Paper Science*, *28*(5), 167–170.

Dence, C. W. and, & Reeve, D. W. (1996). *Pulp Bleaching: Principles and Practice*. TAPPI PRESS.

Duan, C., Li, J., Ma, X., Chen, C., Liu, Y., Stavik, J., & Ni, Y. (2015). Comparison of acid sulfite (AS)- and prehydrolysis kraft (PHK)-based dissolving pulps. *Cellulose*, *22*(6), 4017–4026. https://doi.org/10.1007/s10570-015-0781-1

Duan, C., Verma, S. K., Li, J., Ma, X., & Ni, Y. (2016). Combination of mechanical, alkaline and enzymatic treatments to upgrade paper-grade pulp to dissolving pulp with high reactivity. *Bioresource Technology*, *200*, 458–463. https://doi.org/10.1016/j.biortech.2015.10.067

Dupont, A. L. (2003). Cellulose in lithium chloride/N,N-dimethylacetamide, optimisation of a dissolution method using paper substrates and stability of the solutions. *Polymer*, *44*(15), 4117–4126. https://doi.org/10.1016/S0032-3861(03)00398-7

El-Kafrawy, A. (1982). Investigation of the cellulose/LiCl/dimethylacetamide and cellulose/LiCl/N-methyl-2-pyrrolidinone solutions by 13C NMR spectroscopy. *Journal of Applied Polymer Science*, *27*(7), 2435–2443. https://doi.org/10.1002/app.1982.070270714

Erdei, B., Franká, B., Galbe, M., & Zacchi, G. (2012). Separate hydrolysis and co-fermentation for improved xylose utilization in integrated ethanol production from wheat meal and wheat straw. *Biotechnology for Biofuels*, *5*(March). https://doi.org/10.1186/1754-6834-5-12

Erik Ernø-Kjølhede. (1999). Project Management Theory and the Management of Research Projects. In *MPP Working Paper* (Vol. 3, Issue VI). Copenhagen Business School.

Evans, R., Newman, R. H., Roick, U. C., Suckling, I. D., & Wallis, A. F. A. (1995). Changes in Cellulose Crystallinity During Kraft Pulping. Comparison of Infrared, X-ray Diffraction and Solid State NMR Results. *Holzforschung*, *49*(6), 498–504. https://doi.org/10.1515/hfsg.1995.49.6.498

Evans, R., & Wallis, A. F. A. (1989). Cellulose molecular weights determined by viscometry. *Journal of Applied Polymer Science*, *37*(8), 2331–2340. https://doi.org/10.1002/app.1989.070370822

Fahmy, Y., & Mobarak, F. (1971). *Fine structure and reactivity of cellulose*. *October 1971*, 767–769. https://doi.org/10.1002/pol.1971.110091012

Felgueiras, C., Azoia, N. G., Gonçalves, C., Gama, M., & Dourado, F. (2021). Trends on the Cellulose-Based Textiles: Raw Materials and Technologies. *Frontiers in Bioengineering and Biotechnology*, *9*(March), 1–20. https://doi.org/10.3389/fbioe.2021.608826

Fernandes Diniz, J. M. B., Gil, M. H., & Castro, J. A. A. M. (2004). Hornification - Its origin and interpretation in wood pulps. *Wood Science and Technology*, *37*(6), 489–494. https://doi.org/10.1007/s00226-003-0216-2

Fidale, L. C. ., Ruiz, N., Heinze, T., & Seoud, O. A. E. (2008). *Cellulose Swelling by Aprotic and Protic Solvents : What are the Similarities and Differences ? a*. 1240–1254. https://doi.org/10.1002/macp.200800021

Fidale, L. C., Ruiz, N., Heinze, T., & El Seoud, O. A. (2008). Cellulose swelling by aprotic and protic solvents: What are the similarities and differences? *Macromolecular Chemistry and Physics*, *209*(12), 1240–1254. https://doi.org/10.1002/macp.200800021

Fink, H. P., Weigel, P., Purz, H. J., & Ganster, J. (2001). Structure formation of regenerated cellulose materials from NMMO-solutions. *Progress in Polymer Science (Oxford)*, *26*(9), 1473–1524. https://doi.org/10.1016/S0079-6700(01)00025-9

Fock, W. (1959). A Modified Method for Determining the Reactivity of Viscose-Grade Dissolving Pulps. *Das Papier*, *13*, 92–95.

Foroughi, F., Ghomi, E. R., Dehaghi, F. M., Borayek, R., & Ramakrishna, S. (2021). A review on the life cycle assessment of cellulose: From properties to the potential of making it a low carbon material. *Materials*, *14*(4), 1–23. https://doi.org/10.3390/ma14040714

Gellerstedt, G. (2009). Chemistry of Bleaching of Chemical Pulp. In *Pulping Chemistry and Technology* (pp. 201–238). De Gruyter. https://doi.org/10.1515/9783110213423.201

Ghasemi, S., Eshkiki, R. B., Fatehi, P., & Ni, Y. (2010). Impact of acid washing and chelation on Mg(oh) 2-based hydrogen peroxide bleaching of mixed hardwoods CMP at a high consistency. *BioResources*, *5*(4), 2258–2267.

Glasser, W. G., Atalla, R. H., Blackwell, J., Brown, M. M., Burchard, W., French, A. D., Klemm, D. O., & Nishiyama, Y. (2012). About the structure of cellulose: Debating the Lindman hypothesis. *Cellulose*, *19*(3), 589–598. https://doi.org/10.1007/s10570-012-9691-7

Gong, C., Ni, J., Fan, S., Zhang, Y., Yang, B., & Su, Z. (2022). Upgrading Paper-Grade Pulp as Dissolving Pulp for Lyocell Fiber Preparation. *Coatings*, *13*(1), 3. https://doi.org/10.3390/coatings13010003

Goto, T., Zaccaron, S., Hettegger, H., Bischof, R. H., Fackler, K., Potthast, A., & Rosenau, T. (2023). Evaluating chelating agents and their effects on cellulosic pulps during P-stage bleaching. Part 1: analytical method development. *Cellulose*, *30*(6), 3887–3900. https://doi.org/10.1007/s10570-023-05110-1

Graenacher, C. and, & Sallmann, R. (1939). *Cellulose Solutions and Process of Making Same* (Patent No. 2,179,181).

Granholm, K., Harju, L., & Ivaska, A. (2010). Desorption of metal ions from kraft pulps. Part 1. Chelation of hardwood and softwood kraft pulp with EDTA. *BioResources*, *5*(1), 206–226. https://doi.org/10.15376/biores.5.1.206-226

Gümüskaya, E., Usta, M., & Kirci, H. (2003). The effects of various pulping conditions on crystalline structure of cellulose in cotton linters. *Polymer Degradation and Stability*, *81*(3), 559–564. https://doi.org/10.1016/S0141-3910(03)00157-5

Guo, Y., Cai, J., Sun, T., Xing, L., Cheng, C., Chi, K., Xu, J., & Li, T. (2021). The purification process and side reactions in the N-methylmorpholine-N-oxide (NMMO) recovery system. *Cellulose*, *28*(12), 7609–7617. https://doi.org/10.1007/s10570-021-03929-0

Gustavsson, C. (2006). *On the Interrelation Between Kraft Cooking Conditions and Pulp Composition* (Issue ISSN 1652-2443). Royal Institute of Technology.

Han, N., Zhang, J., Hoang, M., Gray, S., & Xie, Z. (2021). A review of process and wastewater reuse in the recycled paper industry. *Environmental Technology and Innovation*, *24*, 101860. https://doi.org/10.1016/j.eti.2021.101860

Hansen, C. (1967). The Three Dimensional Solubility Parameter and Solvent Diffusion Coefficient. Their Importance in Surface Coating Formulation. *J. Paint Technology*, 104.

Hansen, C. (2007). The Future. In *Hansen Solubility Parameters: A User's Handbook* (2nd ed., pp. 333–355). https://doi.org/10.1515/9780691199917-020

Hansen, C., & Björkman, A. (1998). *The Ultrastructure of Wood from a Solubility Parameter Point of View*. *52*(4), 335–344.

Hasanbeigi, A., & Price, L. (2015). A technical review of emerging technologies for energy and water efficiency and pollution reduction in the textile industry. *Journal of Cleaner Production*, *95*, 30–44. https://doi.org/10.1016/j.jclepro.2015.02.079

Haule, L. V, Carr, C. M., & Rigout, M. (2016). Preparation and physical properties of regenerated cellulose fibres from cotton waste garments. *Journal of Cleaner Production*, *112*, 4445–4451. https://doi.org/10.1016/j.jclepro.2015.08.086

Hearle, J., Kamide, K., Lönnberg, B., Nishiyama, K. and, & Turbak, A. (2001). *Regenerated Cellulose Fibres* (C. Woodings (ed.)). Woodhead Publishing Ltd.

Heinze, T. (2016). Cellulose: Structure and Properties. In O. J. Rojas (Ed.), *Cellulose chemistry and properties: Fibers, Nanocelluloses and advanced materials* (pp. 1–52). Springer International Publishing. https://doi.org/10.1007/978-3-319-26015-0

Henniges, U., Vejdovszky, P., Siller, M., Jeong, M., & Rosenau, T. (2014). *Finally Dissolved ! Activation Procedures to Dissolve Cellulose in DMAc / LiCl Prior to Size Exclusion Chromatography Analysis - A Review*. 52–68.

Henriques, P., Martinho, M., Serrano, M. de L., Mendes de Sousa, A. P., & Brites Alves, A. M. (2021). Xylooligosaccharides production by acid hydrolysis of an alkaline extraction filtrate from Eucalyptus globulus bleached kraft pulp. *Industrial Crops and Products*, *159*, 113066. https://doi.org/10.1016/j.indcrop.2020.113066

Huang, K. ., & Wang, Y. (2022). Recent applications of regenerated cellulose films and hydrogels in food packaging. *Current Opinion in Food Science*, *43*, 7–17. https://doi.org//10.1016/j.cofs.2021.09.003

Hurmekoski, E., Jonsson, R., Korhonen, J., Jänis, J., Mäkinen, M., Leskinen, P., & Hetemäki, L. (2018). Diversification of the forest industries: Role of new wood-based products. *Canadian Journal of Forest Research*, *48*(12), 1417–1432. https://doi.org/10.1139/cjfr-2018-0116

Ingildeev, D., Effenberger, F., Bredereck, K., & Hermanutz, F. (2013). Comparison of direct solvents for regenerated cellulosic fibers via the lyocell process and by means of ionic liquids. *Journal of Applied Polymer Science*, *128*(6), 4141–4150. https://doi.org/10.1002/app.38470

Islam, T., Islam Sarker, M. Z., Uddin, A. H., Yunus, K. Bin, Prasad, R., Mia, M. A. R., & Ferdosh, S. (2020). Kamlet Taft Parameters: A Tool to Alternate the Usage of Hazardous Solvent in Pharmaceutical and Chemical Manufacturing/Synthesis - A Gateway towards Green Technology. *Analytical Chemistry Letters*, *10*(5), 550–561. https://doi.org/10.1080/22297928.2020.1860124

Jadhav, S., Lidhure, A., Thakre, S., & Ganvir, V. (2021). Modified Lyocell process to improve dissolution of cellulosic pulp and pulp blends in NMMO solvent. *Cellulose*, *28*(2), 973–990. https://doi.org/10.1007/s10570-020-03580-1

Jia, F., Yin, S., Chen, L., & Chen, X. (2020). The circular economy in the textile and apparel industry: A systematic literature review. *Journal of Cleaner Production*, *259*, 120728. https://doi.org/10.1016/j.jclepro.2020.120728

Jiang, X., Bai, Y., Chen, X., & Liu, W. (2020). A review on raw materials, commercial production and properties of lyocell fiber. *Journal of Bioresources and Bioproducts*, *5*(1), 16–25.

https://doi.org/10.1016/j.jobab.2020.03.002

Johnson, D. L. (1969). *Compounds Dissolved in Cyclic Amine Oxides* (Patent No. 3,447,939).

Jönsson, L. J., Alriksson, B., & Nilvebrant, N.-O. (2013). Bioconversion of lignocellulose: inhibitors and detoxification. *Biotechnology for Biofuels*, *6*(16), 40.

Kai, D., Tan, M. J., Chee, P. L., Chua, Y. K., Yap, Y. L., & Loh, X. J. (2016). Towards lignin-based functional materials in a sustainable world. *Green Chemistry*, *18*(5), 1175–1200. https://doi.org/10.1039/C5GC02616D

Kamlet, M. J., & Abboud, L. (1975). *The Solvatochromic Comparison Method . 6 . The 7 * Scale of Solvent Polarities1*. *6027*(34), 6027–6038. https://doi.org/10.1021/ja00460a031

Kennedy, J. F., Knill, C. J., & Taylor, D. W. (1998). Conversion of Cellulosic Feedstocks into Useful Products. In S. Dumitriu (Ed.), *Polysaccharides: Structural diversity and functional versatility* (pp. 835–849). Marcel Dekker.

Klemm, D., Philipp, B., Heinze, T., Heinze, U., & Wagenknecht, W. (1998). *Comprehensive cellulose chemistry: Fundamentals and Analytical Methods* (1st ed.). WILEY-VCH Verlag GmbH &Co. KGaA.

Kondo, T. (1998). Hydrogen Bonds in Cellulose and Cellulose Derivatives. In D. Severian (Ed.), *Polysaccharides: Structural diversity and functional versatility* (pp. 131–172).

Köpcke, V. (2010). *Conversion of Wood and Non-wood Paper- grade Pulps to Dissolving-grade Pulps*. KTH Royal Institute of Technology.

Köpcke, V., Ibarra, D., & Ek, M. (2008). Increasing accessibility and reactivity of paper grade pulp by enzymatic treatment for use as dissolving pulp. *Nordic Pulp & Paper Research Journal*, *23*(4), 363–368. https://doi.org/10.3183/npprj-2008-23-04-p363-368

Köpcke, V., Ibarra, D., Larsson, P. T., & Ek, M. (2010). Optimization of treatments for the conversion of eucalyptus kraft pulp to dissolving pulp. *Polymers from Renewable Resources*, *1*(1), 17–34. https://doi.org/10.1177/204124791000100102

Krässig, H. A. (1993). *Cellulose - Structure, accessibility and reactivity*. Gordon and Breach.

Kumar, H., & Christopher, L. P. (2017). Recent trends and developments in dissolving pulp

production and application. *Cellulose*, *24*(6), 2347–2365. https://doi.org/10.1007/s10570-017-1285-y

Lapeña, D., Olsen, P. M., Arntzen, M., Kosa, G., Passoth, V., Eijsink, V. G. H., & Horn, S. J. (2020). Spruce sugars and poultry hydrolysate as growth medium in repeated fed-batch fermentation processes for production of yeast biomass. *Bioprocess and Biosystems Engineering*, *43*(4), 723–736. https://doi.org/10.1007/s00449-019-02271-x

Leipner, H. (2002). *Salzhydratschmelzen als Lösemedien für Cellulose und Cellulosederivate*. Technischen Universität Bergakademie Freiberg.

Li, H., Legere, S., He, Z., Zhang, H., Li, J., Yang, B., Zhang, S., Zhang, L., Zheng, L., & Ni, Y. (2018). Methods to increase the reactivity of dissolving pulp in the viscose rayon production process: a review. *Cellulose*, *25*(7), 3733–3753. https://doi.org/10.1007/s10570-018-1840-1

Lindman, B., Karlström, G., & Stigsson, L. (2010). On the mechanism of dissolution of cellulose. *Journal of Molecular Liquids*, *156*(1), 76–81. https://doi.org/10.1016/j.molliq.2010.04.016

Liu, X., Xiao, W., Ma, X., Huang, L., Ni, Y., Chen, L., Ouyang, X., & Li, J. (2020). Conductive Regenerated Cellulose Film and Its Electronic Devices – A Review. *Carbohydrate Polymers*, *250*, 116969. https://doi.org/10.1016/j.carbpol.2020.116969

López, F., Díaz, M. J., Eugenio, M. E., Ariza, J., Rodríguez, A., & Jiménez, L. (2003). Optimization of hydrogen peroxide in totally chlorine free bleaching of cellulose pulp from olive tree residues. *Bioresource Technology*, *87*(3), 255–261. https://doi.org/10.1016/S0960-8524(02)00239-0

Ma, Y., Hummel, M., Määttänen, M., Särkilahti, A., Harlin, A., & Sixta, H. (2016). Upcycling of waste paper and cardboard to textiles. *Green Chemistry*, *18*(3), 858–866. https://doi.org/10.1039/c5gc01679g

Manimaran, P., Saravanan, S. P., Sanjay, M. R., Siengchin, S., Jawaid, M., & Khan, A. (2019). Characterization of new cellulosic fiber: Dracaena reflexa as a reinforcement for polymer composite structures. *Journal of Materials Research and Technology*, *8*(2), 1952–1963. https://doi.org/10.1016/j.jmrt.2018.12.015

Medronho, B., & Lindman, B. (2014a). Brief overview on cellulose dissolution / regeneration interactions and mechanisms. *Advances in Colloid and Interface Science*, 1–7.

https://doi.org/10.1016/j.cis.2014.05.004

Medronho, B., & Lindman, B. (2014b). Competing forces during cellulose dissolution : From solvents to mechanisms. *Current Opinion in Colloid & Interface Science*, *19*(1), 32–40. https://doi.org/10.1016/j.cocis.2013.12.001

Medronho, B., Romano, A., & Grac, M. (2012). Rationalizing cellulose (in) solubility : reviewing basic physicochemical aspects and role of hydrophobic interactions. *Cellulose*, *19*, 581–587. https://doi.org/10.1007/s10570-011-9644-6

Mendes, I. S. F., Prates, A., & Evtuguin, D. V. (2021). Production of rayon fibres from cellulosic pulps : State of the art and current developments. *Carbohydrate Polymers*, *273*(118466). https://doi.org/10.1016/j.carbpol.2021.118466

Monrroy, M., Renán García, J., Teixeira Mendonça, R., Baeza, J., & Freer, J. (2012). Kraft Pulping of Eucalyptus globulus as a Pretreatment for Bioethanol Production by Simultaneous Saccharification and Fermentation. *Journal of the Chilean Chemical Society*, *57*(2), 1113–1117. https://doi.org/10.4067/S0717-97072012000200012

Nakashima, K., Yamada, L., Satou, Y., Azuma, J., & Satoh, N. (2004). The evolutionary origin of animal cellulose synthase. *Development Genes and Evolution*, *214*(2), 81–88. https://doi.org/10.1007/s00427-003-0379-8

Niaounakis, M. (2017). Regenerated Cellulose. In *Management of Marine Plastic Debris* (p. 40). Elsevier. https://doi.org/10.1016/B978-0-323-44354-8.00001-X

Nishiyama, Y., Sugiyama, J., Chanzy, H., & Langan, P. (2003). Crystal Structure and Hydrogen Bonding System in Cellulose Iα from Synchrotron X-ray and Neutron Fiber Diffraction. *Journal of the American Chemical Society*, *125*(47), 14300–14306. https://doi.org/10.1021/ja037055w

Oliveira Duarte, L., Kohan, L., Pinheiro, L., Fonseca Filho, H., & Baruque-Ramos, J. (2019). Textile natural fibers production regarding the agroforestry approach. *SN Applied Sciences*, *1*(8), 1–10. https://doi.org/10.1007/s42452-019-0937-y

Ono, Y., & Isogai, A. (2021). Analysis of celluloses, plant holocelluloses, and wood pulps by size-exclusion chromatography/multi-angle laser-light scattering. *Carbohydrate Polymers*, *251*(August 2020), 117045. https://doi.org/10.1016/j.carbpol.2020.117045

Philipp, B., & Schleicher, H. (1973). *The Influence of Cellulose Structure on the Swelling of Cellulose in Organic Liquids*. *1543*(42), 1531–1543.

Pinto, I. S. S., Ascenso, O. S., Barros, M. T., & Soares, H. M. V. M. (2015). Pre-treatment of the paper pulp in the bleaching process using biodegradable chelating agents. *International Journal of Environmental Science and Technology*, *12*(3), 975–982. https://doi.org/10.1007/s13762-013-0480-0

Poletto, P., Pereira, G. N., Monteiro, C. R. M., Pereira, M. A. F., Bordignon, S. E., & de Oliveira, D. (2020). Xylooligosaccharides: Transforming the lignocellulosic biomasses into valuable 5-carbon sugar prebiotics. *Process Biochemistry*, *91*(September 2019), 352–363. https://doi.org/10.1016/j.procbio.2020.01.005

Project Management Institute. (2021). *Padrão de gerenciamento de projetos e Guia do conhecimento em gerenciamento de projetos (Guia PMBOK)* (PMI (ed.); 7ª edição). Project Management Institute, Inc.

Ramos, L. A., Assaf, M., Seoud, O. A. El, Frollini, E., Sa, U. De, & Lui, W. (2005). *Influence of the Supramolecular Structure and Physicochemical Properties of Cellulose on Its Dissolution in a Lithium Chloride / N , N-Dimethylacetamide Solvent System*. 2638–2647.

Reyes, P., Márquez, N., Troncoso, E., Parra, C., Mendonça, R. T., & Rodríguez, J. (2016). Evaluation of combined dilute acid-kraft and steam explosion-kraft processes as pretreatment for Enzymatic hydrolysis of pinus radiata wood chips. *BioResources*, *11*(1), 612–625. https://doi.org/10.15376/biores.11.1.612-625

Rosenau, T., Potthast, A., Hofinger, A., Bacher, M., Yoneda, Y., Mereiter, K., Nakatsubo, F., Jäger, C., French, A. D., & Kajiwara, K. (2019). Toward a Better Understanding of Cellulose Swelling , Dissolution , and Regeneration on the Molecular Level. *Cellulose Science and Technology*, 99–125. https://doi.org/10.1002/9781119217619.ch5

Rosenau, T., Potthast, A., Sixta, H., & Kosma, P. (2001). The chemistry of side reactions and byproduct formation in the system NMMO/cellulose (Lyocell process). *Progress in Polymer Science (Oxford)*, *26*(9), 1763–1837. https://doi.org/10.1016/S0079-6700(01)00023-5

Rosenau,T., Potthast, A., Hofinger, A., Sixta, H., & Kosma, P. (2002). Instabilities in the system NMMO/water/cellulose (Lyocell process) caused by polonowski type reactions. *Holzforschung*, *56*(2), 199–208. https://doi.org/10.1515/HF.2002.033

Rosenau, T. ., Hofinger, A. ., Potthast, A. ., & Kosma, P. (2003). On the conformation of the cellulose solvent N-methylmorpholine-N-oxide (NMMO) in solution. *Polymer*, *44*(20), 6153–6158. https://doi.org/10.1016/S0032-3861(03)00663-3

Rosenau, T. ., Potthast, A. ., Adorjan, I. ., Hofinger, A. ., Sixta, H. ., Firgo, H. ., & Kosma, P. (2002). Cellulose solutions in N-methylmorpholine-N-oxide (NMMO) - degradation processes and stabilizers. *Cellulose*, *9*(3–4), 283–291. https://doi.org/10.1023/A:1021127423041

Rowell, R., Pettersen, R., & Tshabalala, M. (2012). Cell Wall Chemistry. In *Handbook of Wood Chemistry and Wood Composites, Second Edition* (pp. 33–72). https://doi.org/10.1201/b12487-5

Saka, S., & Matsumura, H. (2004). Wood pulp manufacturing and quality characteristics. *Macromolecular Symposia*, *208*, 37–48. https://doi.org/10.1002/masy.200450404

Salazar, M. M., Grandis, A., Pattathil, S., Neto, J. L., Camargo, E. L. O., Alves, A., Rodrigues, J. C., Squina, F., Cairo, J. P. F., Buckeridge, M. S., Hahn, M. G., & Pereira, G. A. G. (2016). Eucalyptus Cell Wall Architecture: Clues for Lignocellulosic Biomass Deconstruction. *Bioenergy Research*, *9*(3), 969–979. https://doi.org/10.1007/s12155-016-9770-y

Sayyed, A. J. ., Deshmukh, N. and, & Pinjari, D. V. (2019). A critical review of manufacturing processes used in regenerated cellulosic fibres: viscose, cellulose acetate, cuprammonium, LiCl/DMAc, ionic liquids, and NMMO based lyocell. *Cellulose*, *26*(5), 2913–2940. https://doi.org/10.1007/s10570-019-02318-y

Sayyed, A. J., Mohite, L. V, Deshmukh, N. A., & Pinjari, D. V. (2019). Structural characterization of cellulose pulp in aqueous NMMO solution under the process conditions of lyocell slurry. *Carbohydrate Polymers*, *206*(October 2018), 220–228. https://doi.org/10.1016/j.carbpol.2018.11.004

Schultz, T., & Suresh, A. (2017). *Life Cycle Assessment: Comparing Ten Sources of Manmade Cellulose Fiber*.

Scott, G. M. (2011). Recovered Paper. In *Waste* (pp. 137–149). https://doi.org/10.1016/B978-0-12-381475-3.10010-5

Segal, L., Creely, J. J., Martin, A. E., & Conrad, C. M. (1959). An Empirical Method for Estimating the Degree of Crystallinity of Native Cellulose Using the X-Ray Diffractometer. *Textile*

Research Journal, *29*(10), 786–794. https://doi.org/10.1177/004051755902901003

Sharma, A., Thakur, M. ., Bhattacharya, M. ., Mandal, T. ., & Goswami, S. (2019). Commercial application of cellulose nano-composites – A review. *Biotechnology Reports*, *21*(e00316). https://doi.org/10.1016/j.btre.2019.e00316

Shen, L., & Patel, M. K. (2010). Life cycle assessment of man-made cellulose fibres. *Lenzinger Berichte*, *88*(88), 1–59.

Shen, L., Worrell, E., & Patel, M. K. (2010). Environmental impact assessment of man-made cellulose fibres. *Resources, Conservation and Recycling*, *55*(2), 260–274. https://doi.org/10.1016/j.resconrec.2010.10.001

Shevchenko, A. R., Tyshkunova, I. V., Chukhchin, D. G., Malkov, A. V., Toptunov, E. A., Telitsin, V. D., Rozhkova, A. M., Sinitsyna, O. A., Gofman, I. V., & Aksenov, A. S. (2023). Production of Biomodified Bleached Kraft Pulp by Catalytic Conversion Using Penicillium verruculosum Enzymes: Composition, Properties, Structure, and Application. *Catalysts*, *13*(1). https://doi.org/10.3390/catal13010103

Siller, M., Ahn, K., Pircher, N., Rosenau, T., & Potthast, A. (2014). Dissolution of rayon fibers for size exclusion chromatography: A challenge. *Cellulose*, *21*(5). https://doi.org/10.1007/s10570-014-0356-6

Sixta, H. (2000). Comparative evaluation of TCF bleached hardwood dissolving pulps. *Lenzinger Berichte*, *79*, 119–128.

Sixta, H. (2006). Handbook of Pulp. In *Wiley-Vch* (Vol. 1, Issue 1). WILEY-VCH Verlag GmbH &Co. KGaA.

Sixta, H., Iakovlev, M., Testova, L., & Roselli, A. (2013). Novel concepts of dissolving pulp production. *Cellulose*, *20*, 1547–1561. https://doi.org/10.1007/s10570-013-9943-1

Sjöström, E. (1981). *Wood Chemistry: Fundamentals and Applications*. Academic Press.

Södö, M., Su, P., Granholm, K., Harju, L., & Ivaska, A. (2007). Study on metal ion affinities to oxygen delignified hard-wood kraft pulp by a column chromatographic method. *Nordic Pulp and Paper Research Journal*, *22*(4), 462–467. https://doi.org/10.3183/npprj-2007-22-04-p462-467

Spange, S., Fischer, K., Prause, S., & Heinze, T. (2003). Empirical polarity parameters of celluloses and related materials. *Cellulose*, *10*, 201–212.

Stenutz, R. (2020). *Kamlet-Taft solvent parameters*. http://www.stenutz.eu/chem/kamlettaft.php

Textile Exchange. (2021). *Preferred Fiber & Materials Market Report 2021*. https://textileexchange.org/knowledge-center/reports/preferred-fiber-materials-market-report-2021/

Textile Exchange. (2022a). *Preferred Fiber & Materials Market Report 2022*. http://textileexchange.org/app/uploads/2022/10/Textile-Exchange_PFMR_2022.pdf

Textile Exchange. (2022b). *Sustainable Cotton Challenge 2025*. https://textileexchange.org/knowledge-center/reports/2025-sustainable-cotton-challenge-report/

Tian, C., Zheng, L., Miao, Q., Nash, C., Cao, C., & Ni, Y. (2013). Improvement in the Fock test for determining the reactivity of dissolving pulp. *Tappi Journal*, *12*(11), 21–26. https://doi.org/10.32964/tj12.11.21

Venkatesan, H., & Periyasamy, A. P. (2019). Eco-fibers in the Textile Industry. In *Handbook of Ecomaterials* (pp. 1413–1433). https://doi.org/10.1007/978-3-319-68255-6_25

Venkatram, S., Kim, C., Chandrasekaran, A., & Ramprasad, R. (2019). Critical Assessment of the Hildebrand and Hansen Solubility Parameters for Polymers. *Journal of Chemical Information and Modeling*. https://doi.org/10.1021/acs.jcim.9b00656

Wan, C., Jiao, Y., Wei, S., Zhang, L., Wu, Y., & Li, J. (2019). Functional nanocomposites from sustainable regenerated cellulose aerogels: A review. *Chemical Engineering Journal*, *359*, 459–475. https://doi.org/10.1016/j.cej.2018.11.115

Wang, H., Pang, B., Wu, K., Kong, F., Li, B., & Mu, X. (2014). Two stages of treatments for upgrading bleached softwood paper grade pulp to dissolving pulp for viscose production. *Biochemical Engineering Journal*, *82*, 183–187. https://doi.org/10.1016/j.bej.2013.11.019

Wang, X., Duan, C., Zhao, C., Meng, J., Qin, X., Xu, Y., & Ni, Y. (2018). Heteropoly acid catalytic treatment for reactivity enhancement and viscosity control of dissolving pulp. *Bioresource*

Technology, *253*, 182–187. https://doi.org/10.1016/j.biortech.2018.01.022

Yamane, C., Aoyagi, T., Ago, M., Sato, K., Okajima, K., & Takahashi, T. (2006). Two different surface properties of regenerated cellulose due to structural anisotropy. *Polymer Journal*, *38*(8), 819–826. https://doi.org/10.1295/polymj.PJ2005187

Yaopeng, Z., Miaomiao, C., Xiaodong, W., Gesheng, Y., Fangong, K., Qinghui, L., & Shoujuan, W. (2020). *Method for removing metal ions in waste cotton fabric dissolving pulp* (Patent No. CN111636101B).

Young, R. A., & Rowell, R. M. (Eds.). (1986). *Cellulose: Structure, Modification and Hydrolysis*. John Wiley & Sons, Inc.

Zhang, S., Chen, C., Duan, C., Hu, H., Li, H., Li, J., Liu, Y., Ma, X., Stavik, J. and, & Ni, Y. (2018). Regenerated cellulose by the lyocell process, a brief review of the process and properties. *BioResources*, *13*(2), 1–16. https://doi.org/10.15376/biores.13.2.Zhang

Zhang, X., Li, L., & Xu, F. (2022). Chemical Characteristics of Wood Cell Wall with an Emphasis on Ultrastructure: A Mini-Review. *Forests*, *13*(3). https://doi.org/10.3390/f13030439

Zugenmaier, P. (1998). Supramolecular Structure of Polysaccharides. In S. Dumitriu (Ed.), *Polysaccharides: Structural diversity and functional versatility* (pp. 57–100). Marcel Dekker.

Appendixes

Appendix A: Pulps' properties

Table A.1. General pulp properties and their respective standard deviations.

		DWP FTR	DWP Batch	DWP Commercial	RPP Original	RPP C_3
Kappa Number	Average	1.20	2.02	< 1.00*	49.94	1.28
	Std dev	0.39	0.02	-	0.15	0.09
ISO Brightness	Average	87.84	85.89	88.57	28.98	75.46
	Std dev	0.29	0.17	0.11	0.14	0.25
alpha-cellulose (%)	Average	88.07	90.82	78.01	74.31	70.20
	Std dev	0.36	0.40	0.17	0.05	0.05
Int.Viscosity (cm^3/g)	Average	548.7	873.8	474.1	668.9	413.5
	Std dev	6.8	1.8	7.0	5.6	3.6
Reactivity (%)	Average	71.2	57.1	91.47	45.59	84.09
	Std dev	1.06	1.05	0.26	0.86	0.66
Ash content (%)	Average	0.32	0.29	<0.10*	10.14	1.21
	Std dev	0.10	0.04	-	0.22	0.05

Table A.2. Metal ions content for studied pulps.

Analyte Symbol	DWP FTR	DWP Batch	RPP Original	RPP C3
Na (ppm)	153	255	103	49
Mg (ppm)	77	92	781	163
Al (ppm)	12	12	4616	441
P (ppm)	1	1	80	9
K (ppm)	14	25	170	22
Ca (ppm)	1089	882	32385	2541
Mn (ppm)	4	3	22	4
Fe (ppm)	55	32	681	183
Co (ppm)	0	0	1	0
Ni (ppm)	2	2	3	2
Cu (ppm)	2	1	117	25
Sr (ppm)	1	1	39	3
Ba (ppm)	1	1	24	4
Pb (ppm)	1	0	9	4

Appendix B: RPP properties data

Table B.1. Results of kappa number and intrinsic viscosity of RPP samples presented in Figure 4.3 and their respective standard deviations.

		Original	PH	A_1	A_2	B	C_1	C_2	C_3
Kappa Number unbleached	Average	49.9	-	34.5	30.6	8.8	21.6	20.8	20.9
	Std dev	0.1	-	0.5	1.1	0.2	0.8	0.2	0.2
Kappa Number bleached	Average	-	-	4.7	4.7	2.5	1.8	1.9	1.3
	Std dev	-	-	0.4	0.3	0.7	0.2	0.1	0.1
Intrinsic Viscosity (cm^3/g)	Average	669	554	464	479	351	444	417	414
	Std dev	6	10	5	10	1	13	2	4

Table B.2. Phase 2 RPPs chemical composition and intrinsic viscosity.

		Cellulose (%)	Hemicellulose (%)	Insoluble matter (%)	Intrinsic Viscosity (cm^3/g)
	Original	56.7	7.8	35.5	669±6
	PH	64.0	9.1	26.9	554±10
Unbleached	**C_1**	77.0	6.2	16.8	506±4
	C_2	76.5	6.6	17.0	510±10
	C_3	76.8	4.1	19.1	517±1
Bleached	**C_1**	84.9	5.8	9.3	444±13
	C_2	87.7	4.7	7.6	417±2
	C_3	88.9	4.9	6.3	414±4

Table B.3. Process yields and global yield for phase 2 RPP samples.

	Sample	Process Yield (%)	Global Yield (%)
	Original	100.00	100.00
Prehydrolysis	PH	88.05	88.05
Kraft Cooking	C_1	73.43	64.66
	C_2	76.32	67.20
	C_3	74.34	65.46
ECF Bleaching	C_1	99.81	64.53
	C_2	86.97	58.44
	C_3	90.83	59.45

Appendix C: Reference Chromatograms

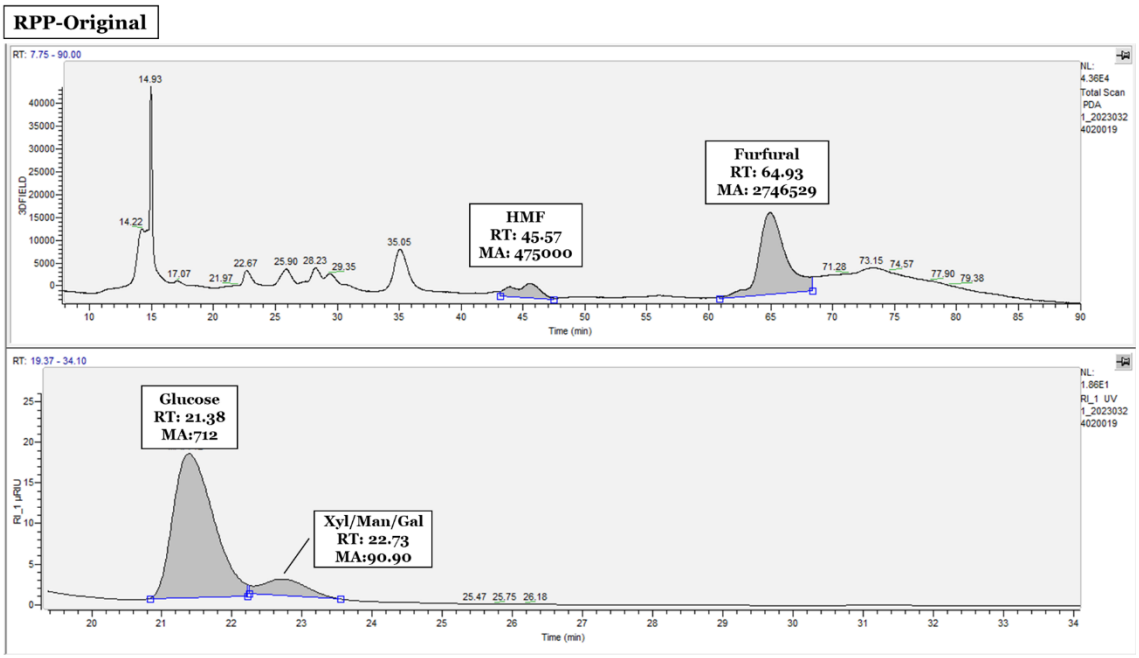

Figure C.1. Chromatograms for RPP-Original. Identification of pics of Hydroxymethylfurfural (degradation product of glucose), Furfural (degradation product of C5 carbohydrates), Glucose (considered as cellulose), Xylose/Mannose/Galactose (considered as hemicellulose).

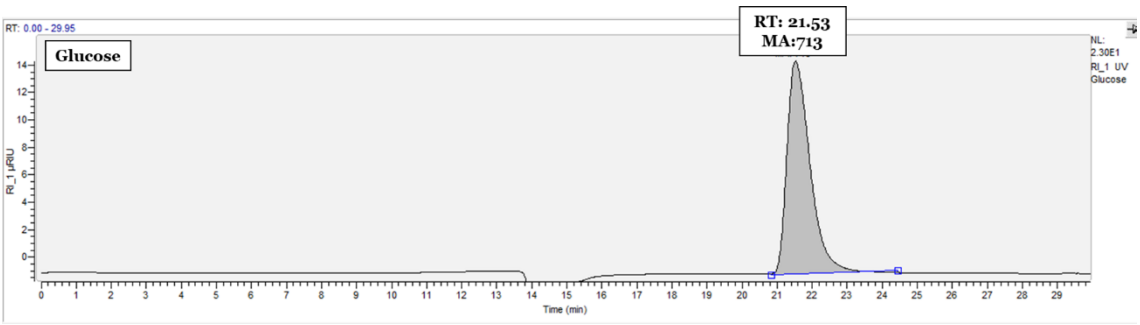

Figure C.2. Reference chromatogram for a standard of Glucose.

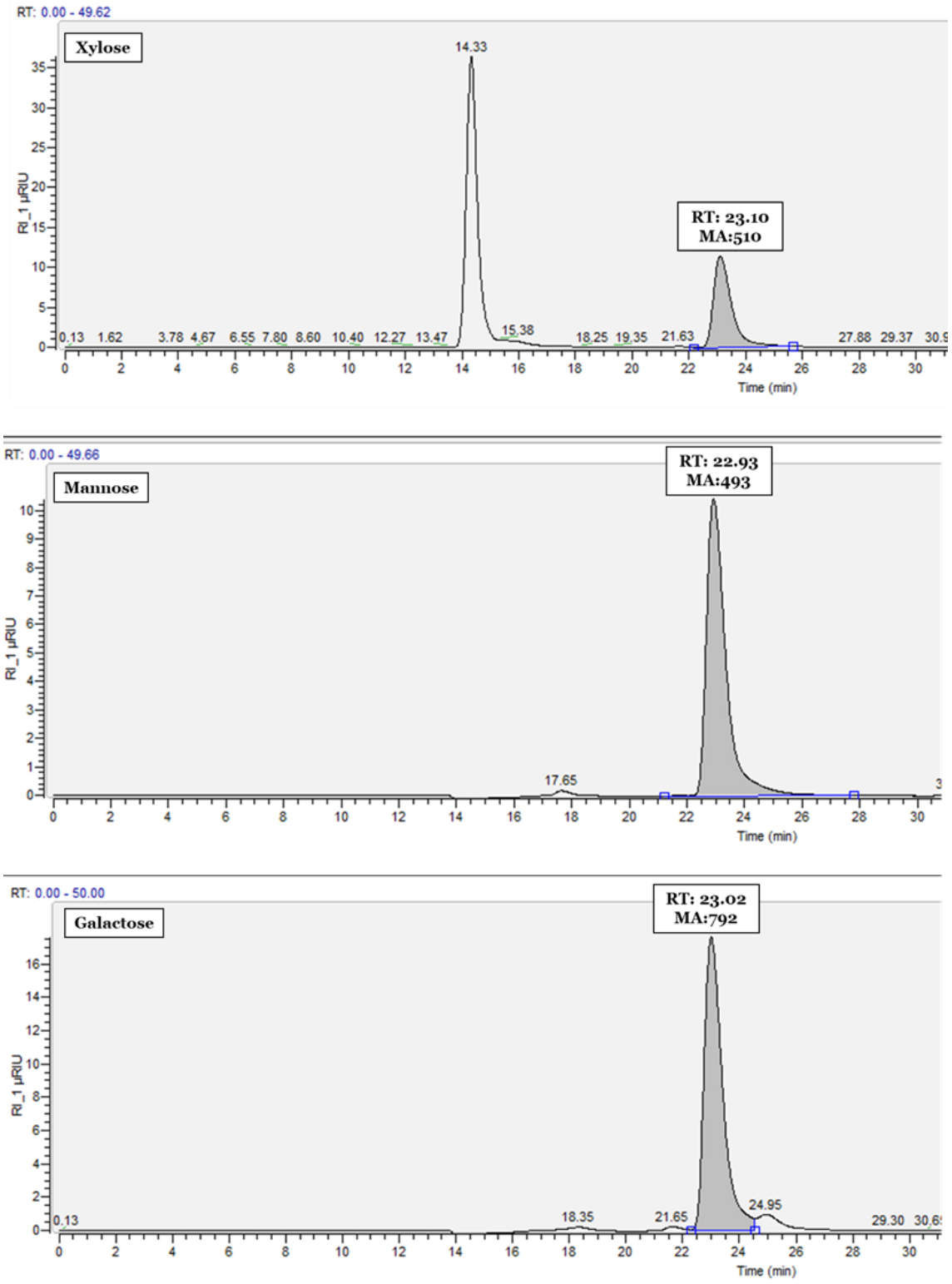

Figure C.3. Reference chromatograms for standards of Xylose, Mannose, and Galactose.

Appendix D: XRD patterns

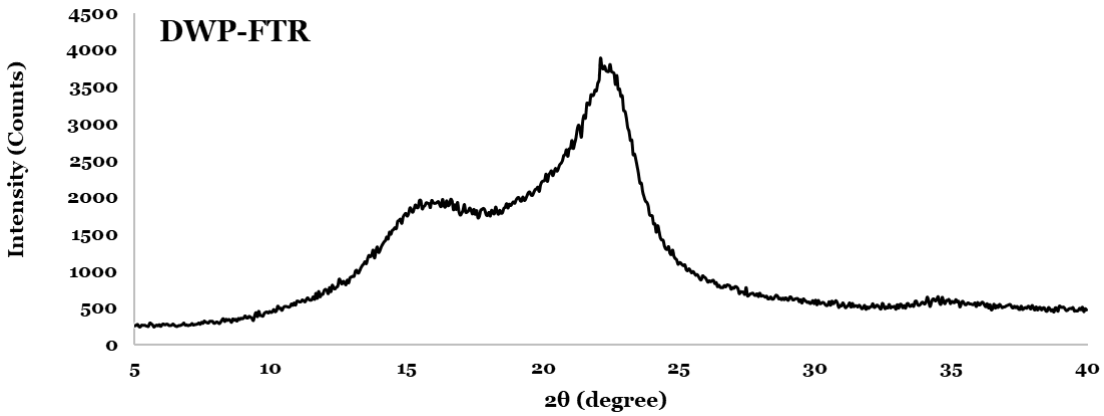

Figure D.1. XRD diffractogram for DWP-FTR.

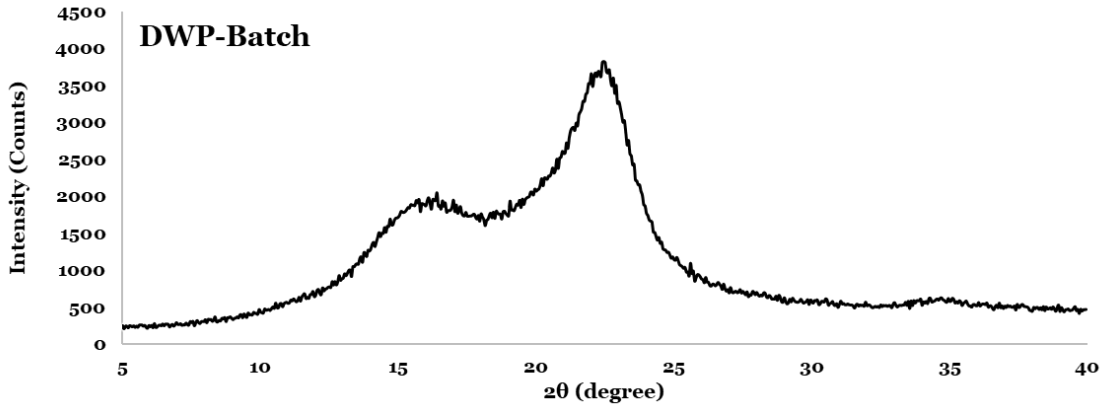

Figure D.2. XRD diffractogram for DWP-Batch.

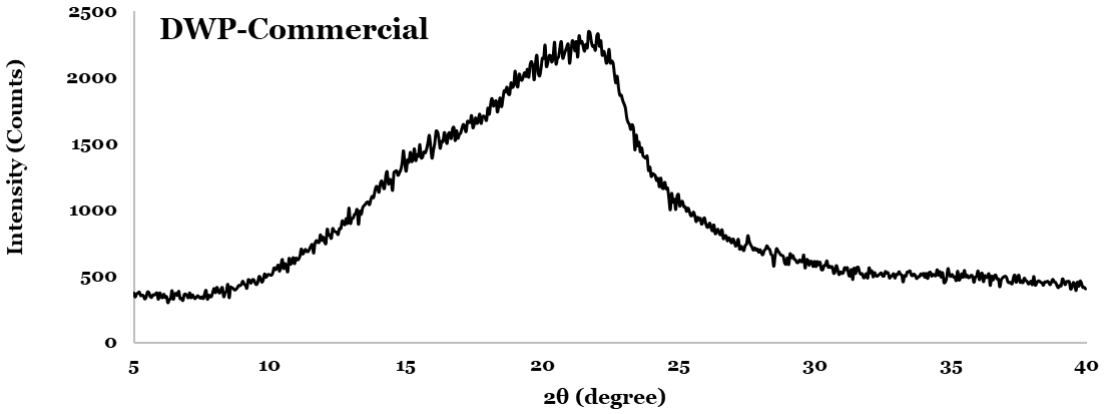

Figure D.3. XRD diffractogram for DWP-Commercial.

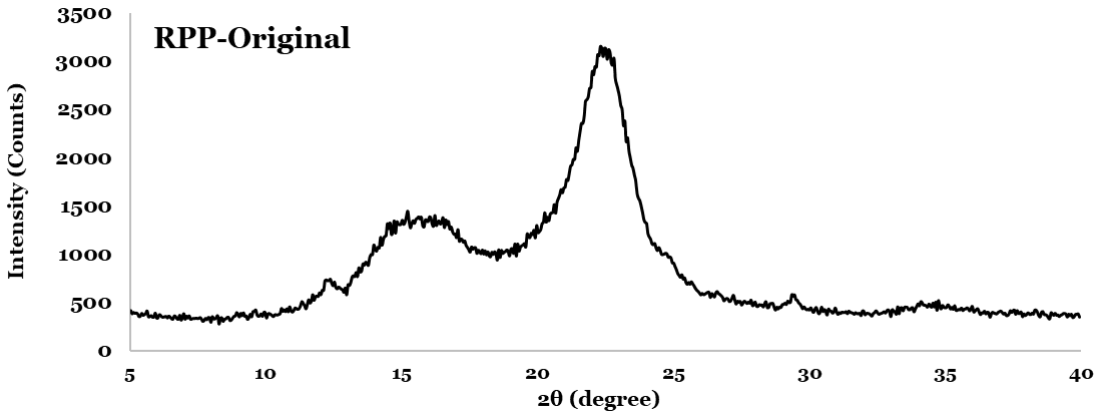

Figure D.4. XRD diffractogram for RPP-Original.

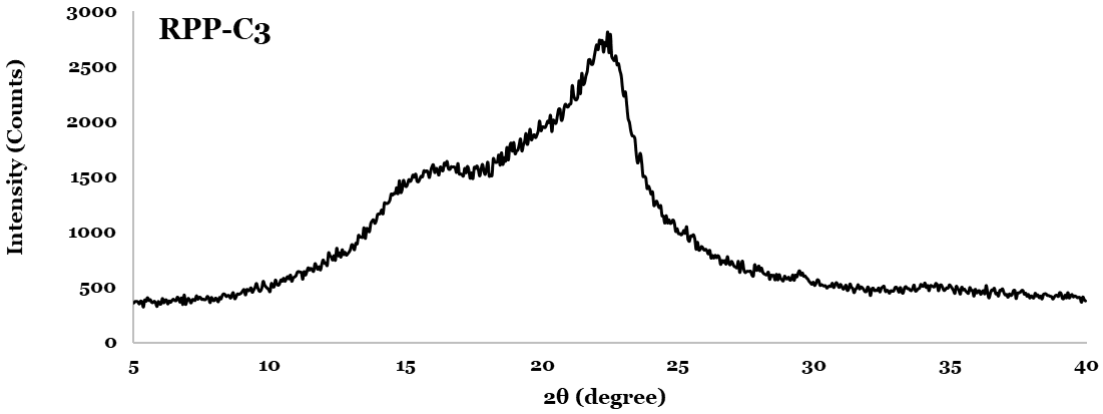

Figure D.5. XRD diffractogram for RPP-C_3.

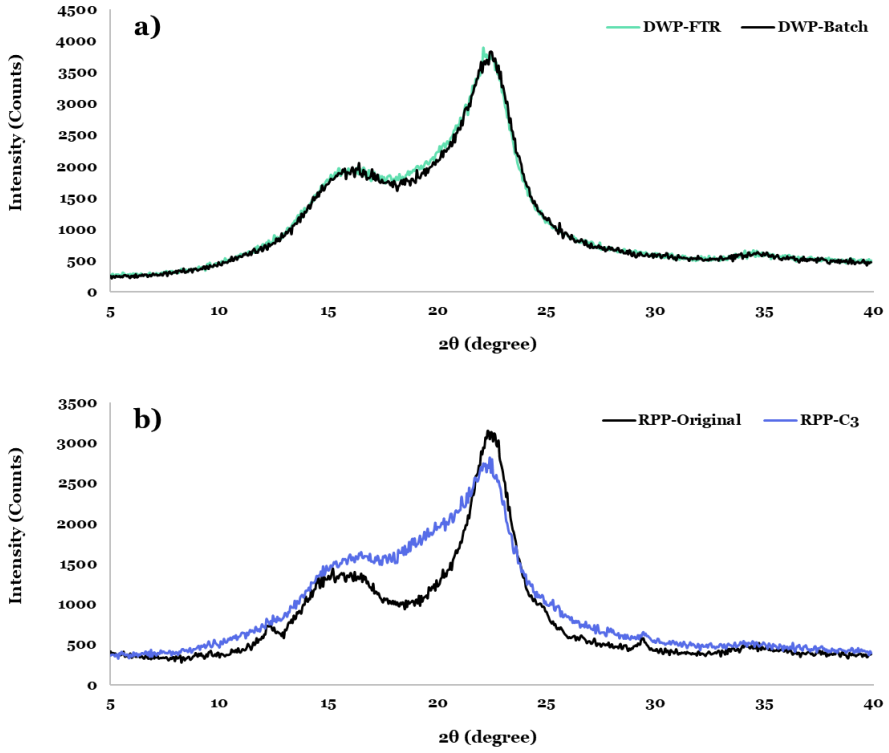

Figure D.6. Comparison of XRD diffractograms for a) DWPs (FTR and Batch), and b) RPPs (Original and C_3).

Appendix E: Dissolution extent in 8% LiCl/DMAc

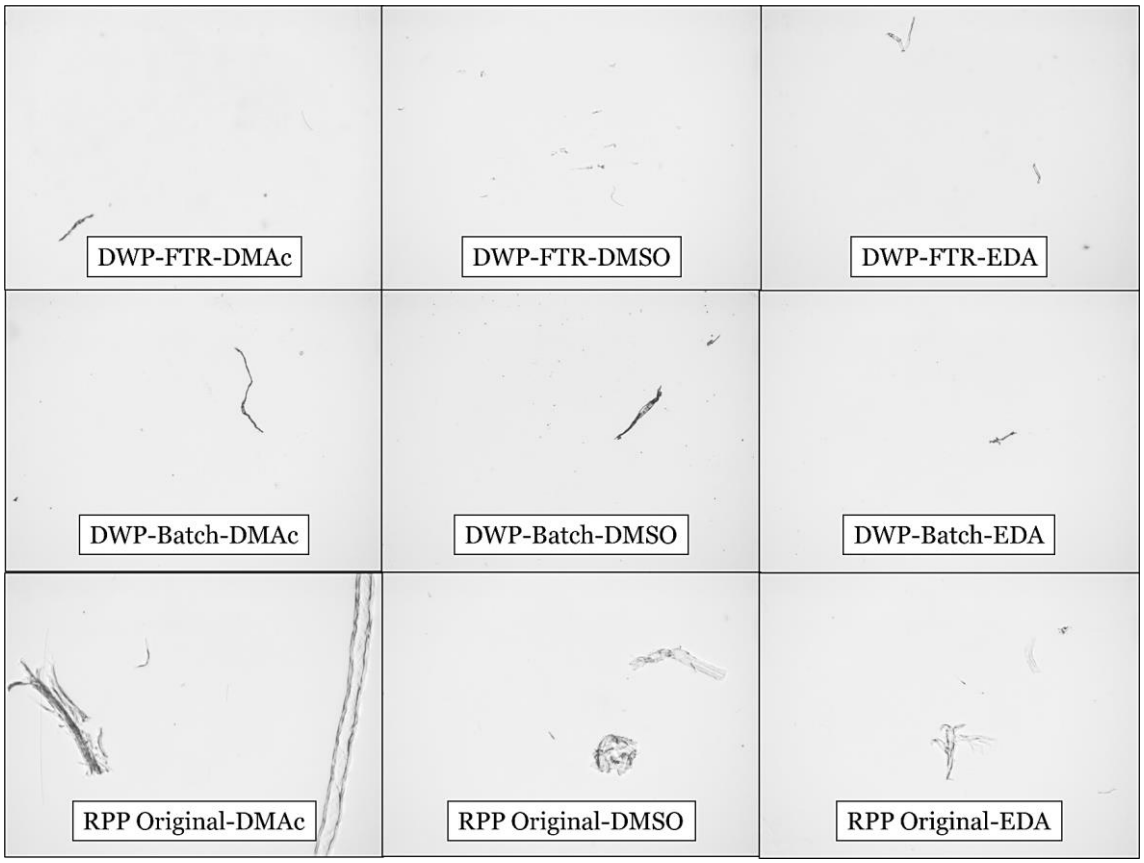

Figure E.1. Microscopy images of dissolution extent of pulps in 8%LiCl/DMAc after the activation processes: H2O→Metanol→DMAc/DMSO and EDA→Metanol→DMAc.

Appendix F: Dissolution extent in NMMO

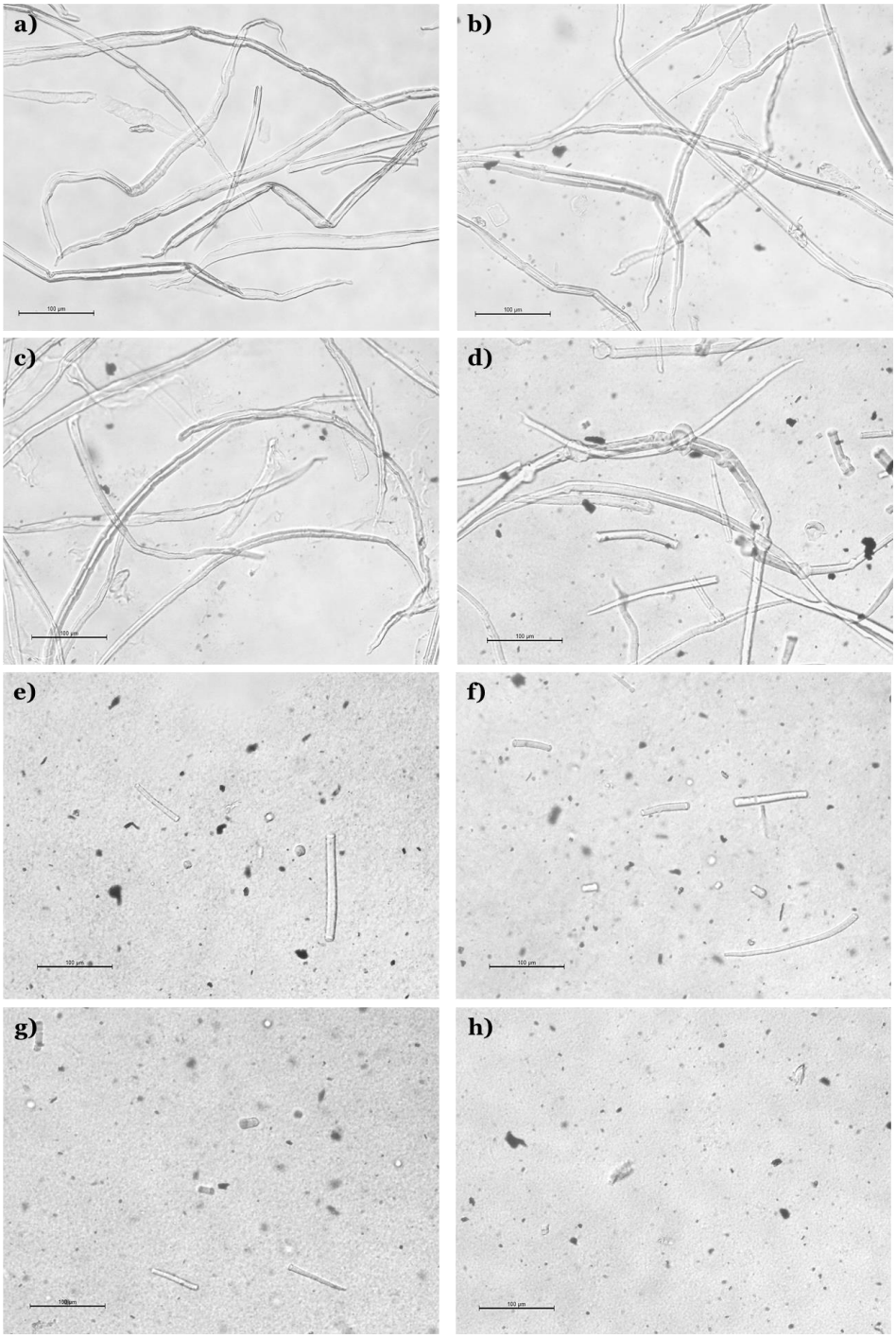

Figure F.1. Microscopy images (100x) of dissolution progress of DWP-FTR in NMMO after a) swelling step; b) 15 min; c) 30 min; d) 45 min; e) 60 min; f) 75 min; g) 90 min; h) 105 min.

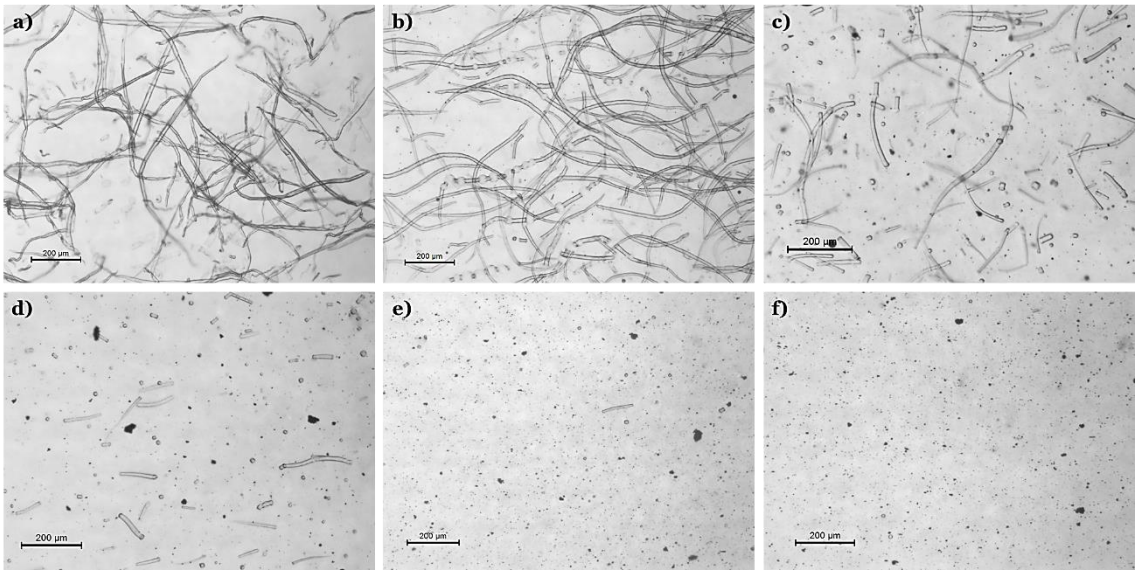

Figure F.2. Images (40x ampified) of the dissolution progress of DWP-Batch in NMMO/H_2O after a) swelling; b) 30 min; c) 60 min; d) 75 min; e) 90 minutes; and f) 105 min.

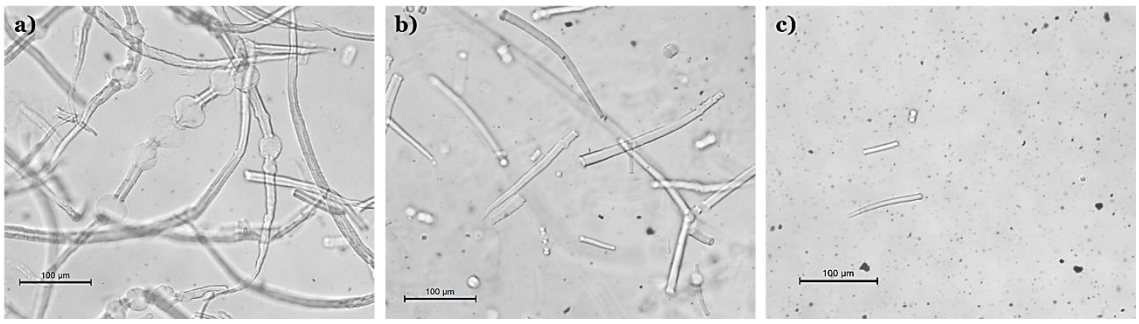

Figure F.3. Images of the critical point of the dissolution development of DWP-Batch between a) 30 min; b) 60 min; and c) 90 min. Evidence of balloons formation, and remaining fiber fragments.

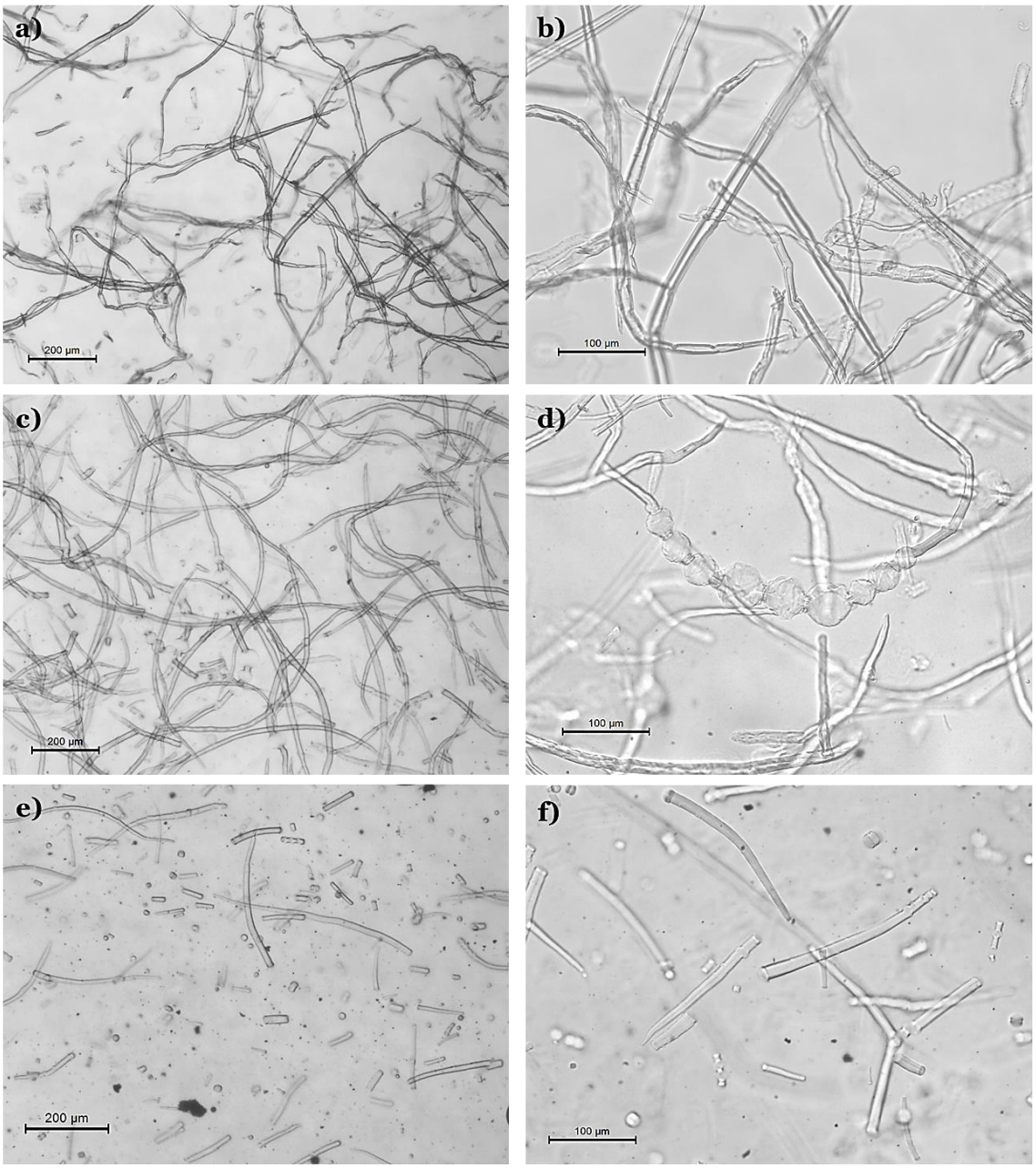

Figure F.4. Microscopy images of dissolution progress of DWP-Batch in NMMO after swelling a) 40x, b) 100x; 30 min c) 40x, d) 100x; 60 min e) 40x, f) 100x.

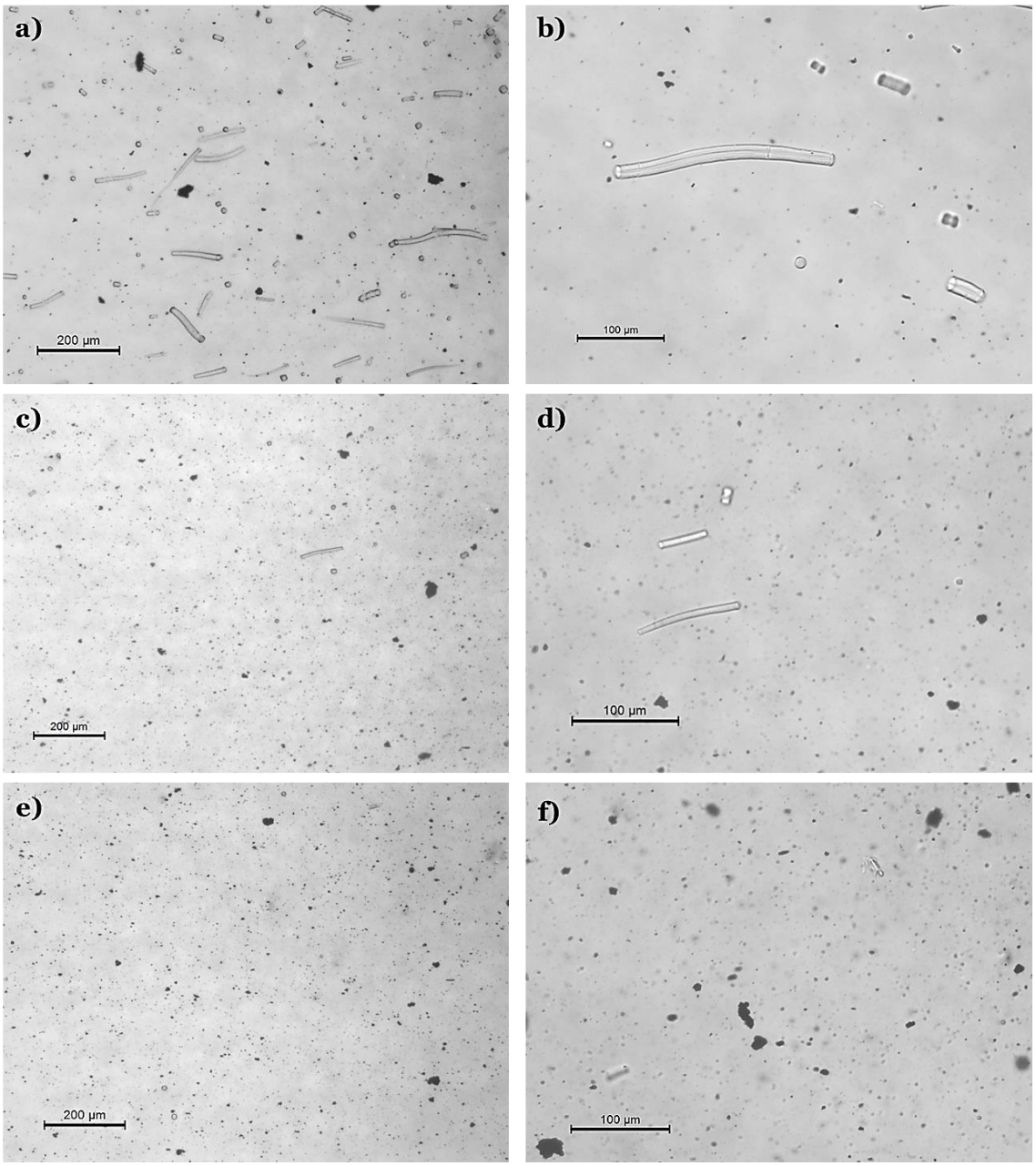

Figure F.5. Microscopy images of dissolution progress of DWP-Batch in NMMO after 75 min a) 40x, b) 100x; 90 min c) 40x, d) 100x; 105 min e) 40x, f) 100x.

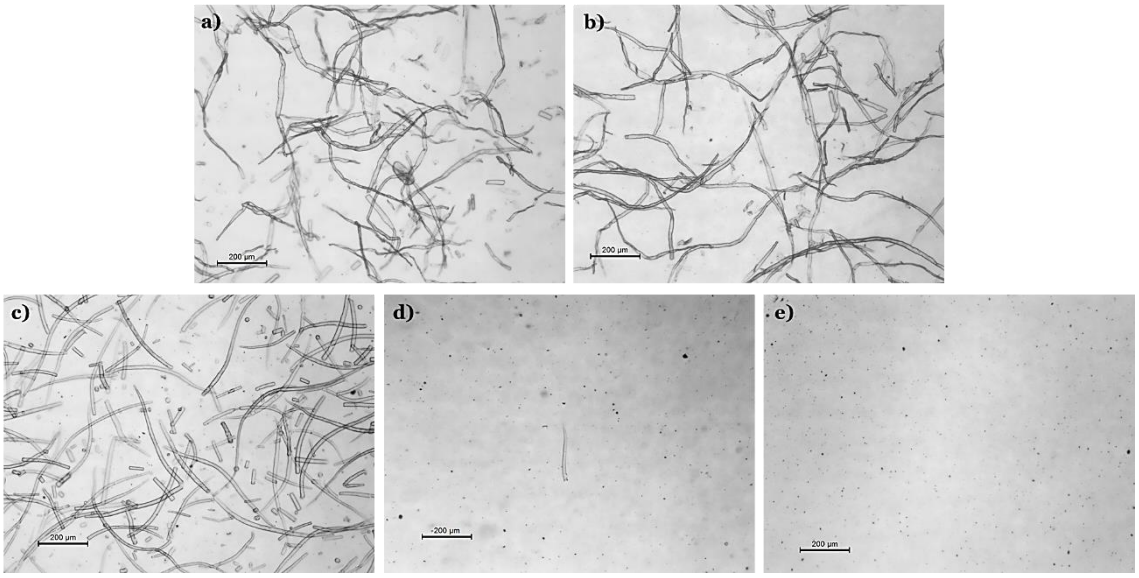

Figure F.6. Images (40x amplified) of the dissolution progress of DWP-Commercial in NMMO/H_2O after a) swelling; b) 15 min; c) 30 min; d) 45 min; and e) 60 minutes.

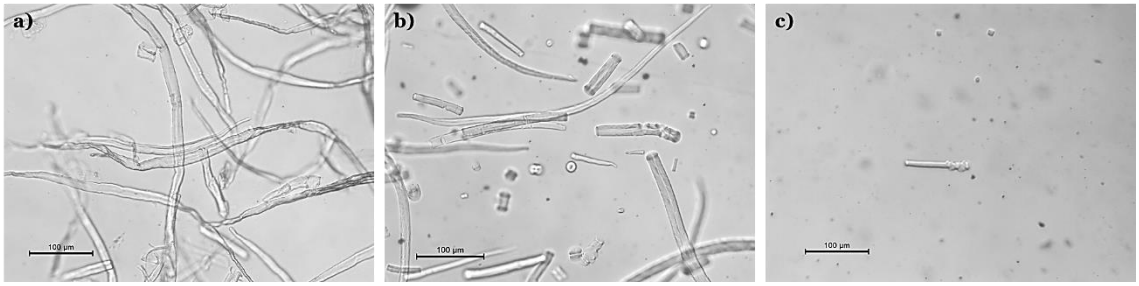

Figure F.7. Images (100x) of the critical point of the dissolution development of DWP-Commercial between a) 15 min; b) 30 min; and c) 60 min. Evidence of a) swelling; b) fiber rupture and ring-like fragments; and c) remaining fiber fragments.

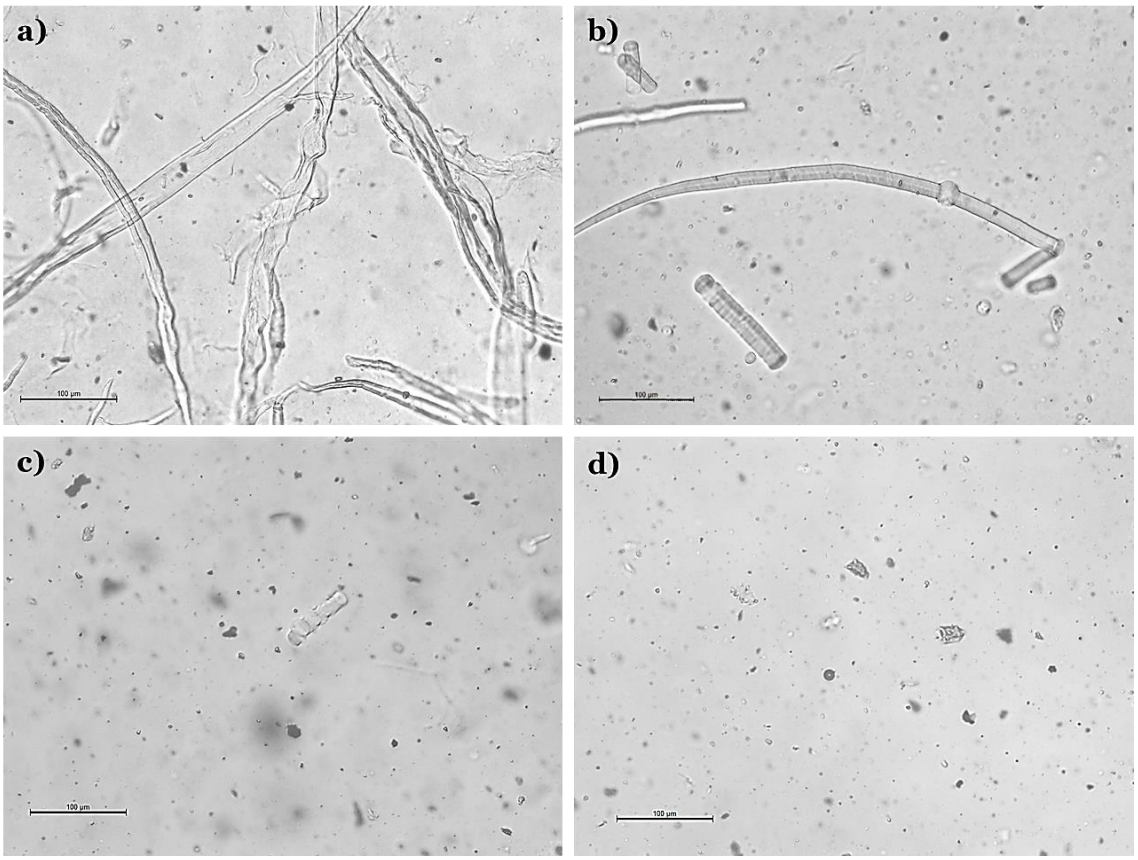

Figure F.8. Microscopy images (100x) of dissolution progress of RPP in NMMO after a) 15 min; b) 30 min; c) 45 min; d) 60 min.